NTNU

Norwegian University of
Science and Technology

Experimental Study of Fracture Toughness in Sedimentary Rocks

Niklas Øystad Brevik

Petroleum Geoscience and Engineering
Submission date: July 2016
Supervisor: Rune Martin Holt, IPT
Co-supervisor: Lars Erik Walle, SINTEF Petroleum

Norwegian University of Science and Technology
Department of Petroleum Engineering and Applied Geophysics

Acknowledgment

I would firstly like to thank my supervisor professor Rune M. Holt for giving me an interesting topic and providing valuable guidance helping me greatly with this work. I would also like to give a special thanks to my co-supervisor Lars Erik Walle, at SINTEF Petroleum for all of his help, as without him this thesis would not have been possible. His help with the technical equipment and for always being open for a discussion helped shape the thesis into what it is today. My gratitude is not enough.

I would also like to thank Anna Stroisz for lending help with the software used, Jørn F. Stenebråten for providing useful solutions to problems encountered during the project, Eyvind Sønstebø for providing a deeper insight into rock mechanics and Alexandre Lavrov for giving me a fundamental insight related to tensile strength issues. In addition, a great thank you is given to Hans Lund and Sigurd Bakheim for their help with the preparations of the samples.

A warm thank you is given to me friends, family and others who provided me with support and encouragement throughout these years at NTNU and TTU. I will cherish the years we spent together.

Lastly, a special thank you is given to my girlfriend, Heidi Langen, for all the help, support and comfort you have given during this thesis. Had it not been for you, I would not be where I am today.

Abstract

This master thesis details the determination of mode I (tensile) fracture toughness, K_{IC}, using the International Society of Rock Mechanics (ISRM) Chevron Bend (CB) method on three sedimentary rock types. Fracture toughness is an important parameter, describing the ability of the rock to avoid fracturing. It has three main purposes: a classification parameter for rock material, index of the rock fragmentation process and a material property used in models. Non-linearity behavior was accounted for through the use of the plasticity factor. The primary motivation for these experiments is to improve on the ability to predict how hydraulic fractures occurs and where they go. Highly important to this is the fracture toughness parameter and its relevance for other parameters such as tensile strength, Brazilian strength etc.

Mode I fracture toughness determination was done on three rock types; Mons chalk, Castlegate sandstone and Mancos shale. The size effect was studied in Castlegate and Mons, using samples sizes of 38 and 50 mm diameter. The uncorrected fracture toughness showed a clear size effect, with increasing fracture toughness for increasing specimen size. Accounting for non-linearity, the fracture toughness for sandstone is independent of size, while the chalk still has a clear size effect. Mancos was used to investigate the anisotropy effect from bedding planes. The fracture toughness was seen to vary greatly with the inclination angle, but to what extent is not properly determined. Mixed mode fracturing is indicated by an increased plasticity factor for higher inclinations. Another finding was that the fractures were seen to follow the bedding planes whenever possible.

For the samples tested, the corrected fracture toughness is 0.153, 0.124, 0.221 and 0.231 $MPa*m^{1/2}$, for Mons chalk of 50 mm diameter, Mons chalk of 38 mm diameter, Castlegate sandstone of 50 mm diameter and Castlegate sandstone of 38 mm diameter, respectively. Mancos shale varied from 0.370 to 1.287 $MPa*m^{1/2}$.

Sammendrag

Denne avhandlingen beskriver bestemmelsen av modus I (strekk) sprekkstyrke[1] (fracture toughness) ved å bruke en av ISRMs anbefalte metoder, CB metoden med et V-formet hakk på midten av prøven på tre sedimentære bergarter. Sprekkstyrken er en viktig parameter som beskriver en bergarts evne til å motstå oppsprekking. Bestemmelsen av sprekkstyrke har flere hovedformål, hvorav to av disse er til klassifisering av bergarter og som en materialegenskap brukt i sammenheng med modellering av sprekker. Ikke-lineær oppførsel er korrigert ved å bruke en plastisitets faktor. Motivasjonen for disse eksperimentene er å forbedre våre evner til å estimere hvordan hydrauliske sprekker oppstår og hvor de går. Aspekter som også er relatert til dette er sprekkstyrken og dens forhold til andre parametere som strekkstyrke, Brasilianer styrke osv.

Modus I sprekkstyrke ble bestemt for tre bergarter; Mons kritt, Castlegate sandstein og Mancos skifer. Størrelseseffekter ble undersøkt hos Mons og Castlegate ved å bruke prøver med en diameter på 38 og 50 mm. Den ukorrigerte sprekkstyrken viste en klar påvirkning av størrelsen på prøven. Sprekkstyrken var større for prøvene med større diameter. Når det ble korrigert for den ikke-lineære oppførselen til prøvene, viste sandsteinprøvene at de var uavhengige av størrelsen på prøven, mens kritt fremdeles hadde en tydelig størrelseseffekt. Mancos ble brukt til å undersøke effekten av anisotropi fra sedimentlagplanene. Her ble det fastslått at sprekkstyrken varierte kraftig med forskjellige helningsvinkler på sedimentlagene, men det var ikke mulig å fastslå i hvilken grad eller hvordan den varierte. Det var indikasjoner på at oppsprekkingen i Mancos skjedde gjennom både skjær- og strekk-laster, såkalt blandet modus, ved at plastisitets faktoren økte for større helningsvinkler. Det ble også sett at sprekkene fulgte lagdelingene der det lot seg gjøre.

Den korrigerte sprekkstyrken ble fastslått til å være 0.153, 0.124, 0.221 og 0.231 MPa*$m^{1/2}$ for henholdsvis Mons kritt med diameter på 50 mm, Mons kritt med diameter på 38 mm, Castlegate sandstein med diameter på 50 mm og Castlegate sandstein med diameter på 38 mm. Mancos skiferen varierte fra 0.370 til 1.287 MPa*$m^{1/2}$.

[1] Fracture toughness har i øyeblikket ikke et tilsvarende ord på norsk, men ordet sprekkstyrke har blitt brukt. Dette er et forslag til en norsk betegnelse på fracture toughness, med bakgrunn i at en norsk standard ikke eksisterer.

Table of Contents

List of Figures

List of Tables

1 Introduction

In petroleum engineering, hydraulic fracturing serves many purposes. The most common is to stimulate low permeability formations, such as tight sands, carbonates and gas or oil shales. Fracturing is also highly relevant for other purposes like water injection and waste storage, and it is the most reliable way of determining in-situ stresses through extended leak off tests.

In hydraulic fracturing modeling, fracture toughness is a highly important parameter that characterizes the fracturing behavior, more specifically a rocks resistance to fracturing. Relating to pure tensile cracks, fracture toughness is defined as the critical stress intensity factor at which a crack starts to grow. Due to its importance, it is highly desirable to experimentally investigate the fracture toughness. An apparatus for measuring fracture toughness has been set up in the Formation Physics Laboratory at SINTEF, and this is the first use of this set-up. Fracture toughness studies found in the literature are however not limited to one testing method alone.

The main purpose of this thesis is therefore to initiate and carry out a fracture toughness testing program using the Chevron Bend method following the standards of ISRM. Three rock types are selected for experimentation, namely Castlegate sandstone, Mancos shale and Mons chalk. The samples are chosen as they are considered analogous to sandstone reservoirs, gas shales and chalk reservoirs found in the North Sea. Chalk and sandstone will be tested for two specimen sizes, while shale is used to investigate potential anisotropy regarding bedding planes. In addition, a literature study will be carried out with the aim of assessing previous experiments, focusing on anisotropy effects, size effects and field scale of fracture toughness, plasticity effects, as well as implementation of fracture toughness in models and how this is used. The literature study will not be limited to the Chevron Bend method alone. The main findings from the experiments will then be presented and discussed. The primary use of the results lies within modeling of fractures as input parameters, most likely used in benchmarking of newly developed models. Additionally, it is believed that results from such experiments can help to achieve a better understanding of fracture mechanics.

2 Theoretical Foundation

2.1 Griffith Theory and the Energy Balance Criterion

Today it is widely accepted and proven that existing cracks in a material leads to changes in the materials inherent properties. An example of this is the fact that the tensile strength of a material decreases due to cracks. This was first realized through the work of Inglis (1913) and later Griffith (1921). Inglis developed a set of equations that could determine the stress magnitudes around an elliptical hole present in a stressed plate**.** This served as the basis for Griffith's work a few years later, when he determined the correlation between fracture stress and crack size, known today as the Griffith energy balance approach.

Using the fact that tensile strength is significantly smaller than what is theoretically predicted, Griffith postulated that typical brittle material contains large quantities of flaws and cracks, too small to even be seen on the submicroscopic level, later commonly known as Griffith cracks. These cracks works as stress concentrators, and hence fracture initiation is the result of stress increase at these cracks.

Griffith investigated the effect of cracks, and through this work, he was able to connect the theory of elasticity to materials containing cracks. Based on his findings, Griffith suggested that failure of brittle materials happens because the cracks inherent in the material extend and that this newly created crack surface absorbs the energy responsible for the crack extension. In order to make a crack grow, two requirements are needed, regarding stress and energy (Fischer-Cripps, 2007). Firstly, the stress at the crack tip needs to be high enough to induce failure of the bonds keeping the solid intact at the crack tip. Secondly, the potential energy released has to be higher than the crack extension resistance. Griffith applied an energy balance to a stressed body and said that the potential energy decreases due to the extension of cracks. At the same time, an increase of surface energy takes place because of the newly created crack surface balancing this. This energy balance was used to determine the strength of brittle solids and hence a correlation between the fracture strength and crack size. Looking at an infinite cracked plate, seen in Figure 2-1 , the total energy for the system can be written as

$$U = U_t + U_c - W + U_s = U_p + U_s \tag{2.1}$$

Here U is the total energy of the infinite cracked plate, U_t is the total initial elastic strain energy of the stressed and uncracked plate and U_c is the elastic strain energy released as a result of the

newly introduced crack length and the relaxation of the material above and below the crack. U_s is the change in the elastic surface energy as a result of the new crack surface being formed, U_p is the change in potential energy and W is work done by any external forces**.** For a more in-depth description at each of the elements in the equation, the reader is referred to chapter 3 of the book "Rock Fracture Mechanics: Principles, Design and Applications" by Whittaker et al. (1992).

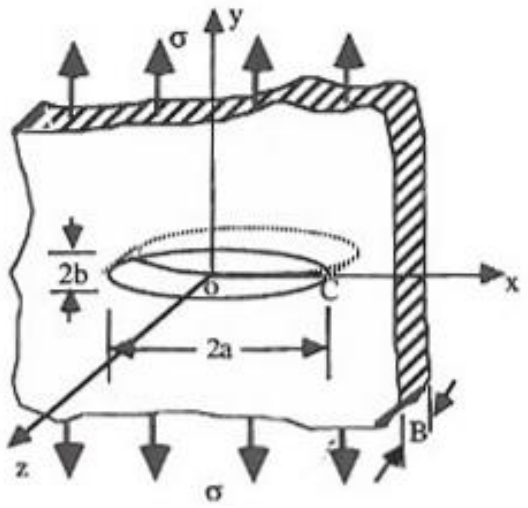

Figure 2-1: An infinite plate containing an elliptical hole. The plate is subject to uniform tension at infinity (Whittaker et al., 1992)

Replacing each of the four elements with their respective mathematical expression, result in the following equation

$$U = \frac{\sigma^2 A}{2E'} \pm \frac{\pi\sigma^2 a^2}{E'} - \frac{\sigma\varepsilon A}{2} + 4a\gamma_s \qquad (2.2)$$

Here A is the infinite area of the thin plate, a is the half crack length, ε is the strain and γ_s is the specific surface energy. σ is the stress, in this case σ_y. E' is the effective Young's modulus, for plane stress $E'=E$ and for plane strain $E'=E/(1-\nu^2)$. For constant displacement, with $W = \frac{\sigma\varepsilon A}{2} = 0$, the behavior of the total potential energy is shown in Figure 2-2. An examination of the equation and the following upper part of the figure reveals that as long as the elastic strain energy released due to crack growth is lower than the surface energy for the same incremental crack growth, the resulting crack extension is stable. If the opposite occurs, the crack propagation is unstable. A more thorough explanation for unstable and stable cracks is given later. From the figure, it is clear that the total energy reaches a peak where this critical condition occurs.

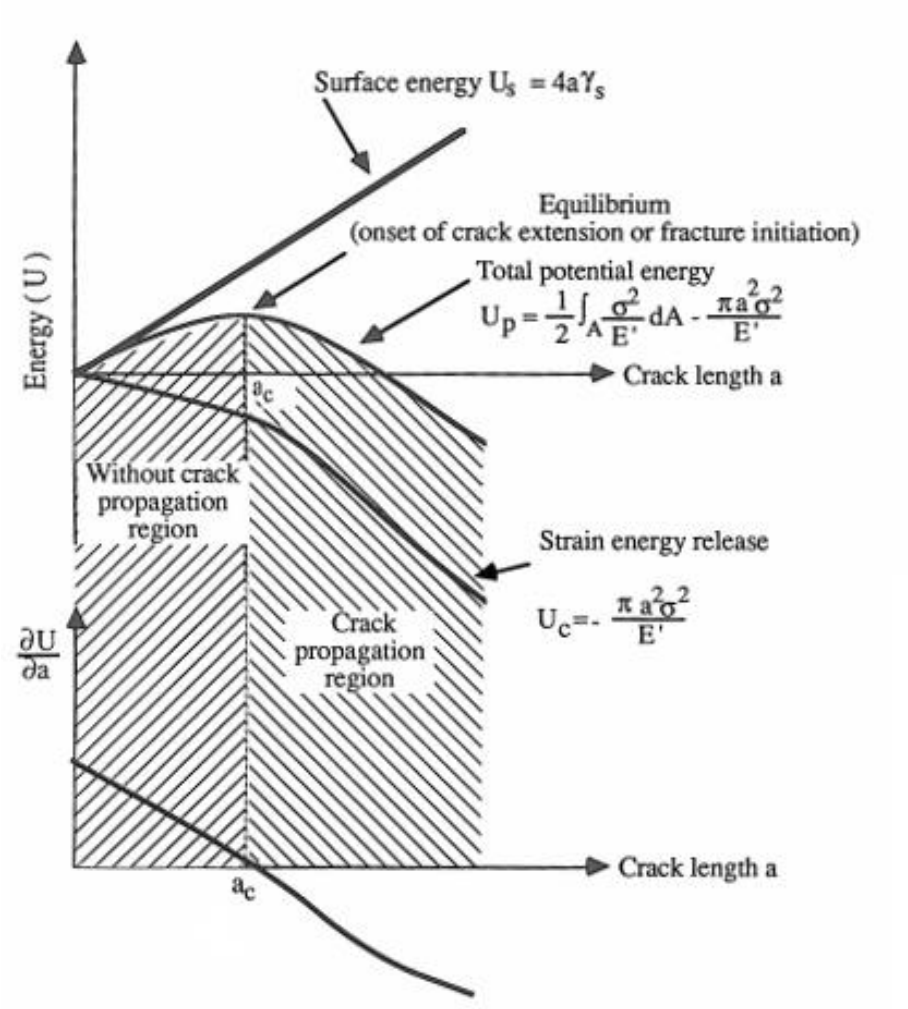

Figure 2-2: Upper half; total energy vs crack length, lower half; differentiation of total energy with respect to the crack length vs crack length. Both shown for a case of constant displacement (Whittaker et al., 1992)

Looking at the lower part of Figure 2-2, this happens when the differentiation of the total energy with respect to crack length satisfy $\partial U / \partial a \leq 0$. By differentiating the equation for the total energy with respect to the crack length a, setting the resulting equation equal to zero and then rearranging, results in the following equation

$$\sigma\sqrt{\pi a} = \sqrt{2E'\gamma_s} \tag{2.3}$$

The terms listed on the right hand side are constants for a given ideally, brittle solid. Based on this, it can be concluded that the fracture initiation occurs when the left hand side of equation 2.3 reaches a constant critical value, called the critical stress intensity factor, also known as the fracture toughness or K_{IC}.

Rearranging the equation further gives the expression for the fracture stress when initiation of a crack occurs.

$$\sigma_f = \sqrt{\frac{2E'\gamma_s}{\pi a}} \tag{2.4}$$

This equation gives the applied fracture stress necessary for crack initiation only, and for the tensile condition, the applied fracture stress is the same as the uniaxial tensile strength, σ_t (Whittaker et al., 1992). For a given ideally brittle solid with either a central crack of length 2a or an edge crack of length a, this fracture stress is a constant. When Griffith reached this conclusion, his derivation was based on balancing the energy for an infinite plate and thereby, the size of the solid was excluded from the derivation. However, several experiments have shown that the size of the sample affects the results.

Rewriting equation 2.3, gives the expression for the elastic energy per unit crack surface, also known as strain energy release rate or G, in honor of Griffith and his work.

$$G = \frac{\partial U_c}{\partial a} = \frac{\pi\sigma^2 a}{E'} \tag{2.5}$$

The G value is another option as a fracture criterion. Once the strain energy release rate, or simply energy release rate, reaches a critical value, failure occurs and the cracks will extend. This will of course happen at the same time as the fracture stress, σ_f , is reached. Another name for the critical energy release rate is fracture toughness, although in this case the fracture toughness is quantified by another parameter. In fact, there are several parameters used in quantifying the fracture toughness. The two most commonly used parameters are the stress intensity factor and the energy release rate, where the stress intensity factor method is the most popular choice, though it does have some limitations that will be addressed later (Chudnovsky et al., 2012). Critical energy release rate is denoted G_{IC} for mode I.

The theory resulting from Griffith's work is considered valid for materials where there is little to no plastic deformation at the crack tip. However, for rocks and other geomaterials, a zone develops near the crack tip where plastic behavior occurs, typically called the fracture process zone (FPZ). The plastic behavior seen here behaves in a non-linear fashion and it has been stated that some of the potential energy goes to creating this area, a fact that was originally not accounted for in Griffith's theory. As a result of this, Griffith's theory was later modified through the work of several researchers, most notably Irwin (1948), where an attempt was made to account for the energy used in the creation of the FPZ. Contemporary to his own work, Irwin, along with Orowan (1949), claimed that the Griffith way, based solely on an elastic analysis,

would provide reasonable estimates for the energy released during extension of cracks, as long as the FPZ was relatively small compared to the crack length and thickness of the specimen.

2.2 Mode of Fracturing

In linear elastic fracture mechanics, the propagating crack for an ideal elastic brittle material is typically described by one of three modes of loading and the resulting mode of fracturing or a combination of these. The three basic modes are simply called mode I, mode II and mode III, each differing in the way the crack behaves, how the two crack faces move relative to each other and the forces behind it. An illustration for these three modes can be seen in Figure 2-3**.**

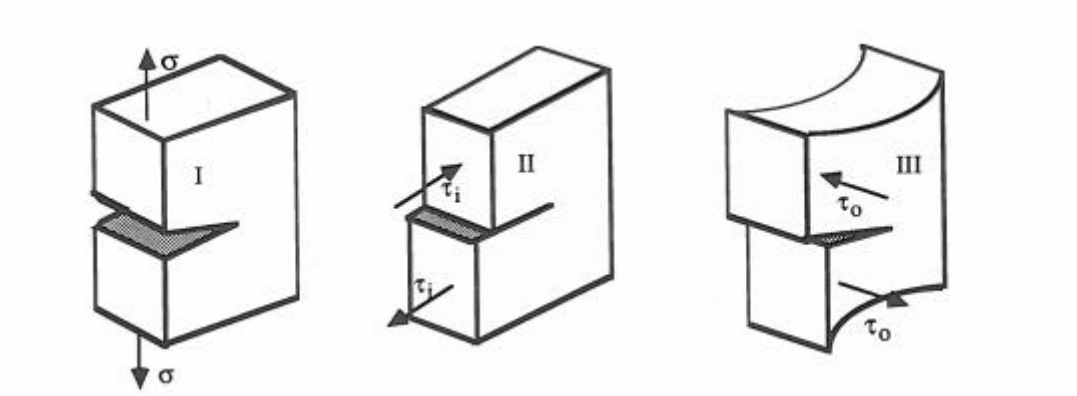

Figure 2-3: Basic modes of loading and the corresponding mode of fracturing, mode I is to the left, mode II is in the middle and mode III is to the right (Whittaker et al., 1992)

For a mode I crack, the two faces will move away from each other, resulting in a crack that opens perpendicular to the movement of the faces. The reason for this is a normal stress that is acting on the crack tip. Another name for mode I is opening mode or tensile mode. This is the most common one and thereby the most important (Whittaker et al., 1992). This is also the simplest and in many situations the dominating mode, and thus a majority of the work done in the past have focused on this mode. This is most evident when regarding the work related to fracture toughness (K_{IC}). It is important to note that even though this mode has achieved most focus, fracture problems in rocks will typically include both mode I and mode II, i.e. a mixed mode between the two.

In a mode II crack, the two faces will slide against each other parallel with the direction of the crack due to an in-plane shear stress acting on the crack tip. This mode is also called sliding mode, due to the movements of the two faces.

The last mode, mode III or tearing mode, happens when an out of plane shear stress acts on the crack tip. This shear stress acts both parallel to the crack front and to the crack plane.

It is also possible to have a combination of any of these three modes, and this can include both two and three of them. It stands to reason that the fracture mode is more complicated when it is a combination of the different modes, where the most complicated is the one that is a combination of all three.

2.3 Linear Elastic Fracture Mechanics

The theoretical foundation provided by Griffith's work eventually resulted in what is today called linear elastic fracture mechanics or LEFM. As mentioned earlier, Irwin continued on the work of Griffith and in 1957, Irwin published a paper where he addressed the stress intensity factor, which provided a theoretical formulation for fracture. The cornerstone of this formulation is the stress intensity factor K. This parameter is a representation of the magnitude of the stress intensity at the crack tip. Additionally, the parameter K relates to the stresses surrounding a crack after the altercation of the stresses due the crack. This means that with a known K value, it is possible to determine the stresses and the displacements surrounding the crack. This however also depends on knowing the mode of loading, as the stress intensity factor is related to this. Said in a different manner, it means that for mode I, mode II and mode III, there is a corresponding K_I, K_{II} and K_{III}.

According to Irwin (1957), it was possible to describe the stress field $\sigma(r,\Theta)$ surrounding an infinitely sharp crack tip by the following equation

$$\sigma_{yy} = \frac{K_I}{\sqrt{2\pi r}} \cos\frac{\theta}{2}\left(1 - \sin\frac{\theta}{2}\sin\frac{3\theta}{2}\right) \tag{2.6}$$

In this equation, the terms with Θ describes the distribution of the stress and K_1 is the stress intensity factor, providing the grade of stress concentration or stress intensity at a crack tip under certain loading, in this case for mode I. It is defined with the following equation

$$K_1 = \sigma Y\sqrt{\pi a} \tag{2.7}$$

Here the Y is a geometry factor, with the right hand side being the same as equation 2.3 with Y=1 for double ended crack in an infinite plate. The subscript I refers to the loading condition, in this case tensile loading. The equation is given for the coordinate system in Figure 2-4. According to Fischer-Cripps (2007), there is an important reason why the definition is like this. Given a particular crack system, the values of π and Y will remain constant and thus the value of K_I will only depend on the externally applied pressure, σ_a, and the square root of the crack half length a.

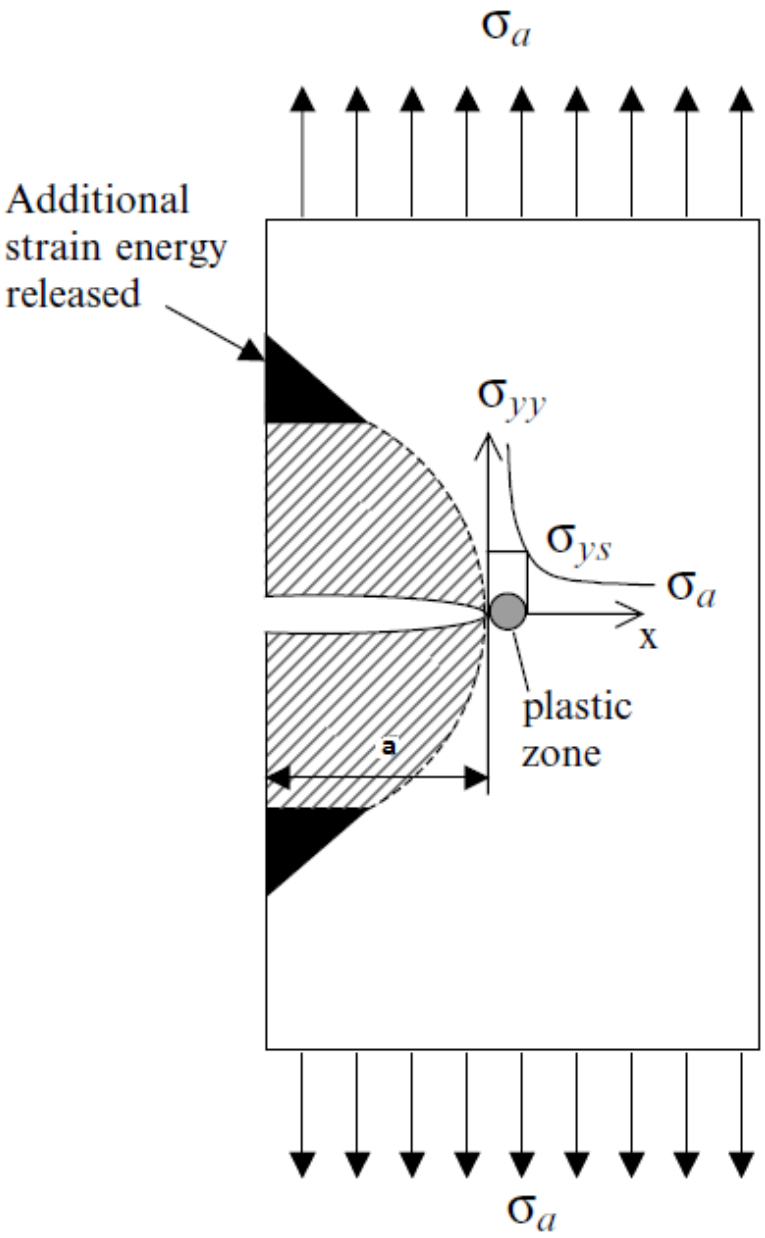

Figure 2-4: Semi-infinite plate under uniformly applied stress with a single ended surface of crack half length a. The additional strain energy release is shown as the dark areas. This happens because of the presence of a surface, as opposed to an infinite solid containing a fully embedded crack (Fischer-Cripps, 2007)

In a doctoral thesis by Backers (2004), a more generalized case for the stress formulations are given, relating to all modes.

$$\sigma_{ij} = \frac{K_k}{\sqrt{2\pi r}} f_{ij}(\theta); i, j = x, y, z; k = I, II, III \tag{2.8}$$

Here the σ_{ij} is the stress tensor in a Cartesian coordinate system, f_{ij} is a geometric stress factor that only relies on the angle Θ and K_k is the stress intensity factor governed by the applied loading conditions as well as the geometry. The subscript k refers to the corresponding mode.

Notations for the system are given in Figure 2-5. The focus of this thesis is on mode I. It should be pointed out that this concept relates to a fracture propagating in its own plane as a result of the mode of loading. However, any deviation from this plane leads to mixed mode conditions.

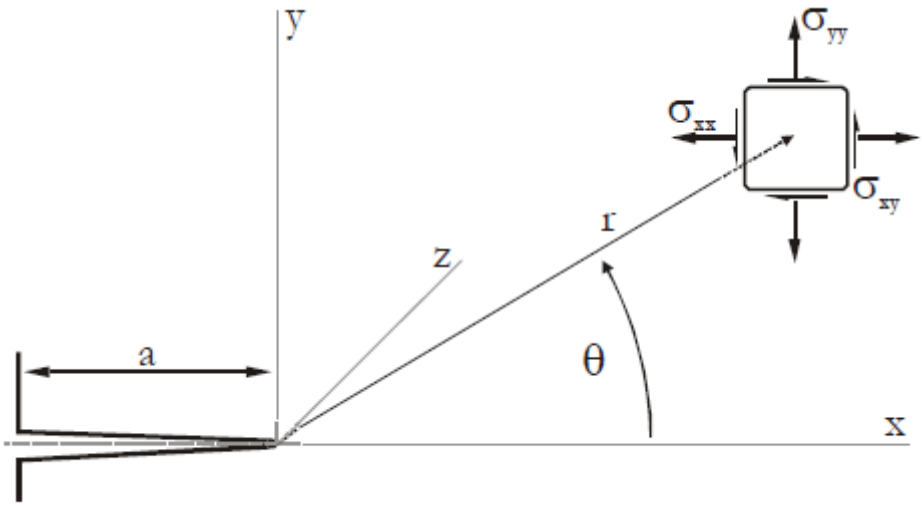

Figure 2-5: Notations for Backers formulation for the stress tensor in a Cartesian coordinate system (Backers, 2004)

From equation 2.6 and 2.8 it is seen that a stress singularity arises at the crack tip where the stress is infinite. Such circumstances do not happen in reality as they are avoided through plastic deformation at the crack tip and in the small region surrounding the crack tip. This area is the same as the FPZ mentioned earlier. Outside of this area, the material behaves mostly in accordance with Hooke's law when external stress is applied, and the equations presented above is applicable.

This theory regarding a plastic zone surrounding the crack tip applies well for metals, but for rocks and other brittle materials there is some ambiguity based on physical evidence (Fischer-Cripps, 2007). In brittle materials, the singularity predicted by equations 2.6 and 2.8 might be avoided if the materials experience deformation in a non-linear, but still elastic fashion. Fischer-Cripps (2007) discusses that for brittle solids, any strain energy absorbed does so by non-linear stretching of the atomic bonds and not through any plastic events, normally seen in ductile metals.

This formulation has increased in popularity over the years, which can to a large degree be attributed to how the critical stress intensity factor is conveniently obtained from testing in the lab. Because of this, it has almost replaced the approach deduced by Griffith. Another

important aspect of the stress intensity factor is that Irwin (1957) was able to show that these two methods are the same, as long as the material in question behaves linear elastically.

Fischer-Cripps (2007) describes the stress intensity factor K_I as a scale factor that describes the stress magnitude at a specific location close to the crack tip. Imagine a specimen with a crack. If the applied stress is increased, the stress intensity factor will increase and eventually the crack will extend once the energy balance criterion is satisfied. At the onset of crack extension, the stress intensity factor will have reached its critical value K_{IC}. Tensile fracturing is dominant in rocks and rock-like material. The reason for this is that K_{IIC} is normally larger than K_{IC} (Backers, 2004). It is worth noticing that K_{IC} is not only an indication of fracture, it also depends on the stability of the crack. Catastrophic failure takes place under unstable conditions. The crack system dictates whether there are stable or unstable conditions. Relating the stress intensity factor to unstable or stable conditions, cracks are stable if $dK_I/da<0$ and hence, unstable if $dK_I/da>0$. Under stable conditions, the case where stress intensity factor equals the critical stress intensity factor indicates that the crack is on the brink of crack extension, only requiring an increase in the applied stress to extend the crack. For unstable conditions however, crack extension will take place immediately and rapidly, leading to failure of the specimen. The critical stress intensity factor is normally considered a material property and its unit is $MPa*m^{1/2}$.

The critical stress intensity factor, K_{IC}, signify the threshold for when the stress intensity factor is large enough to induce crack initiation. This value is often referred to as the fracture toughness in literature. This fracture criterion postulates that fracturing occurs once the stress intensity factor is the same as the fracture toughness. In other words, it describes a rocks resistance to fracturing. According to Sih (1976) the fracture toughness is a constant, independent of specimen dimensions, loading rate, etc. based on how it is conceptually defined, but this is not the case. Experiments have shown that the fracture toughness can vary greatly under different conditions. This will be discussed more in detail later**.** Regarding modeling of fractures and hydraulic fracturing, the stress intensity criterion has seen a widespread usage to predict when fracturing occurs and how to model fracture behavior.

It is possible to mathematically relate the strain energy release rate to the stress intensity factor. Combining equation 2.5 and 2.7, for a double ended crack within an infinite solid where Y=1, results in the following empirical correlation

$$G_I = \frac{K_I^2}{E'} \tag{2.9}$$

By replacing the stress intensity factor with the critical stress intensity factor, the critical strain rate release factor is achieved. The presence of a relationship between these values is important, as it dictates that the critical stress intensity factor is required for the crack extension, as well as being an adequate criterion. The reason for this is that the parameter accounts for two of the criteria presented, the stress criterion and the energy balance criterion (Fischer-Cripps, 2007). Through this relationship it can be said that the value of the critical stress intensity factor both expresses the crack tip stresses and also the strain energy release rate when extension of cracks occur. It should be emphasized that K, and thereby G needs to be corrected when applied to finite body dimensions, but the relationship between these two parameters are still valid through equation 2.9. Critical values also hold true for this equation.

2.4 Terminological Frames

According to Backers (2004) there are two terminological frames that explains the fracture process, each defined by a function. One is defined by the stress intensity factors, while the other relies on the fracture velocity. The former differentiate between a stable and unstable state. Lawn (1993) states that certain criterions need to be in place for a crack to be deemed unstable. Having the stress intensity factor, K_I, equaling the critical stress intensity factor, K_{IC} is not alone sufficient to have an unstable crack, as another requirement is $dK_I/da>0$. The a refers to the crack length. Unstable and stable cracks are differentiated by the fact that stable cracks propagate at slow speeds and can be stopped, meaning that a stress increase is required for it to propagate further. Whereas an unstable crack has an excess of energy that accelerates the propagation, and the crack can potentially reach a terminal velocity controlled by the elastic waves and their speed (Backers, 2004). Unstable cracks are therefore also referred to as dynamic. The second frame, defined by the fracture velocity, differentiate between static and dynamic cracks. Figure 2-6 highlights the different terminological frames and the onset of the different types of fracture growth and is the result of work by Atkinson (1984) – stable vs unstable, and Zhang et al. (1999) – static vs dynamic. Dynamic rock fracturing typically results in crack branching, a phenomenon that increases with higher loading rates. This partially explains why dynamic fracture toughness is higher than static fracture toughness as some energy is used during branching of cracks. The result of this is that rock has a higher resistance to impact loads as opposed to static loads. Zhang (1999) found that the static fracture toughness,

K_{IC} stays nearly constant. For very high loading rates, the test specimens ended up breaking into several pieces as opposed to two halves typically seen in normal fracture toughness experiments.

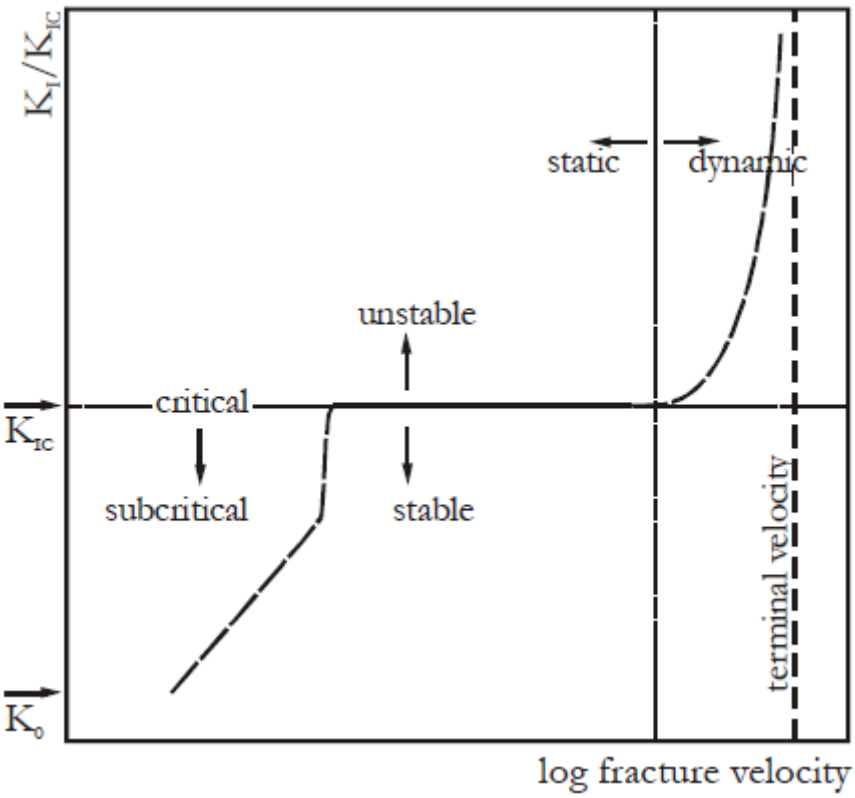

Figure 2-6: Terminological frames for mode I (Backers, 2003)

Instability of cracks happens either by achieving the critical crack length or through impact loading. When the stress intensity factor reaches its critical value, it marks the transition from stable to unstable growth. However, it is possible to have crack growth at stress intensity values below the critical value, called subcritical growth (Atkinson, 1984). Such growth is controlled by several different mechanisms. These mechanisms are stress corrosion, diffusion, dissolution, ion exchange and microplasticity. Each of these mechanisms was investigated by Atkinson (1984), who concluded that the stress corrosion is the main driver for subcritical crack growth below 300^{o} C. When the crack velocity is around 10^{-3} m/s and higher, the crack shifts from being dominated by stress corrosion and towards critical cracking according to Atkinson. Ouchterlony (1988) reported that the effects of stress corrosion is small at crack velocities higher than this. However, in a doctoral thesis by Backers (2004) this topic was briefly discussed. Having performed fracture toughness tests on Flechtingen sandstone, three loading rates were used below this value. Had stress corrosion cracking been the dominating mechanism for these rates, the peak load would have been lowered as the loading rate decreased due to

subcritical growth resulting in a reduction of the rock ligament between load point and crack tip. However, this was not seen in the experiment, with even the displacement at peak load staying the same. The K_o is the lower limit for crack growth. Stress intensities below this limit means no growth occurs. Atkinson called this value the stress corrosion crack growth limit.

2.5 Determination of Stress Intensity Factors

The Griffith theory and linear elastic fracture mechanics are presented above, focusing on the stress intensity factor and its relevance to these theories. However, methods for determining this parameter have been left out until now. According to Whittaker et al. (1992) there are four categories of methods for determining K. These four categories are analytical methods, numerical methods, experimental methods and approximate or estimating methods. These are all based on calculating the stress intensity factor, however the experimental method is the closest to getting an actual measurement, as will be explained shortly below. For each of these categories, there exist multiple different sub-methods. The focus will be on their accuracy and what separates them. Some of the methods are limited to certain modes of loading, while others work across different loading modes.

Analytical methods can use a multitude of different complicated functions, including stress concentration factors and complex stress functions to name a few, to determine the value of K. These methods provide solutions that are either exact or close to the actual value, thereby being a highly accurate method.

The numerical methods can be divided into several sub-groups, depending on what mathematical foundation they utilizes. Examples here include finite element method (FEM), boundary element method (BEM) and modified discrete element method (MDEM). Such methods are often chosen because of the complicated systems and geometries that arises due to cracks, and different loading conditions makes it impossible to achieve closed form solutions. The accuracy of such methods will be dependent on the grid systems used; a finer grid system will be more expensive, require more data and a larger storage capacity, but will ultimately result in better solutions. The boundary collocation method (BCM) have errors of up to 2% while the FEM may have an error of up to 6%. A downside with these methods is that they are often oversimplified and hence they introduce large uncertainties to their solutions.

Experimental methods utilize different approaches in which the stress intensity factor is determined from loading a specific crack sample in a laboratory and then determining the K value based on the measurements collected. It is worth noticing however, that it is not possible

to directly measure the stress intensity factor during an experiment, instead its value is found based on mathematical relationship with parameters it is possible to measure, including stresses and displacements. Methods here include the photoelastic technique and the compliance method. Whittaker et al. (1992) argues that these methods are less accurate and reliable than the other methods, thereby it is important to pay great care to the measurements of such methods. The method used in this thesis falls within this category, experimental methods, and it is a part of a group of methods suggested by the International Society for Rock Mechanics (ISRM) for testing and determination of fracture toughness.

If the previously mentioned categories does not provide an opportunity to determine the fracture toughness directly, an approximate method might be more useful, for instance the superposition method, not detailed here. For more details about this method or any of the other, the reader is referred to Whittaker et al. (1992).

2.5.1 ISRM Methods for Determination of Fracture Toughness

Until the middle of the 1980s, a great deal of different tests were invented and utilized inside rock mechanics, however the results from these tests were not comparable with each other, as they took place under highly different loads and specimen configurations (Ouchterlony, 1988). This indicates that the fracture toughness values does not represent a material property. To combat this, ISRM have so far acknowledged four Suggested Methods for mode I fracture toughness. In 1988, ISRM presented the two methods called the Short Rod (SR) method and the Chevron Bend (CB) method, and in 1995, a third test was presented, called the Cracked Chevron Notched Brazilian Disc (CCNBD) method (Ouchterlony, 1988, Fowell, 1995). In 2013, a fourth test was introduced as a Suggested Method, the Semi-Circular Bend (SCB) method (Kuruppu et al., 2014). It is important to emphasize that these methods existed before ISRM presented them, but that these papers instead had collected all information relevant for said tests and developed a best practice for each such that comparisons of different rock types became possible. Included in these methods are the precautions one need to take, the relative dimensions of the samples used, what information should be collected during the tests, how to calculate and determine any relevant information and lastly what should generally be presented when fracture toughness results are published. The main reason for presenting the Suggested Methods and for being so thorough was to introduce a few methods that would produce precise and accurate results consistently. Figure 2-7 shows the notches for the different Suggested Methods.

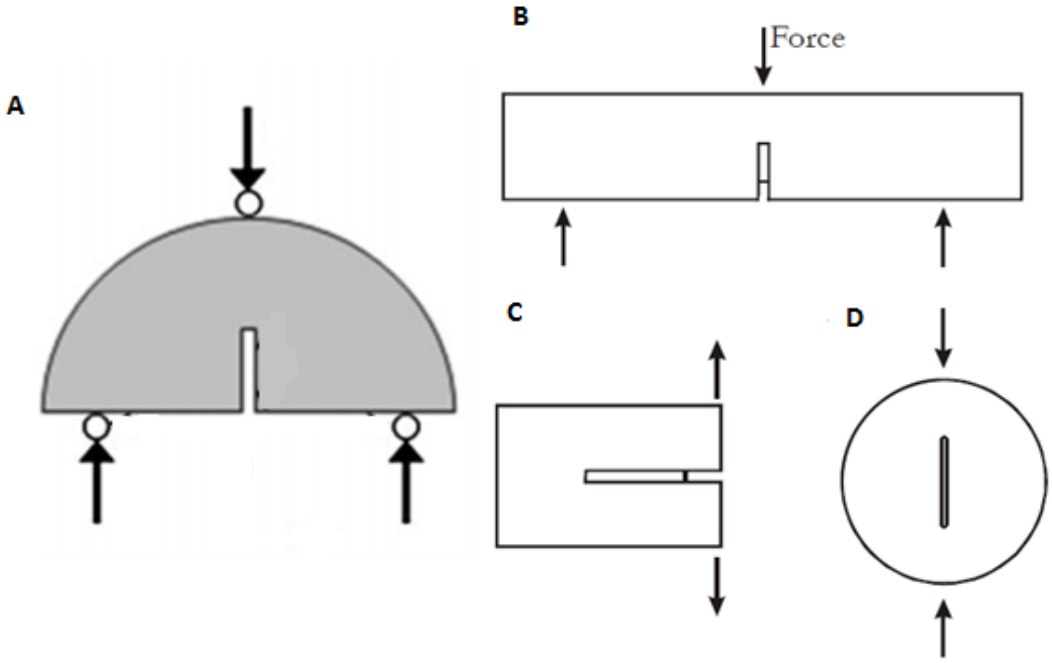

Figure 2-7: Configuration of the different Suggested Methods. Arrows indicate the locations of the applied force. A: Semi-Circular Bend, B: Chevron Bend, C: Short Rod, and D: Cracked Chevron Notched Brazilian Disc (Modified from Fowell, 1995 and Kuruppu et al., 2014).

In the Suggested Methods, there are three applications specifically mentioned for the use of fracture toughness. The first one is as a classification parameter for rock material, the second is as an index of the fragmentation process and the third is as a material property used in modeling work. Further, depending on the method used, determination of fracture toughness values also provides a corrected value, accounting for non-linear behavior (Ouchterlony, 1988). Before continuing with a brief introduction into these four methods, it is worth mentioning that there also exist a Suggested Method for mode II fracture toughness. However, this method is not presented here, as the focus of this thesis is on Mode I fracture toughness. The reader is referred to the doctoral thesis of Backers (2004) and the ISRM Suggested Methods for Rock Characterization, Testing and Monitoring 2007-2014 (Ulusay, 2015). Whittaker et al. (1992) comments on several of the advantages of the first two ISRM methods, the CB and the SR. Among these is the use of core samples, easily obtainable from rock characterization procedures and geological prospecting, the use of the chevron notches resulting in a stable crack initiation and propagation and the fact that level I testing gives a good estimate of the fracture toughness while level II testing gives a more accurate material property. The same advantages apply to the other two methods except that they do not have level I and level II testing.

2.5.1.1 Chevron Bend Method and the Short Rod Method

Both the CB and the SR method were presented as Suggested Methods in 1988, as previously mentioned. CB uses cores with prefabricated V-shaped notches in a three point bending test to determine the fracture toughness. During the test, a crack is induced at the tip of the prefabricated notch that propagates in the plane of the notch. The sample is meant to undergo stable crack propagation until it reaches a peak load. The specimen is split into two halves at the end of the experiment. This is the method utilized in this thesis and hence more thorough details will be given later.

The SR method uses the two halves left from the CB experiment. A V-shaped notch is machined into the core in the direction of the rod axis**.** Similarly, to the CB, the applied external force splits the rod in half by inducing a crack at the notch tip. The crack will propagate in a stable manner until it reaches a peak load, at which the sample will fail in an unstable manner (Whittaker et al., 1992). A side effect of being able to use the remaining halves of the CB is that it provides an excellent opportunity to investigate the anisotropy of K_{IC} as the fracture toughness is determined both parallel and perpendicular to the core axis (Backers, 2004). However, both methods are fairly strict when it comes to both preparation of the samples and the apparatus used.

2.5.1.2 Cracked Chevron Notched Brazilian Disc

The introduction of the CCNBD method into the Suggested Methods was motivated by the fact that it provided an opportunity to investigate the complete fracture toughness anisotropy of rocks as the cracks of the respective methods can be machined in such a way that they all lie perpendicular to one another. Fewer restrictions are given to the apparatus and the samples are not subjected to the strict regime as the CB and SR are. Additionally, results from this method provide a smaller scatter and the procedure is simpler (Fowell, 1995). The notch of the core specimen is machined into the sample as a V-notch along the core diameter. During the testing, a crack is induced at the notch tip and the crack continues to propagate radially outwards from the notch, in a stable manner. During the determination of the fracture toughness for the CB and the SR methods, a corrected fracture toughness is also determined aimed at providing a result that accounts for non-linearity behavior. Such a correctional factor is not provided in the Complete ISRM Suggested Methods for Rock Characterization, Testing and Monitoring: 1974-2006 (Ulusay & Hudson, 2007), nor in the original paper (Fowell, 1995), but it was expected to be added at a later time.

2.5.1.3 Semi-Circular Bend

The SCB method is the fourth method that allows for a determination of the fracture toughness. The fracture toughness is measured using a rather slow loading rate, under which dynamic effects are so small they are negligible. This method can replace one of the other three methods to conduct a complete fracture toughness anisotropy analysis (Kuruppa et al., 2014). Its main advantages is that the method is quite simple, only small and easy machining work is required of the samples prior to testing and low material requirements as well as the fact that the experiment can be carried out using three point compressive loading by the use of a simple loading frame. Additionally, it is able to use the remaining halves after either the CB method or the SR method.

3 Previous Work

In an effort to understand more about the work previously done regarding fracture toughness with focus on mode I, a literature study was conducted. This survey centered around four topics in particular; lab to field scale, effect of plasticity, use of fracture toughness in models and tensile strength vs fracture toughness. These next sections are designed to summarize what was learned about each of these fields through the survey. Note that they only cover a portion of the literature identified, and there are still many remarks that need further and more thorough investigation.

3.1 Lab to Field Scale

One issue with the fracture toughness determined from laboratory experiments is its relevance to use in models, and whether or not it is a proper representation of the in-situ value (Thiercelin, 1989). The experiments where the in-situ fracture toughness predication has been the topic are scarce and there exist only a limited amount of information. In one of the few papers that address the in-situ fracture toughness, hydraulic fracturing of impermeable rock indicated that the values were one to two magnitudes higher than the values achieved in laboratory experiments (Shlyapobersky, 1985). The values obtained based on these field tests are seen in Table 3-1. The field test showed that an increase of K_{IC} always resulted in an increase of the fracture size. However, these values suffer from the fact that their determination are greatly associated with uncertainty, as the method used to calculate the fracture toughness in this particular case relied on knowing the shape and the in-situ stress of the formation. Such information proved difficult to obtain and thus the values are highly ambiguous (Thiercelin, 1989, Thiercelin et al., 1989). At the time, Thiercelin hypothesized that the discrepancies are attributed to the use of small samples in the laboratory compared to actual field sizes. Even though he was able to simulate downhole conditions, it was theorized that the apparent fracture toughness determined from such small sample experiments would fail to capture, and therefore underestimate, the actual value of the apparent fracture toughness. Macdonald et al. (1991) also reported stress intensity factor values that were much higher than typical laboratory results.

Injected Volume [m^3]	K_{IC} [$MPa*m^{1/2}$]
22	9.7
57	15.6
114	21.5

Table 3-1: Calculations of in-situ fracture toughness values (Shlyapobersky, 1985)

Over the years, several explanations have been presented that explains the discrepancies between in-situ fracture toughness and laboratory fracture toughness. The reason for the high values might originate from several effects, including scale effects, confining stress, micro-cracking and plasticity (Papanastasiou, 1999, Khanna & Kotousov, 2016). Plasticity effects have been shown to affect the fracture toughness value. This will be discussed more in detail later. Zhao & Roegiers (1993), Thiercelin (1989) and Al-Shayea et al. (2000) all presented evidence based on modeling and laboratory experiments that the confining in-situ stress tends to increase the fracture toughness. According to Thiercelin, this increase is due to different behavior of the process zone ahead of the crack tip and the size of the increase is dependent on the material of the specimen. Al-Shayea et al. found that in some cases the fracture toughness for mode I increases by a factor of 3.7 using the Straight Notched Brazilian Disk (SNBD) method. Other authors have reported similar results. They argued that the increase in fracture toughness could be attributed to the energy increase required to initiate cracks in ductile materials. Under a triaxial loading with confining pressure, rock materials are believed to behave more ductile compared to little to no confining pressure.

Scale effect for material strength is a fact that has been known for a long time and it has been subject to a lot of research (Chudnovsky et al., 2012). Studies on the scale effect in fracture toughness on the other hand is somewhat limited. This parameter is dependent on several factors, including size and shape of the test specimen and aspects related to the microstructure. Chudnovsky et al. (2012) conducted an analysis of size effect of fracture toughness based upon the results from a thorough fracture toughness experiment involving over 250 concrete samples with a large range of specimen sizes and different aggregate sizes (Issa et al., 2000). The calculated fracture toughness values, K_{IC}, showed a scale effect where the critical stress intensity factor increased when aggregate size or specimen size increased. However, the focus of the following analysis was the fracture toughness parameter G_{IC}, the energy release rate. This was done because the stress intensity factor method has several limitations, including that it is a theoretical parameter not possible to measure, and in most tests, there were evidence for mixed

mode fracturing. The behavior of the G_{IC} was the same as the critical stress intensity factor. During their analysis, they were able to find a simple scaling rule in which they could calculate the G_{IC} for larger specimens for the same aggregate size. However, this rule does not have any data available to limit its domain application. Even though the focus was on the energy release rate, the results strongly indicates that there is a relationship between the critical stress intensity factor and the specimen size.

In Shlyapobersky et al. (1998), an explanation for the results by Issa et al. (2000) is provided. The reasons for the trends seen regarding aggregate size and specimen size are twofold. Aggregates are much stronger than the surrounding paste and thus it requires less energy for the crack to travel around the aggregate than through it. This results in a more tortuous path, where larger aggregates leads to an even more tortuous path resulting in a larger bridging effect or interlocking of fracture surfaces. The link between specimen size and fracture toughness and the increase of these is thought to be the ratio between specimen size and process zone size where it is believed that larger ratios lead to smaller resistance to fracturing. For small samples, this ratio is rather high resulting in a weaker stone. When the sample becomes larger, this ratio decreases and the sample is stronger.

A series of SR experiments on marble and sandstone carried out by Scavia et al. (1995), yielded similar results as Chudnovsky, with proportionality between fracture toughness and the specimen size. The size effect law, which initially was proposed by Bazant (1984) to explain the decrease in tensile strength as the specimen size gets larger, was utilized. Based on energy related considerations, they were able to find a good match between the experimental data and the scale law for level I testing of SR specimens. The meaning of level I testing will be explained later. The scale effect law is given as

$$K_{IC} = Q\left(1+\frac{B}{D}\right)^{-0.5} \tag{3.1}$$

D is the specimen diameter in mm, while Q and B are constants found experimentally. According to the law, fracture toughness will reach a constant value for sufficiently large diameters, as seen in Figure 3-1. For small diameters, the fracture toughness should approach zero. However, the diameter for when the fracture toughness reaches a constant value was far outside of the diameter range used in the experiment.

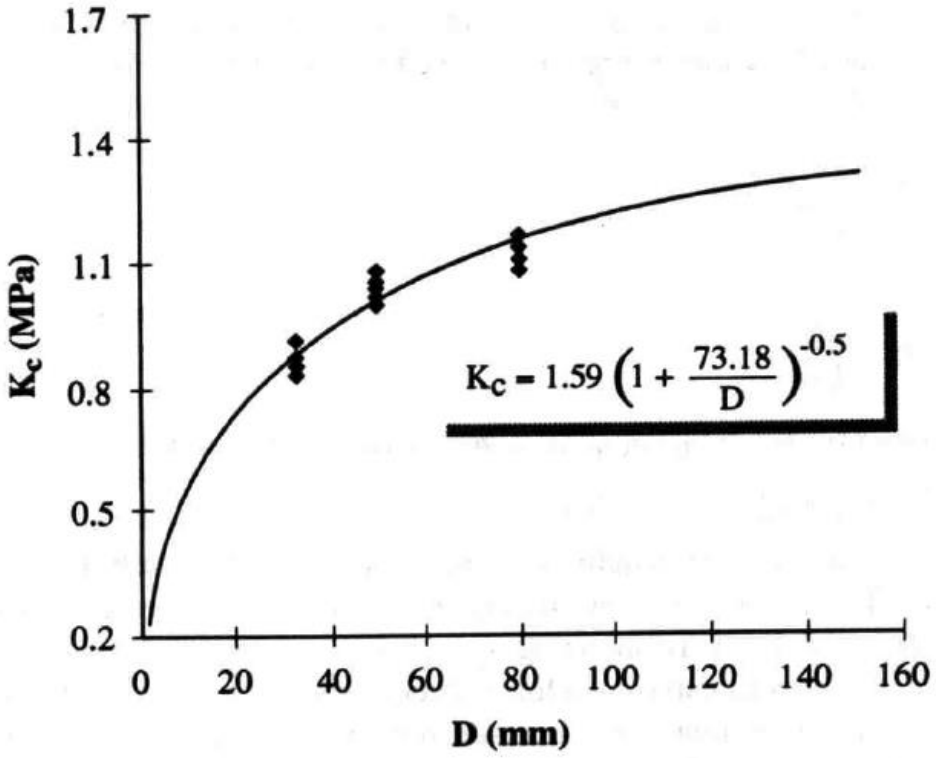

*Figure 3-1: Mode I fracture toughness vs diameter based on the size effect law for a sandstone under level I testing of short rod specimens. Note that there is an error in the unit of the fracture toughness, it ought to be MPa*m$^{1/2}$ (Scavia et al., 1995)*

Over the years, several methods have been proposed to calculate the in-situ fracture toughness, primarily based on pressure data (e.g. Shlyapobersky, 1985, Chavez et al., 2015). However, it appears that most of these methods have either failed to achieve a more widespread use or that they are currently still in development.

3.2 Plasticity effects

A topic of many scientific papers have been focused on understanding the effect of plasticity during rock fracturing as they are often the source of the mismatches seen between fracture models and reality. Griffith theory assumes that no energy is absorbed at the fracture tip and that energy is either used for elastic deformation or rupturing of the material. In reality, some degree of plastic deformation is seen in all materials pre-failure but it is typically assumed that this is insignificant in hydraulic fracturing (Martin, 2000). This assumption held true for the type of fracturing typically done through the 1990s but since then, more and more focus have been on soft, ductile formations, including shales, evaporates and soft carbonates, where such assumptions are no longer valid. Martin (2000) states that formations with low yield stress and high fracture toughness are prone to exhibit large degrees of plasticity.

Papanastasiou (1999) driven by the inconsistencies between net pressures from the field and simulations, concluded that the effective fracture toughness in the field can be more than an order of magnitude higher due to plastic yielding that occurs close to the tip during fracturing, thereby providing an effective shield that increases the effective fracture toughness. Another name for the effective fracture toughness is the apparent fracture toughness (Papanastasiou & Atkinson, 2015). To accomplish this, a model was developed using finite element analysis resulting in a fully deterministic elasto-plastic model. This model was used to find the effective fracture toughness value, which was then implanted into a purely elastic model. This allowed for a comparison between the two methods regarding fracture width and propagation pressure. Figure 3-2 shows the width profiles for one of the cases tested. A better match is achieved when using the effective fracture toughness. The size of the plastic zones that developed in the elasto-plastic model was directly linked to the effective fracture toughness value, where a larger plastic zone resulted in a larger effective fracture toughness value. Further, when using this value in the purely elastic model, a good match was achieved between the two models. The size of the plastic zone and thus the value of the effective fracture toughness were found to increase with larger differences in the in-situ stress magnitude. Building upon the work done by Papanastasiou (1999), van Dam et al. (2002) concluded from numerical work that the LEFM method does not satisfyingly describe the rock behavior exhibited at the crack tip.

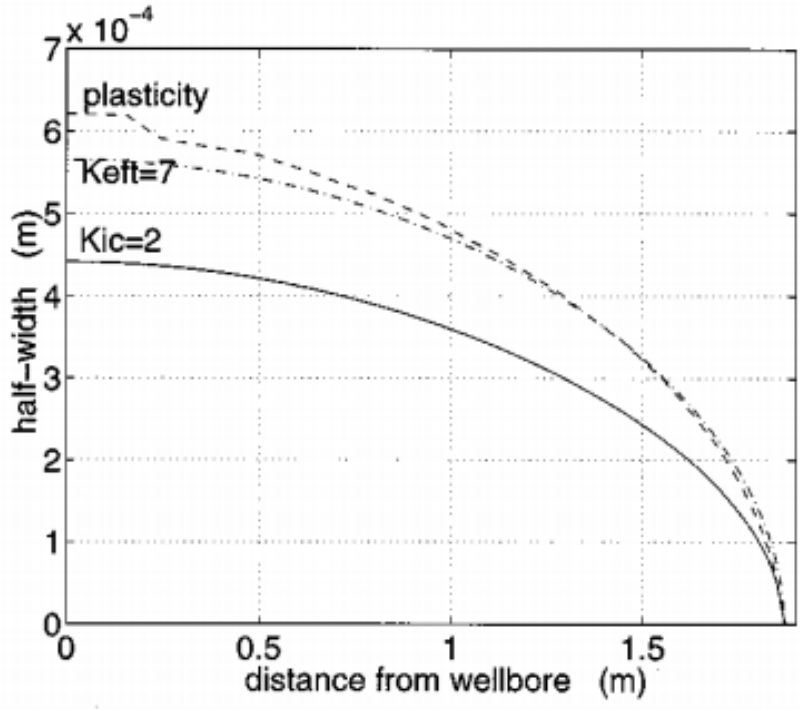

Figure 3-2: Width profiles for the different methods tested (Papanastasiou, 1999)

Wang et al. (2014) discussed the use of the LEFM method, typically used in hard rock formations where it gives reasonable results, for soft and unconsolidated formations and its inadequate performance relating to the accuracy it achieves. The reason that the LEFM method falls short is that it is not possible to ignore the fracture process zone ahead of the tip, elasto-plastic behavior and the strong coupling that exist between flow and stress. The work done by Papanastasiou (1999) is a possible solution to this, however Wang et al. (2014) points out that the work presented, as well as later work, ignored the pressure diffusion and the porous behavior that occurs during deformation of rock. Because of this, Wang et al. (2014) developed models for poroelastic and poroplastic formations, using the cohesive zone method. Additionally, the results for plastic deformation were compared with the effective fracture toughness method. Comparing the poroelastic solution with the poroplastic solution, the latter gave higher net pressures and wider fractures. This is the same as seen in the work of Papanastasiou (1999), when comparing the plastic model with an elastic model. Wang et al. (2014) also reached a good agreement between net pressure and the maximum fracture width between effective fracture toughness method and the poroplastic method. When looking at the fracture width profiles, Figure 3-3, the effective fracture toughness method underestimate the fracture width and overestimate the fracture length for the same net pressure, as this method only account for the plastic deformation that occurs close to the fracture tip.

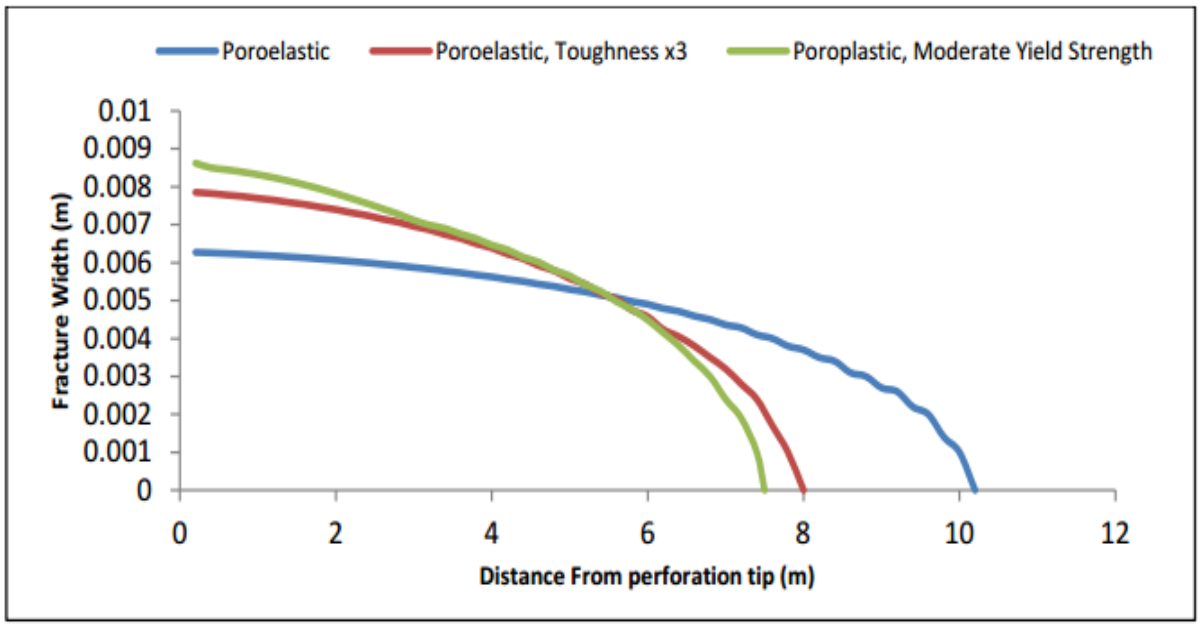

Figure 3-3: Fracture width profiles after a 2 minute injection period (Wang et al., 2014)

It was further found that formations with lower cohesion strength i.e. more plastic formations, have larger areas affected by the plastic deformation, which in turn results in shorter fractures. The same formations also require higher propagation pressure with the result being wider fractures. Lastly, the contribution of poroelastic backstress as well as the plasticity of the formation increases the net pressure. However, their impact upon the fracture width is different. The latter will typically reduce the width while the former usually increases it.

3.3 Anisotropy Effects

The effect of anisotropy on geo-mechanical properties is a topic that has undergone extensive studies over the years, including the effects it has on fracture toughness, especially in the last few years. The investigation of anisotropy regarding fracture toughness is often either solely focused on examining the effect of bedding planes and how their relative angle towards the propagating crack affects the value of the fracture toughness, or on the grain size distribution within rocks. Most of the work seems to primarily focus on two methods, namely the SCB method and the CCNBD method.

An experiment recently conducted by Ghamgosar et al. (2015) utilized the CCNBD method on Brisbane sandstone with clear laminations. For the experiment, four inclination angles were chosen – 0°, 30°, 45° and 90°, where five samples for each angle were prepared. The samples had an average diameter of 51.5 mm. Inclination angle is given as the angle between bedding and the embedded crack, i.e. a bedding parallel with the embedded crack means an inclination of 0°. The value of the fracture toughness increased from 0° before reaching its maximum value when the inclination angle was 45° before decreasing again and reaching its minimum value when the inclination angle was 90°. The results are shown in Figure 3-4. An investigation of the results showed that a pure tensile fracture was not achieved when the inclination angle surpassed 0°, indicating mixed mode fractures. Different crack behavior was also encountered. For 0° inclination, the crack initiation occurred at the embedded crack tip, while for larger inclination angles the crack was initiated closer to the center of the samples, see Figure 2-7, part D. The appearance of mixed mode fractures was the result of shear displacement between the layers when the propagating fracture tried to align itself with the anisotropy of the sandstone. Additionally it was found that as the inclination angle increased, the behavior of the fractures moved from brittle towards ductile. This was thought to be the result of the increase in micro-fractures that accompanies mixed mode fracturing.

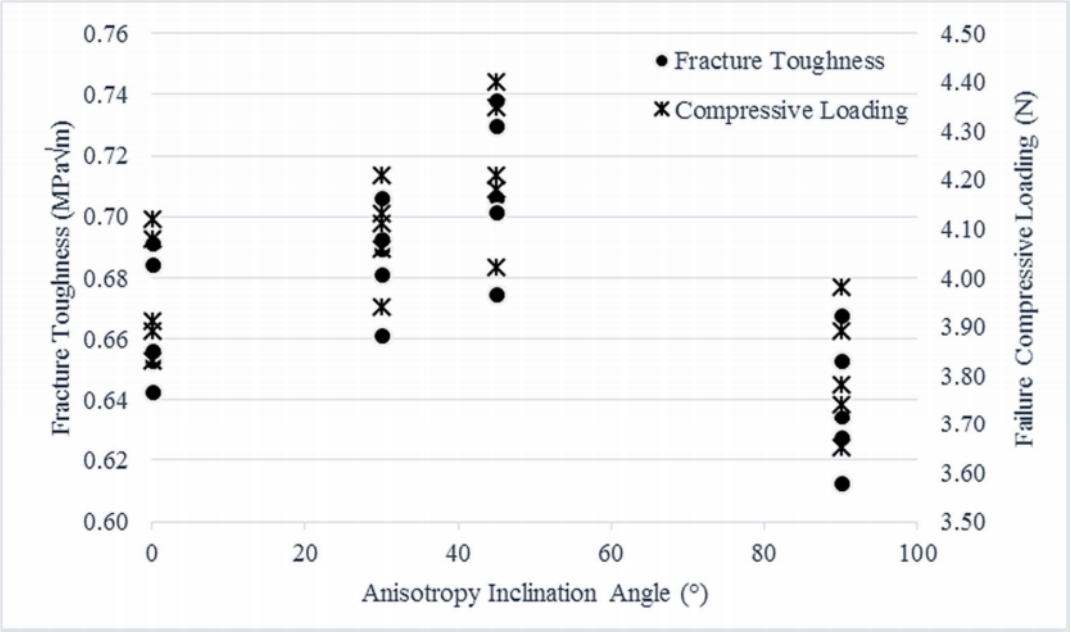

Figure 3-4: Fracture toughness and failure (maximum) loads for Brisbane laminated sandstone using CCNBD specimens (Ghamgosar et al., 2015)

Another experiment, conducted by Amrollahi & Baghbanan (2009), investigated the effect of grain size distribution. In this particular experiment, three crystalline marbles were selected, each containing the same mineralogy – crystalline calcite, but with different distributions in grain size. The three marbles were Neiriz, Baghat and Maron. Investigations of the stones revealed that the grain size distribution was the *only* difference between the marbles, and thus it provided an opportunity to investigate the relationship between the grain size distribution and the mode I fracture toughness. Two methods were utilized; the CCNBD method following ISRM standards and the hollow center cracked disc (HCCD). Samples prepared for each method were 75 mm in diameter and the samples were drilled along two different axes to investigate differences in fracture toughness values. Figure 3-5 shows the resulting cracks after the experiment where the cracks propagated in tensile mode**.** The results showed similar values between the two methods and they indicated that there is a negative correlation between grain size and mode I fracture toughness, where higher grain sizes resulted in lower fracture toughness values. Neiriz marble, containing medium sized particles were the one with the highest fracture toughness in both directions, while Baghat marble, made from coarse particles, had by far the lowest values in both directions. The last marble, Maron, contains a mixture of fine to coarse particles resulting in medium sized values. Figure 3-6 shows the effect of grain size distribution upon fracture toughness determined by Amrollahi & Baghbanan (2009).

Figure 3-5: Fractured samples from the CCNBD and HCCD experiment. Notice the cracks that have propagated in tensile mode. CCNBD is to the left, HCCD is to the right (Amrollahi &Baghbanan, 2009)

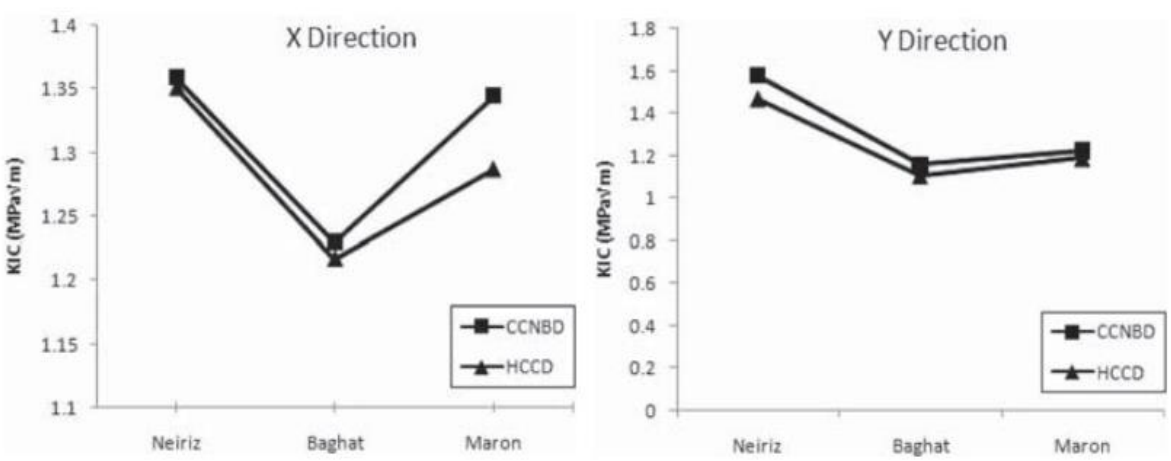

Figure 3-6: The effect of grain size distribution upon fracture toughness, K_{IC}. The cracks have been induced in different directions for the two plots, but on the same samples (Amrollahi & Baghbanan, 2009)

Thorough investigations of anisotropic granitic rocks have shown that they are more connected with microcracks and their orientation than they are with grain size (Nasseri & Mohanty, 2008). Four granites were selected for a series of CCNBD test, and these were Laurentian, Barre, Stanstead and Bigwood, selected for their varying microstructural properties. The highest average fracture toughness values determined were *always* encountered when the cracks

propagated perpendicular to the plane containing the mesocraks often found in the granites. Additionally, the value of the fracture toughness was always found to be larger whenever cracks crossed zones of weakness in the granites. When investigating the Stanstead granite, it was found that there was a mismatch regarding the microcracks and the preferred orientation of the mineral fabric. The authors concluded that this misalignment was both responsible for the lower anisotropy seen in this granite, but more importantly it points out that the microcrack alignment has a more dominant role regarding the fracture toughness value than grain size. The Bigwood granite stood out as it was dominated by mesocracks of larger lengths. Because of these mesocracks, the Bigwood granite experienced a much higher fracture toughness anisotropy than the rest, where the highest fracture toughness value was 2.4 times larger than the smallest one recorded. Due to these weak mesocracks being so long, they are suitable zones where the stress relief occurs when the fracture propagates parallel to the plane with the mesocracks, while at the same time they override the effect from perpendicular microcracks.

Two of the granites, Barre and Stanstead, later underwent additional testing that further validated these results, both regarding the effect of grain size distribution and orientation of microcracks (Nasseri et al., 2007 & 2011). An investigation of the Barre granite revealed a possible explanation for the differences in the value of the fracture toughness when it was forced to propagate perpendicular to microcracks as opposed to when it was forced to propagate parallel to them. In the former case the fracture damage zone, being the final form of the FPZ, had certain characteristics compared to the latter case. Firstly, the fracture surface area was twice as large, explained as a representation of stress shielding effects**,** and secondly, it contained ten times the amount of induced porosity, something that is similar to the effects of stress amplification. These two effects combined are thought to explain why the fracture toughness value for perpendicular cracks were twice as large as those for parallel cracks.

However, an interpretation of the results from a series of SCB tests under different water vapor pressures provided results contradictive to the results of Nasseri & Mohanty (2008) (Kataoka et al., 2011 & 2015). The experiments, conducted on African granodiorite and Korean granite, further emphasized the fracture toughness anisotropy seen in other experiments but when examining the samples, another conclusion was reached on whether microcracks and their orientation or grain size distribution is the dominant factor. It was found that the fracture toughness value was higher when the crack propagated parallel with the plane containing many of the microcracks, axis-1, and not when it propagated perpendicularly, in axis-3. See Figure 3-7 for the definition of the planes and axes.

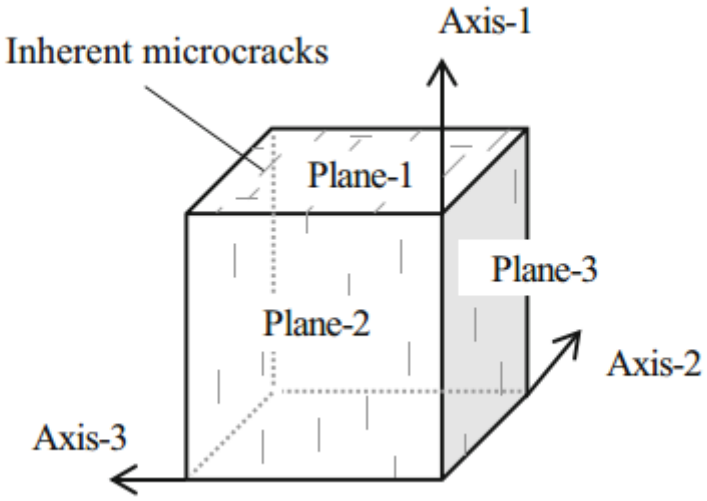

Figure 3-7: Axis and plane definition, showing the inherent cracks (Kataoka et al., 2015)

The same trend was seen at all water vapor pressures used in the experiment. Based on a deeper investigation of the induced cracks for different directions, it was concluded that fractures tended to be initiated at the boundaries of the grains while they would also avoid going through grains of higher density. The reasons for this was the differences in fracture initiation resistance, higher density grains have higher resistance to fracture initiation, compared to initiation along the boundaries of the grains. This then gave the anisotropic fracture toughness values seen. Based on this, it was concluded that the mode I fracture toughness was more dependent on grain size distribution and their orientation, and not the presence of microcracks. Further support to this was given by the larger grain sizes of axis-3 and the fact that fractures had a harder time to propagate through grains. This resulted in an increase of the fracture resistance and hence the mode I fracture toughness for cracks propagating in the direction of the microcracks were larger than those propagating normal to them as the fractures needed more energy to initiate and propagate.

Similar experiments were conducted on Kimiachi sandstone, Rustenberg granodiorite and Iksan granite with the SCB method (Kataoka & Obara, 2015). The conclusion that the mode I fracture toughness value was more dependent on grain size distribution and the orientation rather than microcracks was also found here for the Rustenberg granodiorite and the Iksan granite with the same argumentation. Regarding the Kimiachi sandstone, it was found that the anisotropy value was dependent on the compaction seen in the sandstone. It was believed that one of the axes was more compacted than the others, which was assumed to result in a higher

fracture initiation resistance perpendicular to this direction and hence an increase in the fracture toughness value.

Kimiachi sandstone was also the test material used in another SCB testing program (Funatsu et al., 2012). For this particular batch of sandstone, the bedding planes were clearly visible and therefore a limited amount of tests were conducted on different angles relative to the bedding plane. Inclination here is defined as the angle between the notch and bedding, i.e. an inclination of 0° means the notch is parallel with the bedding. Here it was found that the fracture toughness values were lower between 45° and 60°. However, the authors did not discuss the reason behind this in their paper, other than stating that different mechanisms of microcracking caused it.

3.4 Tensile Strength vs Fracture Toughness

A topic of several investigations have been to determine the relationship between fracture toughness and tensile strength. This work however, has been somewhat limited, as fracture toughness experiments have not achieved any widespread use due to the lengthy experimental processes and inconsistencies with the methods used (Zhang, 2002). This has led to many of the results being used multiple times and the work might not be as diverse as one might initially believe. Additionally, in many of the papers found, the main topic is not related to the relationship between these two parameters, and correlations between them are then seldom discussed, if mentioned at all. Despite this, the work has led to several interesting and important findings.

An important argument and one of the main motivations for investigating this relationship, has been to find ways to study the fracture behavior by looking a different parameter relationships (Zhang, 2002). If a relationship between the two parameters exist, it could be possible to determine the value of the fracture toughness through the tensile strength, a parameter that is much more common to investigate and also cheaper to determine. One of the most thorough investigations of the relationship between tensile strength and fracture toughness was conducted by Zhang (2002), where an empirical relationship between these two parameters was determined. By looking at both existing and newly discovered data, Zhang was able to determine a correlation where the tensile strength is given as

$$\sigma_t = 6.88K_{IC} \tag{3.2}$$

Here the tensile strength is given in MPa and K_{IC} in MPa*$m^{1/2}$, while the correction factor has a unit of $m^{-1/2}$.Similarly for the other equations given later, the tensile strength and the fracture toughness use the same units as here, while most of the constants have the unit of $m^{-1/2}$. The correlation has a coefficient of determination of r^2=0.94, providing one of the best fits among all of the correlations seen in the literature survey. This correlation is built upon the results from more than 50 different rock types, including coals, shales and sandstones. In addition to this, several different methods for determining the fracture toughness were used, mainly SR and CB. Based upon the rock types used, Zhang (2002) argued that this correlation would yield satisfying results for soft to hard rocks under quasi-static or low-speed impact loading. The results from Zhang agrees fairly well with similar investigations conducted by Bearman (1999) and Whittaker et al. (1992), although their resulting correlations differed from the one found by Zhang. Similar results can also be seen in the work of Backers (2004) where a correlation between the fracture toughness and the tensile strength was achieved. Some of the other correlations seen have a coefficient of determination ranging between 0.6 and 0.75, indicating that there are inaccuracies related to them. Further, even though they all agree that there is positive correlation between the parameters, none of them agree completely on the same relationship. A major reason is of course the different methods utilized. Previously it has been stated that the different methods for measuring the fracture toughness results in different values for the same rock but it is believed that this is not the only source responsible for the differences as the rocks consist of different layering, different porosities etc.

Both Backers (2004) and Zhang (2002), after having conducted a regression analysis, commented upon the correlation found by Whittaker et al. (1992). The correlation of Whittaker et al. was

$$\sigma_t = 9.35K_{IC} - 2.53 \tag{3.3}$$

The coefficient of determination for this correlation was r^2=0.62. The regression analysis showed that this correlation yields a non-zero value for K_{IC} if the tensile strength is zero, meaning that it would be possible for a rock to resist crack propagation, something that it should not be able to do under zero tensile strength. Based on this, both of them determined that a correlation should be passing through the origin.

Previous work from Zhang (Zhang et al., 2000, Yu et al., 1998) found that there were fracture pattern similarities between fractures seen in tensile strength experiments and in fracture toughness experiments. Based on evidence from such work, two similarities where

identified. First, the samples used in such tests usually result in two fractured surfaces when subjected to static or low-speed impact loading, hereby indicating the samples fail due to single crack extension. Thereby, the resulting fractures from both types of tests are similar. Secondly, by looking at the characteristics of the fracture surfaces from each test type, it was found that the fractures are made up from micro- and mesocracks resulting from loading.

Additionally, in Whitaker et al. (1992), a total of three basic criterions for fractures are given, namely maximum principal stress, maximum energy release rate and strain energy density. In the same book, Whittaker et al. argues that the maximum principal stress (i.e. tensile strength) is the governing factor for fracture toughness relating to rocks, thereby indicating that there is a relationship between tensile strength and fracture toughness inherent to the rock.

The most relevant correlations found in the literature survey are summarized in the table below, along with the respective coefficient of determination and where it was published.

Author	**σ_t**	**r^2**
Whittaker et al. (1992)	$9.35K_{IC}-2.53$	0.62
Zhang et al. (1998)	$8.88K_{IC}^{0.62}$	0.94
Zhang (2002)	$6.88K_{IC}$	0.94
Backers (2004)	$4K_{IC}$	-

Table 3-2: Tensile strength vs fracture toughness correlations. Backers did not provide a coefficient of determination

3.5 Use of Fracture Toughness in Modeling

Fracture toughness was for a long time thought to have little effect in hydraulic fracturing, where the exception was for small fractures, when performing very low viscosity injections (Thiercelin et al., 1989). This was mainly due to the usage of fracture toughness values that turned out to be unrepresentative for the in-situ values, while at the time most models were limited to 2-D. Developments in these fields led to a re-evaluation of the importance of fracture toughness by Thiercelin et al. (1989). They conducted an investigation where the fracture toughness effect on different models was assessed. For basic 2-D fractures, uniformly pressurized in a uniform stress field, it was seen that the fracture toughness did not become insignificant as a fracture propagates. In this particular case, the fracture toughness is the only factor constraining the fracture length and thus the fracture length is highly sensitive to the value of the fracture toughness. However, a fracture such as the one described above is not

representative for an actual case, regarding geometry and the pressure distribution. Moving on to 3-D numerical results, the growth of penny-shaped fractures was found to be highly affected by fracture toughness (Abe et al., 1976, Shoji et al., 1985). Thiercelin et al. (1989) attempted to verify these results. The main model used incorporated both viscous friction and fracture toughness effects. Two additional models were also used to investigate the limiting cases of the main model; one model ignores the fluid friction effects while the other ignores the fracture toughness effects. A typical trend appeared where the higher fracture toughness values accompanied smaller fractures in all of the cases tested. One case used a high injection rate of 78.5 bbls/min and a viscosity of 100 cP. For this particular case, the geometry was not highly affected by the fracture toughness and the wellbore pressure did not differentiate by much for all the different fracture toughness values tested. Thus, it is possible to have large fracture diameters without significant differences in wellbore pressure.

An investigation of the effect of toughness contrasts was accomplished using a 3-D model developed by Thiercelin et al., as well as a simple pseudo 3-D (P3DH) model. Such models had earlier been shown to be valid for elongated fractures. One example of such a model, a discrete P3DH model, was developed by Settari (1988) incorporating fracture toughness variations between layers and its effect on vertical growth, while at the same time accounting for the energy used to overcome both viscous friction and fracture toughness. Thiercelin et al. (1989) found that the two models used provided similar fracture geometry where it was seen that large toughness differences could lead to unwanted propagation of fractures into the surrounding layers. This happened whenever the pay zone had higher toughness than the surrounding layers and was much more pronounced the higher the toughness difference was. However, only the 3-D model was able to simulate such a situation. The effect of fracture toughness contrasts is shown in Figure 3-8.

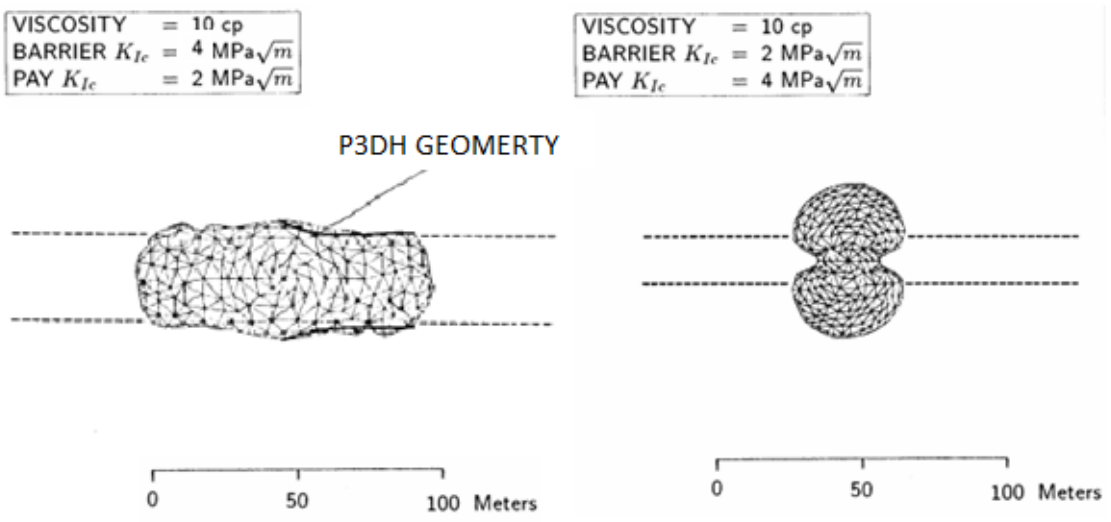

Figure 3-8: Effects of fracture toughness contrasts. In the left figure, the fracture toughness of the pay zone is twice as high as the barriers, while in the right figure the opposite is the case (Thiercelin et al., 1989)

One example of the use of fracture toughness in modeling is FRACOD. This is a two-dimensional code based on the principals of the displacement discontinuity model (DDM), used to predict the fracturing process where it explicitly determines fracture initiation and propagation, as well as fracture opening and sliding (Shen & Rinne, 2007). The model uses the F-criterion, a modification of the G-criterion to determine when fracturing occurs, developed by Shen & Stephansson (1993), which uses the strain energy release rate for mode I and II. This parameter has been shown to be directly related to the mode I and II fracture toughness, K_{IC} and K_{IIC}. Modifications to the code have implemented the direct use of the fracture toughness parameters. One example of this is the modeling of sub-critical crack growth (Shen & Rinne, 2007). Sub-critical crack growth takes place when the stress intensity factor is below its critical value and the fracture toughness is then used as a limiting factor. Simply explained, the code calculates at each time step a time dependent crack length. If this crack length is larger than the element lengths used in the code, a new tip element is added to the already existing tip. Otherwise, this length is stored and added to the next tip length calculated until the combined length is longer than an element. Attempts were made to try to reproduce the results from laboratory experiments on coal and diorite specimens. The models produced from this achieved generally good agreements regarding the creep strain and failure time for both rock types. However, the limitations of the FRACOD towards the modeling capacity, specifically regarding its ability to consider large quantities of microcracks lead to it often underestimating the creep strain when close to failure.

Another use of fracture toughness in FRACOD, was the implementation of an anisotropic function (Shen at al., 2014). The F-criterion underwent modifications so that it instead of being expressed by the strain energy release rate, was expressed by stress intensity factors and then implemented as a fracture propagation criterion. Due to fracture toughness being a direction dependent parameter in anisotropic rock, several F-values are calculated. The direction of where this value is the highest is the potential direction of fracture propagation. Combined with a set of criterions for fracture initiation based on the Mohr-Coulomb criterion, the FRACOD calculates if a fracture is initiated and/ or if it propagates. Testing of the code was done against two scenarios. In the first one, a tensile fracture propagating in an anisotropic rock mass was investigated. The fracture propagated as expected where it curved towards the weakest plane. The other showed that the compressive strength of a sample was direction dependent when simulating a uniaxial compressive test in an anisotropic sample, in accordance with what is often seen in textbooks. The code has also been verified against other rock related situations.

4 Samples and Experimental Set-up

Below is a description of the loading equipment as well as the software used for determination of mode I fracture toughness using the CB method. Selected properties of the materials tested, shale, chalk and sandstone are also presented. As time did not allow for separate testing of the properties for each of the different materials, the information provided here is based on information available, either at the courtesy of SINTEF Petroleum or from the manufacturer themselves. The majority of these tests have been done on previous sample batches, but it is believed that they are of similar properties. Because of this, there are limitations to the information available. Figure 4-1 shows a sample for each rock type tested next to each other.

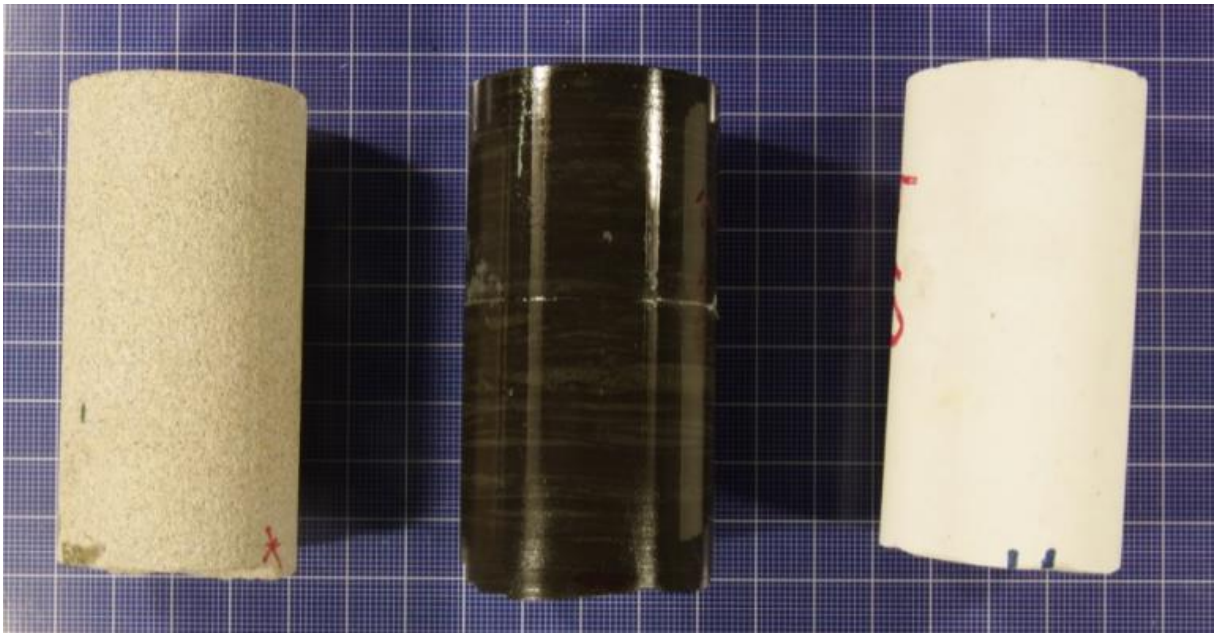

Figure 4-1: Picture of the three rock types used. To the left is Castlegate sandstone, in the middle is Mancos shale and to the right is Mons chalk

4.1 Loading Equipment

An electro mechanical loading frame called 2/M purchased from MTS (Material Test Systems Inc.) was used, capable of providing a total of 10 kN confining force. The system was controlled with MTS Testworks 4 and logging of data was done through both the loading frame and with a HBM QuantumX MX440A. The data from the latter was logged with HBM Catman software. In addition to this, a HMB QuantumX MX878A was used to transform the analog signal from the clip-gage into a guiding signal for the loading frame. Figure 4-2 shows the loading frame.

Figure 4-2: Loading frame used

4.2 Materials

4.2.1 Castlegate Sandstone

Terratek Inc, Salt Lake City, provided the Castlegate outcrop sandstone. The bulk density is reported to be 1.93-1.94 g/cm^3 with a high porosity typically in the range 27-29%. The unconfined compressive strength is around 16.0 MPa with Young's modulus of 1.72-2.07 GPa. The permeability ranges from 400 mD to 1400 mD. Brazilian tests gave a tensile strength of 1.072 ± 0.095 MPa (Simpson, 2013). The structural makeup for Castlegate sandstone consists of 70% quartz and 30% feldspar & rock fragments. It is a beige sandstone defined as homogenous with no layering and it's considered analogous to sandstone reservoirs, which is one of the reasons it was chosen along with its high porosity. Prior to testing the samples were stored at ambient conditions.

4.2.2 Mons Chalk

The Mons outcrop chalk originates from Mons in Belgium and is considered analogue to chalk reservoirs of the North Sea. Its main component is calcite, accounting for 99.8% of the chalk. Its porosity lie in the range of 40-44% and it has a permeability of around 2 mD (Walle & Papamichos, 2015). The dry bulk density is 1.515-1.550 g/cm^3. Currently there are no data for the unconfined compressive strength and Young's modulus at ambient conditions, but based on data from SINTEF as well as Papamichos (personal communication, 2016), the UCS is expected to lie between 11 and 12 MPa and the Young's modulus at around 5 MPa. Likewise, the Poisson's ratio is expected to be around 0.11. Brazilian tests gave a tensile strength of 0.867 ± 0.368 MPa (Simpson, 2013). It appears to be homogenous with no preferred orientations. The material consists of small parts of irregularities in addition to the calcite. It is not known what this material is, and it is seen as yellow/ golden grains sporadically spread, not necessarily present in all samples. The specimens were stored at ambient conditions prior to the experiments.

4.2.3 Mancos Shale

The Mancos outcrop shale utilized in this experiment was purchased from Terratek Inc., Salt Lake City. Prior to testing the rock was kept in inert oil at room temperature such that desiccation effects did not take place. The only time the sample was taken out of the inert oil was during sample preparation and right before the experiment took place. Mancos is made up from 40-45% quartz, 20-25% clay, roughly 20% carbonates and around 1% organic material (Simpson et al., 2014). The respective porosity and bulk density are 6-8% and 2.57 g/cm^3, determined from core testing. Mancos was chosen because it is a good analogy to gas shales, however it fails to classify as a shale because of its low content of clay in a geological context. Despite this, Mancos shale is highly relevant for investigations as it exhibits interesting features, particularly anisotropy. Figure 4-3 shows the anisotropic features of the Mancos shale highlighting the bedding planes. Testing of the Mancos shale will occur at predefined inclinations at 0°, 15°, 30°, 45°, 60°, 75° and 90° in relation to the bedding planes. This inclination angle is defined as the angle between the bedding planes and the applied load, see Figure 4-5. Previously, the uniaxial compressive strength and the Young's modulus have been determined by Fjær & Nes (2013) to be between 45-82 MPa and 18-29 GPa respectively, varying with the inclination. Tensile strength obtained with Brazilian tests by Simpson et al. (2014) is seen in Figure 4-4.

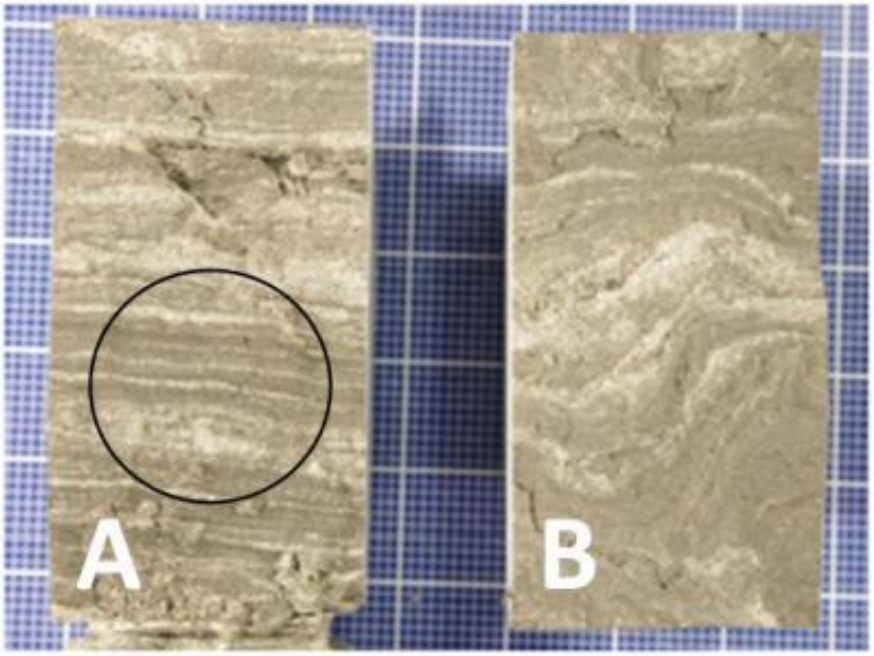

Figure 4-3: Cross sections of Mancos shale. Sample A shows the bedding planes of Mancos shale most samples exhibit while sample B shows how some samples exhibit a more complex structure with less clearly defined bedding planes. Both samples are cored parallel to the bedding planes (Simpson et al., 2014)

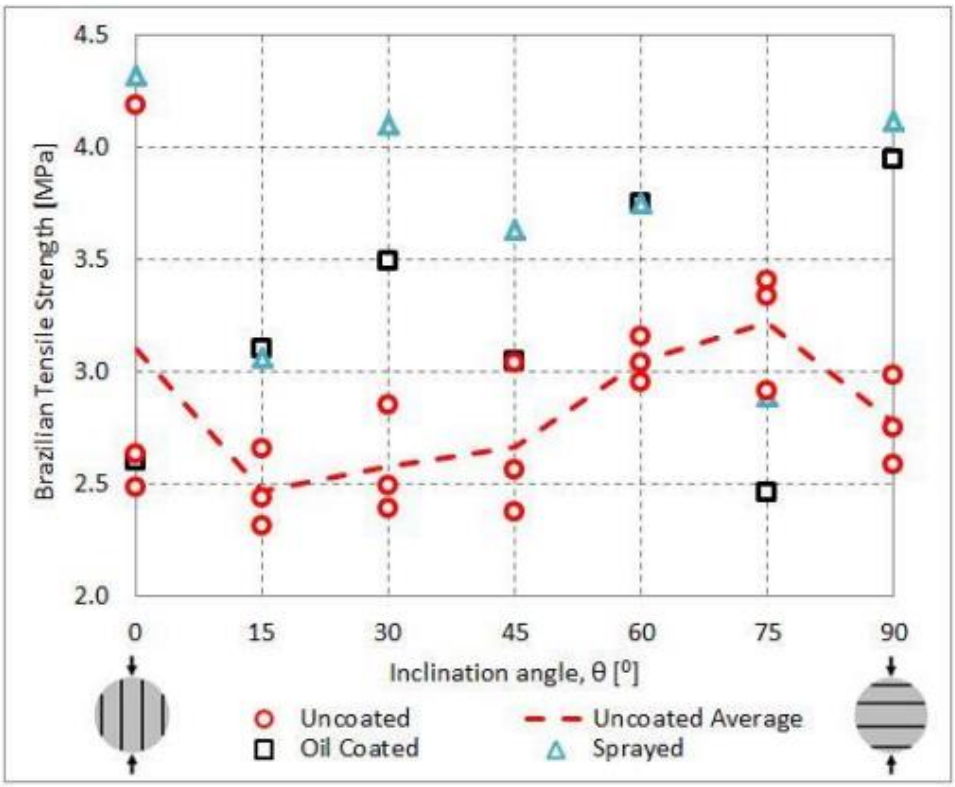

Figure 4-4: Tensile strength data from Brazilian tests. The average value is marked by the dashed line (Simpson et al., 2014)

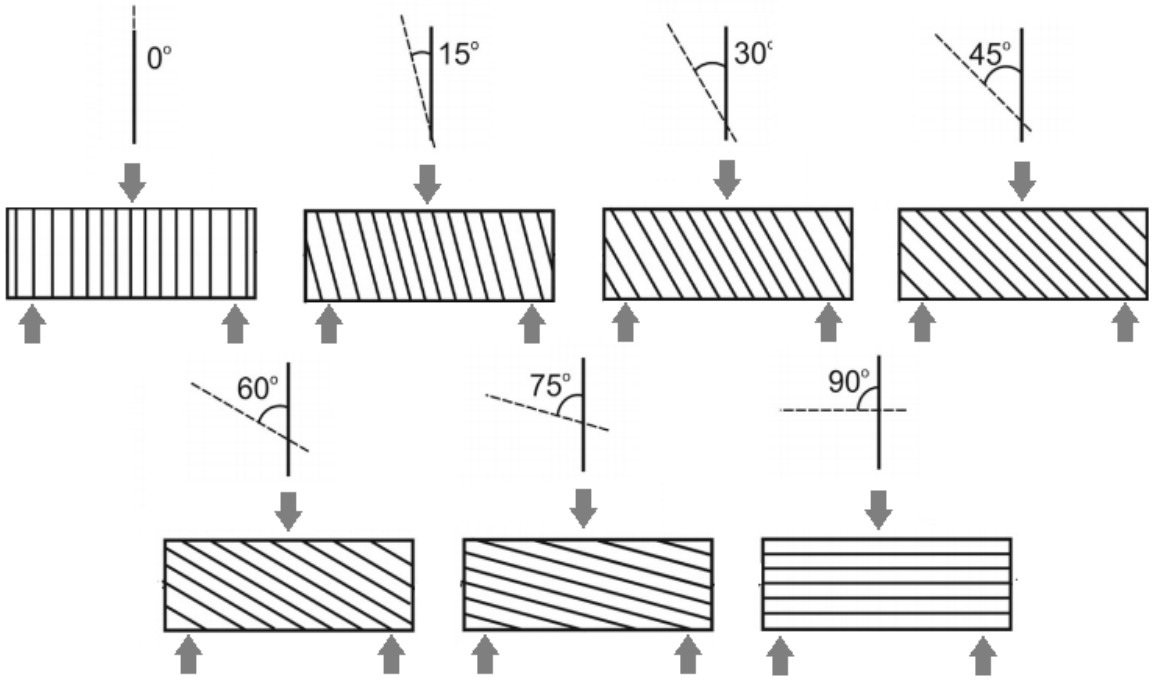

Figure 4-5: Inclination of samples between the bedding plane and the applied load. Note that the notch is not shown here

During the mode I fracture toughness experiments, the notch will be made both parallel and normal to the bedding planes for each inclination. Figure 4-6 shows the differences between these two.

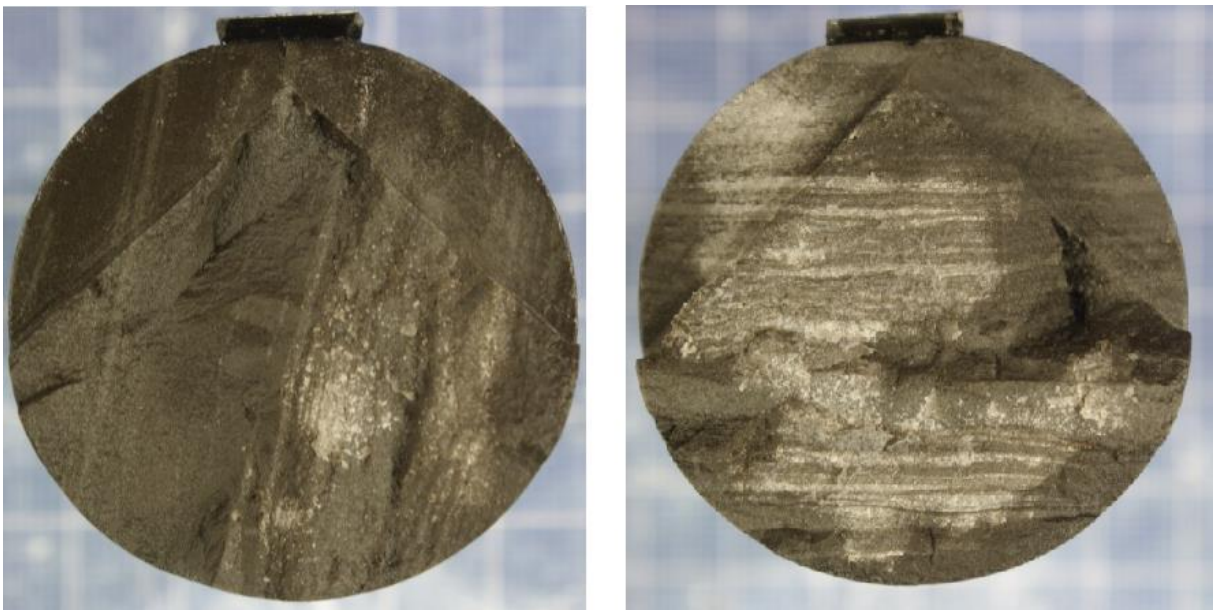

Figure 4-6: The picture to the left show a notch parallel with the bedding planes, the picture to the right shows a notch perpendicular to the bedding planes. Both pictures are of samples with an inclination of 75°

Table 4-1 summarizes the specimen properties for all rock types.

Sample	Castlegate	Mancos	Mons
Unconfined Comp. Strength [MPa]	16.0	45-82	11-12*
Young's Modulus [GPa]	1.72-2.07	18-29	5*
Tensile Strength [MPa]	1.072±0.095	-	0.867±0.368
Bulk Density [g/cm^3]	1.93-1.94	2.57	1.515-1.55
Porosity [%]	27-29	6-8	40-44
Poisson's Ration	0.07-0.4	-	0.11
Permeability [mD]	400-1400	very low	2

*Table 4-1: Rock properties. The tensile strength for Mancos is given in another figure. * means the values have not been obtained, but guessed based on previous experiments. Permeability for Mancos is in the nanoD range*

4.3 Bend Fixture

The three point bending fixture used is a model 642.10 purchased from MTS. All rollers have a diameter of 1 inch or 25.4 mm allowing for a maximum span of 12 inches or 308.4 mm between the two support rollers. Minor modifications were done to the bend fixture such that it was possible to stabilize the samples. This did not have an effect on the measurements.

4.4 The Chevron Bend Method

The experiment was done according to the ISRM Suggested Methods for mode I determination of fracture toughness using the Chevron bend method. The schematic set-up is shown in Figure 4-7 while Figure 4-8 is a picture taken of the actual set-up in the loading frame. Two rollers are for support, while the third roller positioned in the middle applies a compressive load.

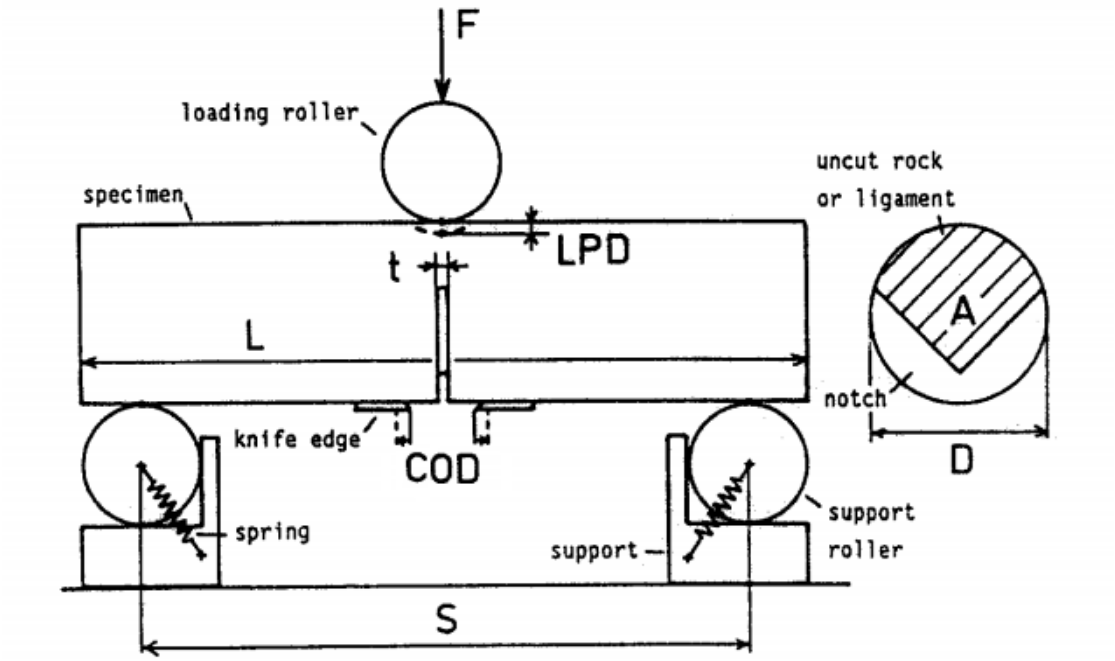

Figure 4-7: Simple drawing of the set-up (Modified from Ouchterlony, 1988)

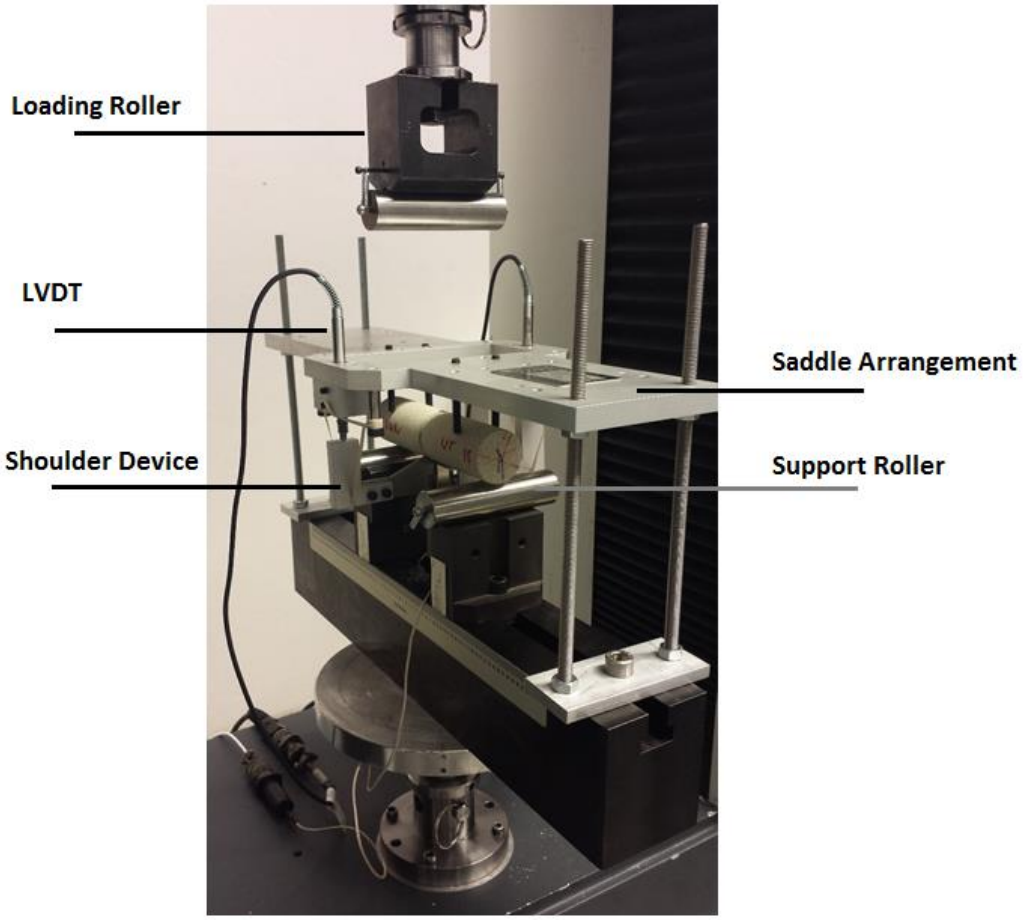

Figure 4-8: Bend fixture with a sandstone highlighting the different aspects of the set-up. The COD tool is not seen.

4.4.1 Sample Preparation and Set-Up

In preparation of the samples, the requirements of the ISRM Suggested Methods were followed. For Mons chalk and Castlegate sandstone, specimens of 38 and 50 mm were used, in an attempt to investigate size effect, while for Mancos a diameter of 38 and 40 mm were used, 40 mm for the specimens with no inclination and 38 mm for the rest. The reason for this was that samples of 38 mm with 0° inclination was not available during the testing period, nor was there time to make new samples. In designing the specimens, the requirements as well as the desired values seen in Table 4-2 were followed when practically feasible.

Geometry parameter	Value	Tolerance
Specimen diameter, D	D	>10x grain size
Specimen length, L	4D	>3.5D
Support span, S	3.33D	±0.02D
Chevron angle, Θ	90.0	±1.0
Chevron v tip position, a_0	0.15D	±0.1D
Notch width, t	≤0.03 or 1mm*	

*Table 4-2: Specimen dimensions for the Chevron Bend method. * use whichever is greater (Ouchterlony, 1988)*

Design problems occurred for the notch width, as there was no cutting blade available for making sufficiently thin notches. Therefore, a decision was made to make these specimens with the smallest blade available, with a width of roughly 2.2 mm. Additionally, the length of the samples all satisfied the minimum length requirement, but not all of them were of the desired length for different reasons. The Mons chalk encountered some difficulties when trying to cut them into 4D long specimens, but all of them satisfied the minimum requirement. The Mancos shale was impossible to cut when the specimen length got longer than 2D and the samples tended to break. As a solution to this, the samples where instead prepared as pieces with a length of roughly 2D. To achieve the correct length, a second set of specimens where prepared with the same length, which was then cut into two pieces of equal length. These pieces were then glued to each side of the main component with quick hardening glue, making the total length of the sample close to 4D. This was done as it was believed that the middle section would be unaltered by the pieces glued on and that the main reason for such long specimens was for support, allowing the specimen to rest on the support rollers on each side of the middle roller. The support specimens were all made from the same inclination, 0^o, as this was the inclination where there were least issues with obtaining samples. Once the samples were glued, they were allowed to rest in inert oil for a minimum of two days to ensure that the glue had hardened properly.

Following the Suggested Method, each specimen had a chevron notch (V-notch) machined into the middle of the specimen in the axial direction. The chevron angle was within the tolerance for all samples. For measuring purposes two metal knife-edges were glued centered around the notch with a distance of 5 and 6 mm between the knife-edges using a two component epoxy glue. Prior to gluing of the metal knife-edges, the location for where the gluing would take place was grinded carefully to allow the glue to stick to both the sample and the knife-edge. Without the blunted section, the knife-edges did not stick properly making it difficult if not impossible to use them for measuring purposes. To make sure the knife-edges were correctly centered with a correct distance between them, alignment tools were used, shown in Figure 4-9. With the knife-edges glued on, the samples were stored in inert oil for at least two days allowing the glue to harden.

Figure 4-9: Alignment tools for positioning of the knife-edges

With the samples properly prepared and ready, they were loaded onto the bend fixture. The distance between the two rollers were approximately 3.33D. Each specimen was positioned such that the notch faced downwards, with the notch located at an equal distance from each roller. A third roller applied the compressive load on the opposite side, hitting the specimen directly above the notch. This accuracy was obtained using a pendulum-like device, made up by a thin thread and small metal nut that hang from two points at an equal distance from each side of the third roller indicating the location of where the roller would hit the sample. Having previously marked the middle of the specimen, this allowed for an easy way to determine if the specimen was correctly positioned.

Two measuring tools were used during the experiment. One measured the clip-gage opening displacement (COD) using a clip-gage attached to the metal knife-edges. The other used two LVDT's (linear variable differential transducers) to measure the load point

displacement (LPD) of the sample. The LVDT's rested on a shoulder device positioned around the notch as seen in Figure 4-10. This device was held in position by common rubber bands attached to a saddle. The saddle device was used as a way of holding the sample in place while at the same time verifying that the specimen has been correctly positioned. Prior to use, both tools were calibrated against known values allowing for a sufficient level of accuracy. Figure 4-8**,** seen earlier, shows the complete set-up, highlighting the different aspects of the assembly.

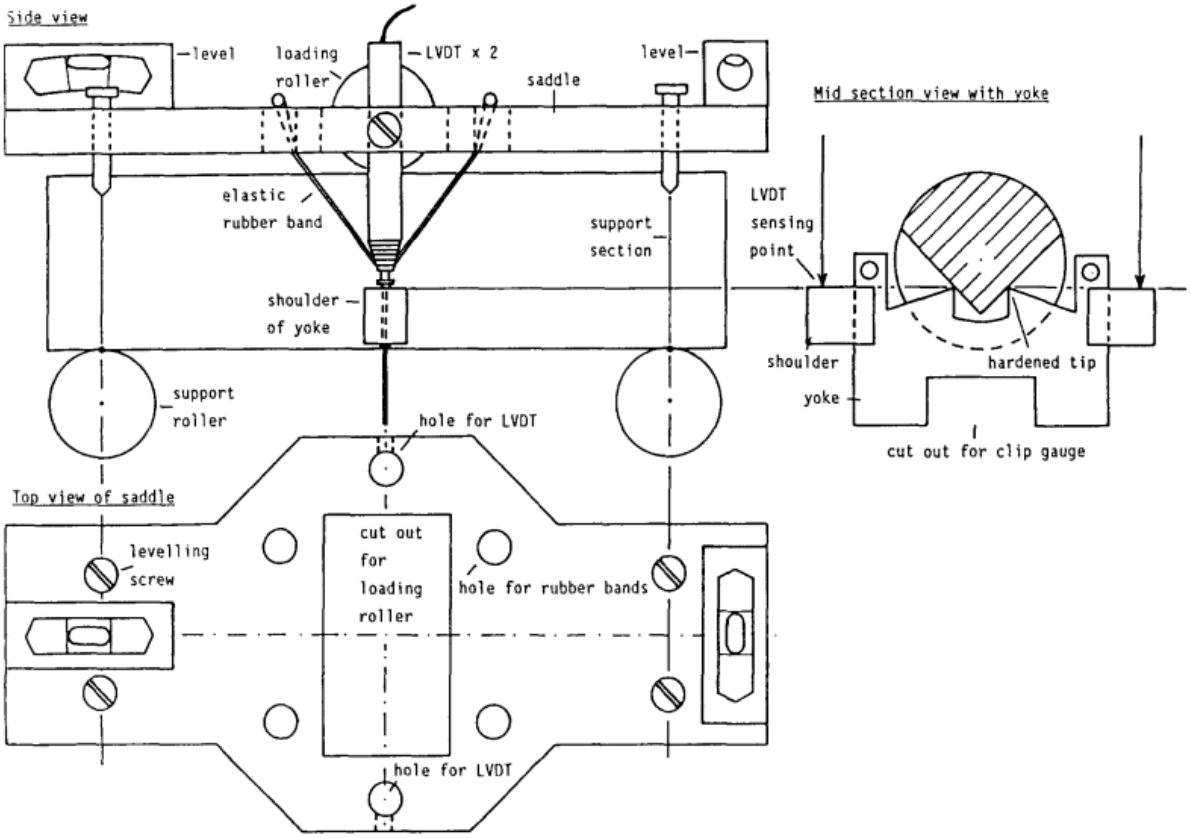

Figure 4-10: Saddle arrangement for the Chevron Bend method (Ouchterlony, 1988)

4.4.2 Experimental Procedure

When conducting experiments with the CB method, one has the option to run the system in either level I or level II, with level I being the cheapest and fastest method, while level II provides the most accurate determination of the fracture toughness as it accounts for non-linear behavior. In level I mode, the system is run under load control and only the load is measured. The test lasts until the specimen fails, when the propagating fracture becomes unstable, which should happen within 10 seconds. In level II mode, the selected method for this thesis, the system is run under displacement control, requiring both the load and the displacement to be

measured and recorded. During testing, at least four loading/ unloading cycles shall take place to allow for a proper calculation of the correction factor p. How to calculate p and an explanation for this parameter is given later. Two of these cycles should happen pre-peak load and two post-peak load. This was not always possible for these experiments as the samples often failed abruptly and the system was too slow to detect it. Unloading ends and reloading begins when the load is around 10-20 % of the maximum load. Level II mode was run with COD control. The majority of the experiments were run with either a loading rate of 0.006 or 0.003 mm/min. Converted to m/s this is $1*10^{-7}$ and $5*10^{-8}$ m/s, respectively. The loading rates chosen are based on the rates used by Backers (2004). These values were initially picked to investigate subcritical crack growth. However, the numbers chosen in this thesis is not done for investigation of subcritical crack growth but instead to allow for proper control of the experiment as it is run manually. With such loading rates, the system could easily be controlled and cycles initiated at a given time without leading to sudden failure. If higher loading rates had been used, it would not have been possible to run the system manually, as the load would have been applied too fast for intervention**.** Depending on the loading rates used, an experiment can last from anywhere between a few minutes and up to several days. The running time for these experiments varied between 15-30 minutes for the chalk to over 90 minutes and more for some of the shale and sandstone. Subcritical growth is not commented upon, as it is not the objective to investigate it.

As mentioned earlier, Testworks 4 was used to control the experiment. Within this program, a procedure was developed that allowed the frame to apply load at a certain rate, specified above. The system had the option to either use automated and pre-specified cycles or initiate the cycles manually. Due to no existing knowledge about the behavior of the rock types used during CB testing, it was decided to initiate the cycles manually during the experiment. This meant that no experiment was carried out at the exact same displacement. However, this was the better option as only a limited amount of samples were available and having an automated system to initiate the cycles at specific displacements would have been difficult without using several samples to properly determine the onset of cycle initiation. Similarly, for the Mancos shale it would have been impossible to use an automated program because only one test sample was available for each inclination and prior to testing there was no way of telling if they would behave similarly or differently from each other. Each sample is preloaded to 20 N before the experiment is commenced.

4.4.3 Calculation Procedure

This section is designed to show the steps involved for determination of the fracture toughness, the corrected fracture toughness and other values related to this such as the p value previously mentioned. In addition to this, the idea behind the steps is explained when necessary. This procedure will show the entire calculation, step by step. The original ISRM Suggested Method was designed to be done by hand, but it is quite possible to do it through a software program such as Microsoft Excel or Matlab. In this thesis, Excel was used.

For level I testing the fracture toughness is simply calculated by applying the following formula

$$K_{IC} = \frac{A_{min} F_{max}}{D^{1.5}} \tag{4.1}$$

Here F_{max} is the maximum load during the experiment given in kN and D is the diameter given in cm. A_{min} is a dimensionless parameter calculated as

$$A_{min} = \left(1.835 + 7.15 \frac{a_0}{D} + 9.85 \left(\frac{a_0}{D} \right)^2 \right) \frac{S}{D} \tag{4.2}$$

with S being the span mentioned earlier in Table 4-2 along with a_o being the chevron tip position. S, D and a_o use the same notations. Using these notations gives the fracture toughness in MPa*$m^{1/2}$. The complete derivations of these two equations are outlined in Ouchterlony (1986, 1989) and in Barker (1977). The derivation was obtained through empirical relationships assuming stable crack growth until the crack achieves a critical length, at which point the specimen is evaluated. The method requires the specimen to propagate steadily under plane strain-conditions (Barker, 1977).

The requirements for the notch tip are easy to achieve due to its relatively large tolerance values. However, an accurate measurement of this position is difficult to accomplish. Instead, the Suggested Method recommends to measure the depth of the flanks, h, and then calculate the notch tip position with the equation below. It is believed by ISRM that this most likely will give a more accurate result.

$$a_0 = 1.414h - 0.207D \tag{4.3}$$

Level I testing is the simplest and fastest way to determine the fracture toughness, but the method assumes that the specimen behaves in an ideally linear elastic fashion. To account for

the non-linear behavior of the specimens, Barker (1979) developed a procedure using the SR method. However, the developed method also applies to the CB method. This procedure is used in level II testing, where a corrected fracture toughness is determined based on this correction factor. A plot should be made with either the load vs LPD or the load vs COD. The Suggested Method uses LPD data, but allows for the use of COD. In Funatsu et al. (2014) COD data is stated to be the only source of data used, and it also appears that Backers used this. The following procedure as outlined is independent of the use of either LPD or COD, the method is the same. Its details now follows, using load vs COD data.

For all the unloading-reloading slopes, a straight line is drawn by defining two points on each cycle and drawing a line between these two. The high point is located were the COD starts to decrease on the unloading part of the cycle. The low point is located on the reloading part of the cycle at the point where

$$F_L = \frac{F_H}{2} \tag{4.4}$$

This is done for all cycles. The next step is then to determine the slope of each line, which is easily done when using software. The two slopes that most closely match the span given by the following equation is where the fracture toughness is to be evaluated.

$$s_c = \left[1.05 - 2.15\frac{a_0}{D} + 4.21\left(\frac{a_0}{D}\right)^2 \right] s_{\text{initial slope}} \tag{4.5}$$

If none of the lines span the evaluation point, it is still possible to continue. If the evaluation point lie before the first cycle, the two finalized lines shall be the initial slope and the line obtained from the first cycle obtained in the same sense as below. If the point lies after the last cycle, the last two cycles shall be chosen and the procedure continues as described in the following. For future testing of similar specimens, more cycles should be made, such that the slopes span the evaluation point.

Once these two lines have been determined, the next step is to translate these vertically downwards. For each line, the amount of translating is defined by the low point's position. The difference between F at the low point and at the location on the unloading line directly below it is designated ΔF. The final straight line is located $0.5\Delta F$ below its current position. See Figure 4-11 for an example of a translated line.

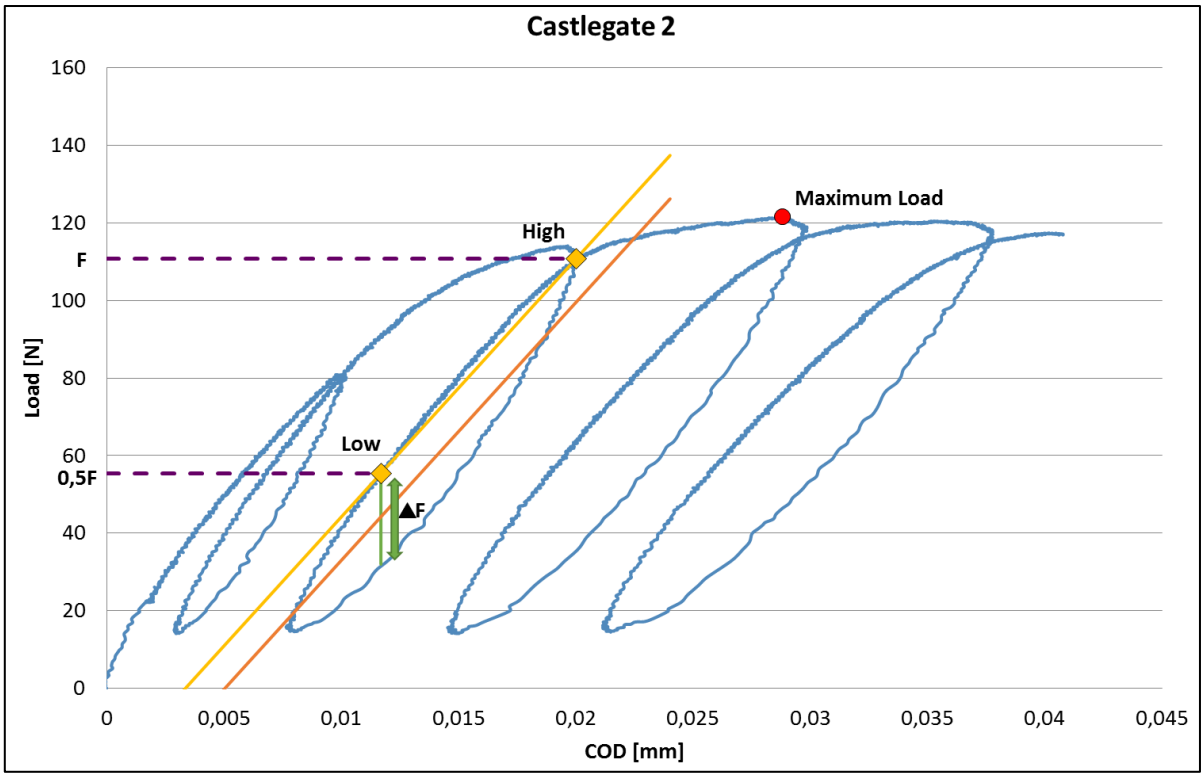

Figure 4-11: The principles for how to translate a line. The yellow line is the initial line one start with, while the orange line is a final linearized unloading line

A smooth approximation is drawn ignoring the unloading dips and connecting the two sides of the curve as if there is no unloading-reloading cycle. When the initial slope is used, the first slope shall not be translated. Each finalized line, designated as the final linearized unloading line in the Suggest Method, are then extrapolated at both ends. It is extrapolated downwards until it intersects the COD axis, and upwards until it crosses the smoothed load vs COD curve ignoring the dips of the cycles. The distance between the two lines where they intersect the COD axis, defines the residual displacement in an unloaded state. This difference is designated x_u and calculated.

The loads at the location where the lines intersect the load vs COD curve are labeled F_1 and F_2 respectively. Using these two values, an average load is found by

$$\bar{F} = \frac{F_1 + F_2}{2} \tag{4.6}$$

Should the span between these two loads include F_{max}, the largest of these is replaced with F_{max}. A horizontal line is drawn between the two finalized lines at this load, defining the displacement between two matching loaded states for the final lines. This displacement is designated x_l. Figure 4-12 illustrates how this is done.

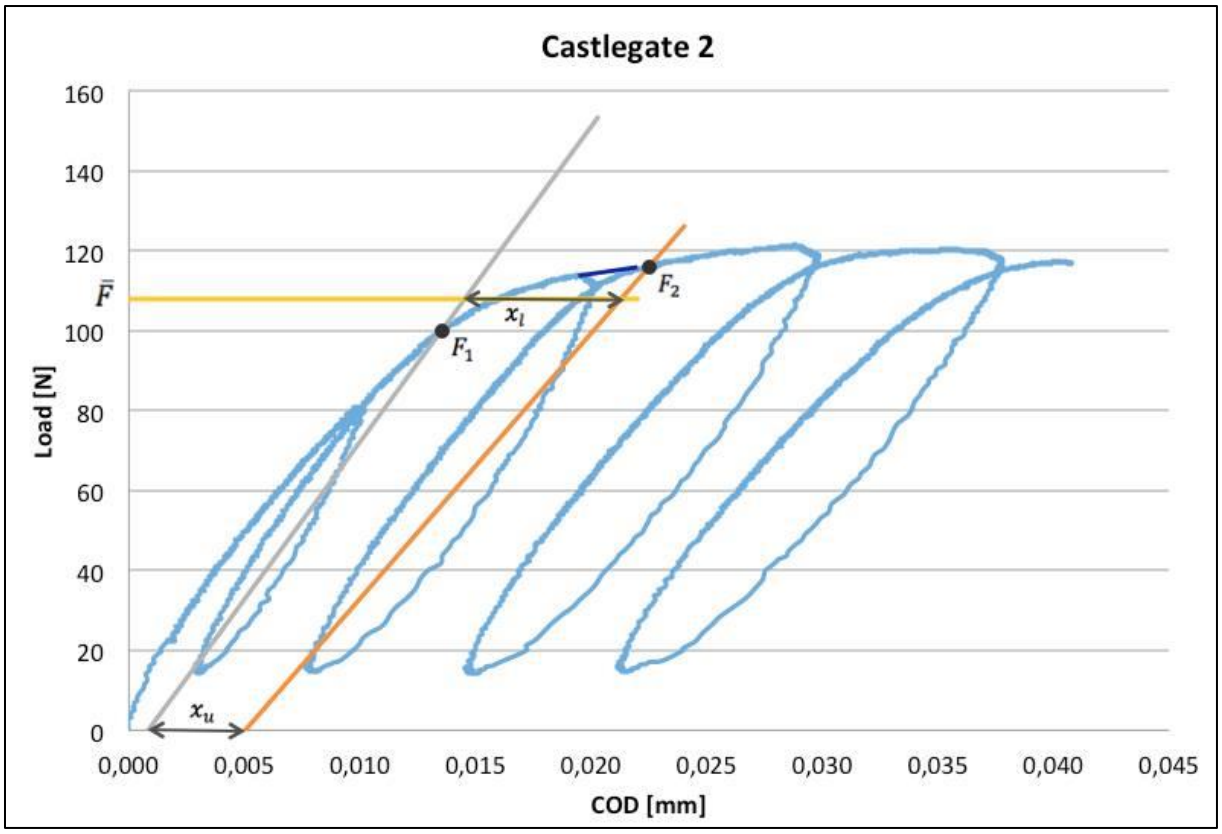

Figure 4-12: An illustration of how to find the displacement at zero loading and at the average load. The dark blue line shows a smooth approximation ignoring the cycle. These two values are chosen because they span the slope given by equation 4.5

The p-value can then be calculated as

$$p = \frac{x_u}{x_l} \tag{4.7}$$

This value defines the amount of non-linearity, and according to Barker (1979), it defines the amount of plasticity exhibited by the specimen between these two points**.** A value of 0 means that the fracture growth that occurred was completely elastic, experiencing no additional plastic deformation while a p-value of 1 represents a completely irreversible fracture growth. If the p-value ends up being negative or if it varies greatly between different specimens of the same origin, an error has most likely occurred during the evaluation. For large variations in the p-value, ISRM suggests a correction by using the average p-value over two or three cycles. If this is done, the system recorder settings should be changed. This technique was not applied here.

If the value of the average load is higher than 98% of the maximum load and at the same time the two chosen finalized lines span the evaluation point, the corrected fracture toughness is calculated as

$$K_{IC}^{C} = \left[\frac{(1+p)}{(1-p)}\right]^{0.5} K_{IC} \tag{4.8}$$

However, if either of these requirements is not met, linear extrapolation or interpolation, depending on the location of the evaluation point, shall be used to draw a line with a slope of s_c. The technique is the same, with linear extrapolation referring to a point located after the last cycle and linear interpolation referring to a point located between two finalized lines. Start by determining the horizontal distance along the COD axis, between the point where the second finalized line intersects the COD axis, and where the line intersects the curve. This distance is designated x_2. Next, find the location along the first line that goes through F_1 and that leads to a horizontal displacement of x_2 from where this line crosses the COD axis. This point is designated F_1'. Then draw a line between this point and F_2. Find the point along this line where the load is

$$F_e = s_c x_2 \tag{4.9}$$

Should the two lines not span the evaluation point, the line is extended beyond these two points until F_e appears on the line. The next step is to find the position along the COD axis that leads to a displacement of x_2 upon unloading for this new line. A line is then drawn between two points, F_e and the location along the COD axis, and possibly extended until it intersects the curve. By following the procedure correctly, this new line should have a displacement of x_2 upon unloading with a slope of s_c. The final step is to determine the load at the intersection between this line and the curve, F_c. Figure 4-13 shows how this is done for linear interpolation.

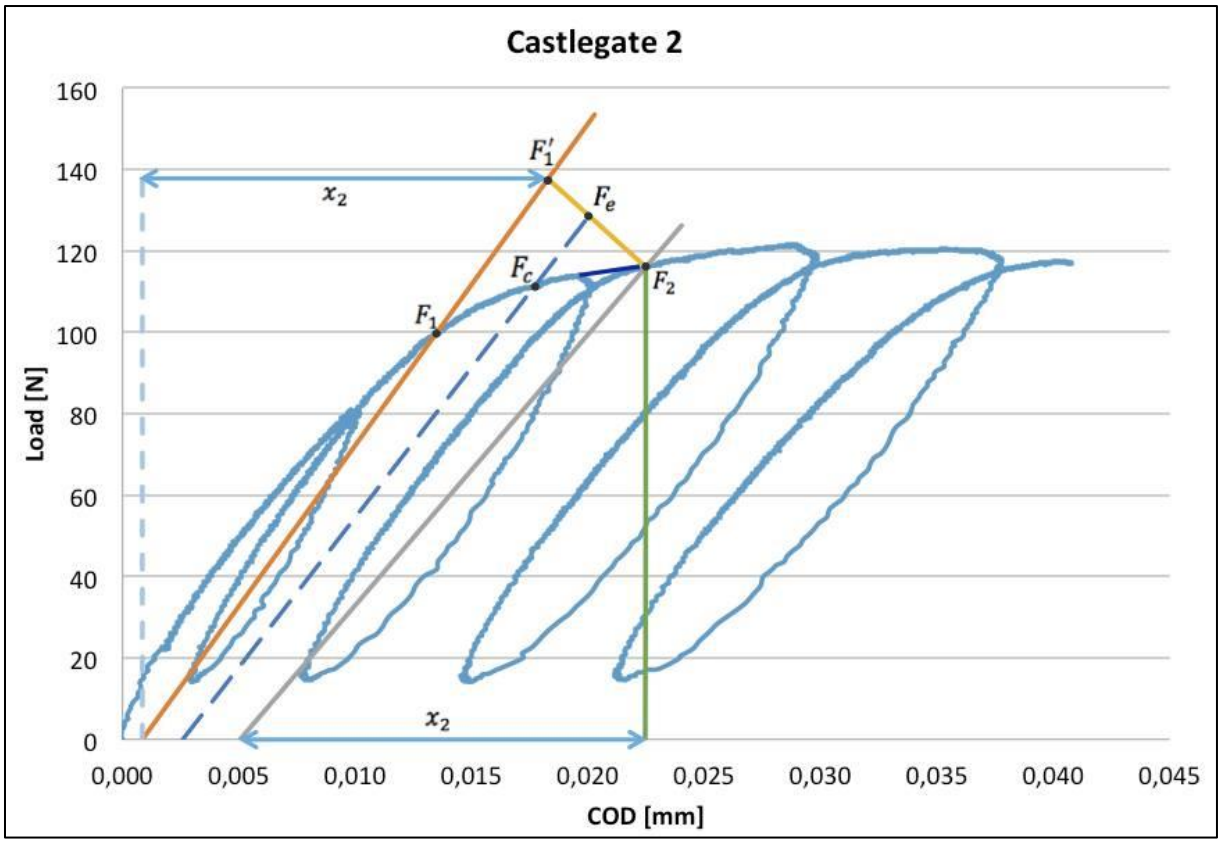

Figure 4-13: An illustration of how to find the corrected peak load with the relevant points shown for linear interpolation

This load, designated the corrected peak load or F_c, is used to calculate the corrected fracture toughness with the following equation

$$K_{IC}^{c} = \left[\frac{(1+p)}{(1-p)}\right]^{0.5} \frac{F_c}{F_{max}} K_{IC} \tag{4.10}$$

Young's modulus can be calculated if the load point displacement measuring equipment has been properly calibrated.

$$E = \frac{g_0 s_{\text{initial slope}}}{D} \tag{4.11}$$

Where

$$g_0 = 20.8 + 19.4\frac{a_0}{D} + 142.3\left(\frac{a_0}{D}\right)^2 \tag{4.12}$$

Here $s_{\text{initial slope}}$ is given in kN/mm and D in mm, such that Young's Modulus is given in GPa. This equation will only work for load vs LPD data.

4.4.4 The Plasticity Factor

Assume a specimen has been loaded to a certain point, A, along a load vs LPD/ COD curve and that a cycle is initiated at this point. The unloading slope is assumed to be elastic, with no further crack growth and with the amount of plastic deformation being negligible. If the deformation has occurred in a completely elastic fashion, the unloading slopes will lead back to the origin, as seen in Figure 4-14. Now, consider instead the same scenario, except that unloading lines lead to a point along the LPD/ COD axis, offset from origin due to some plastic deformation that occurred near the crack tip while the crack propagated. Next, imagine yet again the same scenario, but now the crack is allowed to propagate beyond point A to point B. Unloading from this point, using the same assumption as for the previous cycle results in the unloading line intersecting the LPD/ COD axis further away from the origin than the unloading line from point A. This occurs because of additional plastic deformation that takes place during crack propagation from point A to B. According to Barker (1979), it is assumed that the additional irrecoverable work that occurs is used up when creating this new crack area**.** In Figure 4-15 the additional work required to extend the crack from point A to B is shown. The p-value is in fact defined as the ratio of the two bases defined by the trapezoid seen in the figure. Barker noted that this value could be interpreted as the amount of plasticity exhibited by the specimen between two such points, point A and B. During testing, the p-value is determined from two such unloading slopes as presented in Figure 4-15. Considering Figure 4-14 again, this shows why the p-value is zero for elastic behavior; from a point B, the unloading will lead back to the same position as unloading from point A and hence there is no difference between these two points in an unloaded state. The reason that a F_c value is determined following this, is that the peak load, F_{max}, found from level I testing responds to a true LEFM sample. This does not represent the true peak load for elasto-plastic specimens. Instead, the two slopes used to determine the p-value can also be used to determine the location of the new peak load for elasto-plastic specimens, as seen in the procedure above.

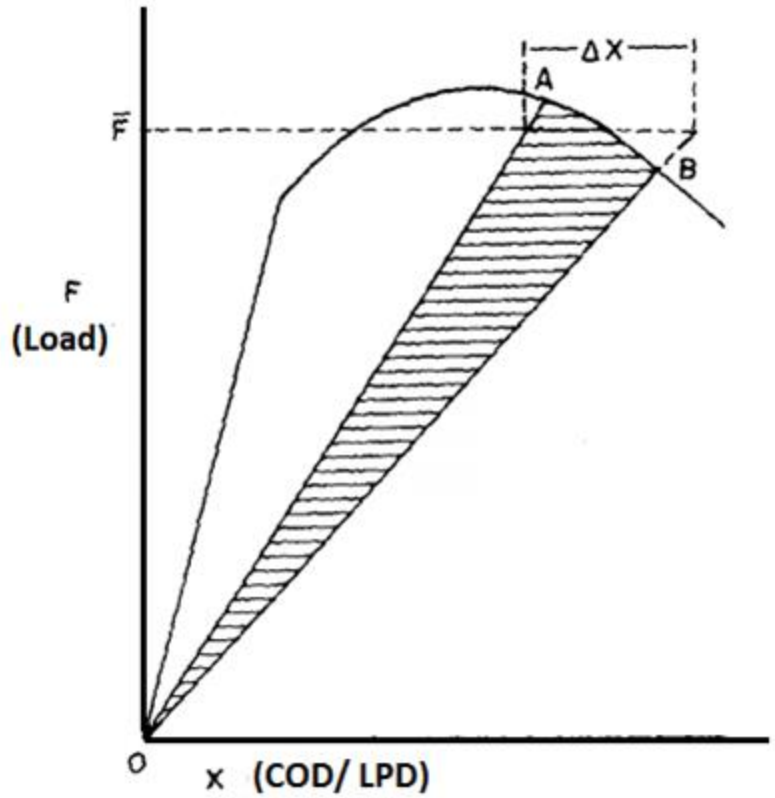

Figure 4-14: Elastic specimen behavior (modified from Barker, 1979)

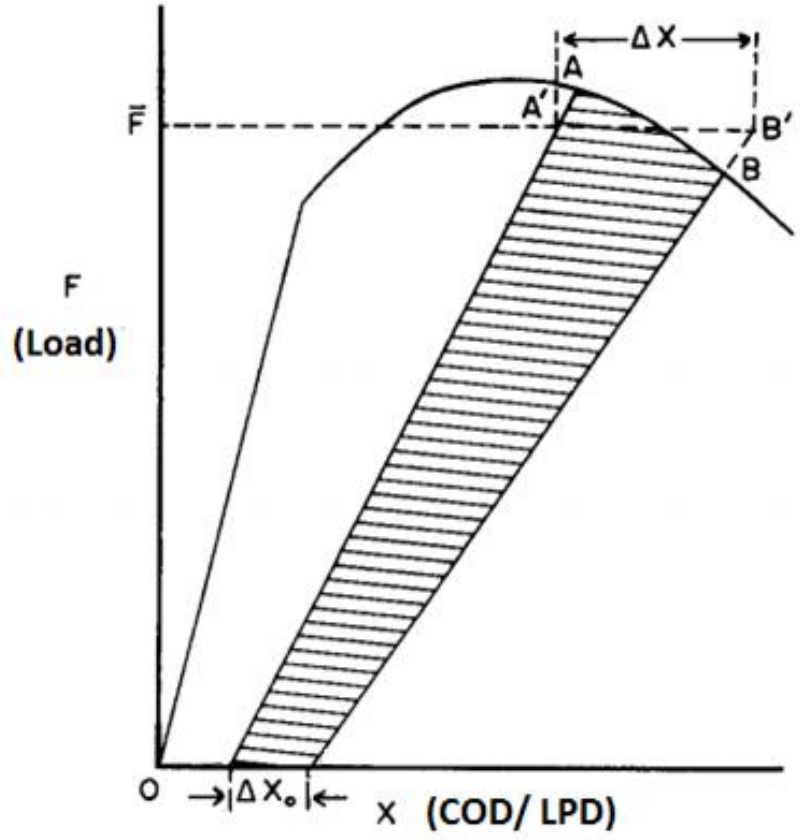

Figure 4-15: Elasto-plastic specimen behavior (modified from Barker, 1979)

5 Results

The Suggested Method for CB primarily focuses on the use of LPD data when determining the corrected fracture toughness, however it does allow for the use of COD data. As mentioned above, both Backers (2004) and Funatsu et al. (2004) use this type of data. For the determination of fracture toughness, both methods were utilized, however, the focus ended up being on the COD data for a number of reasons that will be explained later. Appendix 11.2 contains a summary of all relevant data for each specimen, including uncorrected and corrected fracture toughness, p-values and sample dimensions. The fracture toughness values are generally very low, as expected based on the rock types being classified as weak to very weak rocks, and their order of magnitude is in agreement with other known values from the literature (Whittaker et al., 1992, Backers, 2004, Ouchterlony, 1988).

Some of the specimens tested for chalk and sandstone had a different loading rate than the majority. This is a result of running the system manually, as some of the tested loading rates either went too fast for proper control or too slow, such that it would take a very long time to complete the experiment. However, based on the data there appears to be little differences between the results for different loading rates, and the differences that do occur is most likely a result of the nature of the rock and not the loading rate. Similar results are given in Backers (2004). The loading rate will briefly be mentioned when changed, and if there are any differences.

5.1 Fracture Toughness for Mons Chalk and Castlegate Sandstone

5.1.1 Determined from Load vs COD

Figure 5-1 and Figure 5-2 shows both the uncorrected and corrected fracture toughness for all samples of Mons chalk and Castlegate sandstone, including average values for the fracture toughness for the corresponding specimens and sample diameter. There is a clear correlation between the size of the sample and the uncorrected fracture toughness, and this is more evident for chalk than sandstone. The uncorrected fracture toughness increases with the size of the specimen for both the chalk and the sandstone. The scatter of the data points are much larger for the former than the latter, i.e. it appears that the chalk increases more with increased specimen size than the sandstone. However, due to the scatter of the chalk it is difficult to say if this is actually the case. The corrected fracture toughness for chalk is less scattered and still show a clear size effect, as the smaller sample yield lower values. For sandstone, the opposite occurs as the scatter increases somewhat compared to uncorrected values. There appears to be

little distinction between the smaller and larger specimens, with the average value being a little higher for the small specimens than for the large ones. Table 5-1 summarizes the data for both.

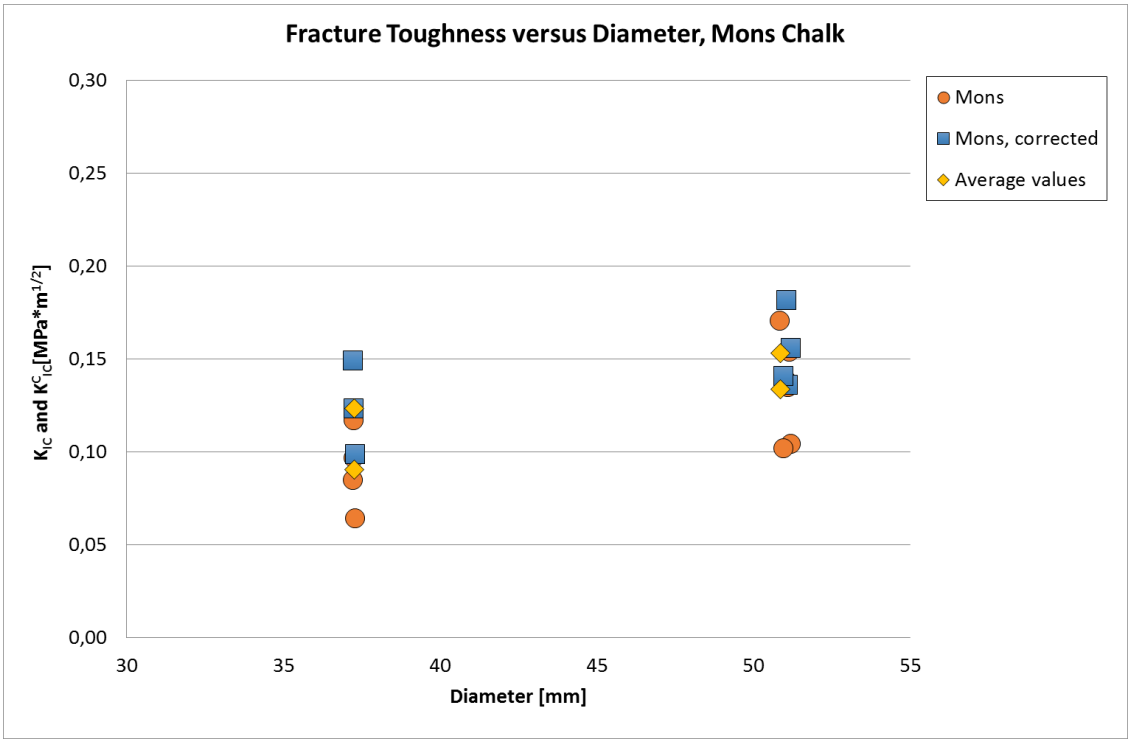

Figure 5-1: Uncorrected and corrected fracture toughness for Mons chalk using load vs COD data

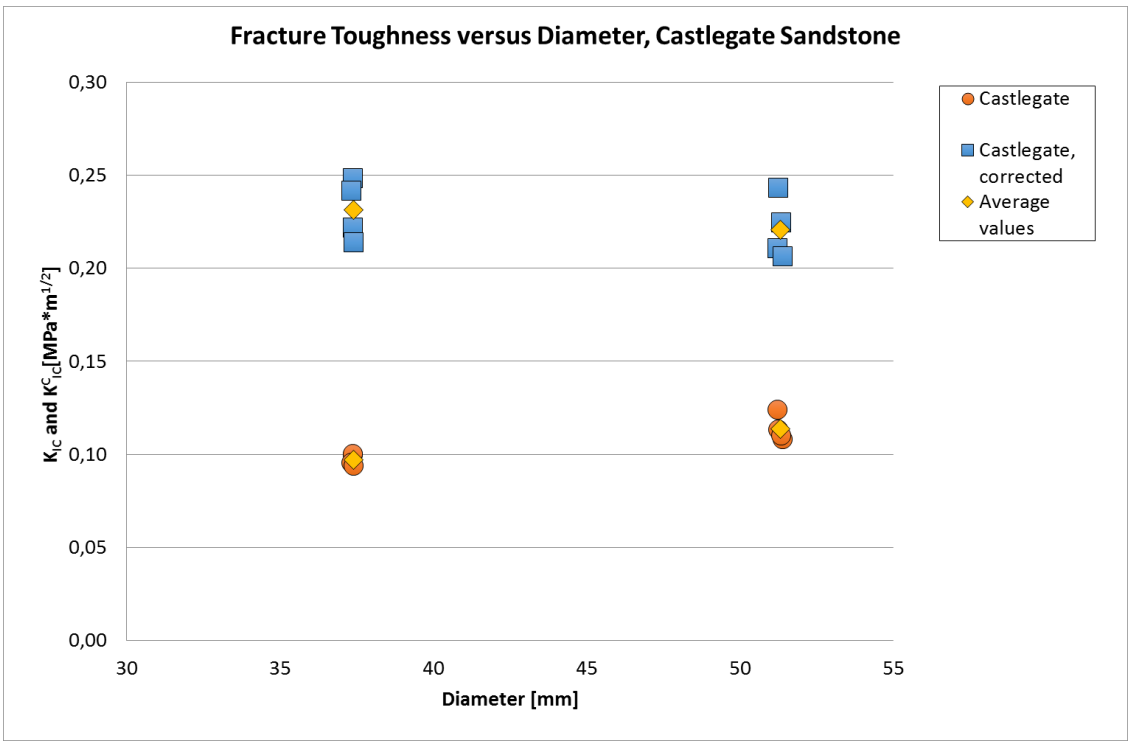

Figure 5-2: Uncorrected and corrected fracture toughness for Castlegate sandstone using load vs COD data

	K_{IC}	p	K_{IC}^{C}
Mons, 50 mm	0.134±0.027	0.30±0.16	0.153±0.020
Mons, 38 mm	0.091±0.022	0.49±0.14	0.124±0.025
Castlegate, 50 mm	0.114±0.007	0.65±0.02	0.221±0.017
Castlegate, 38 mm	0.097±0.003	0.76±0.03	0.231±0.016

Table 5-1: Mode I fracture toughness data for Mons chalk and Castlegate sandstone using load vs COD. Uncorrected fracture toughness is also included

An inspection of the entire range of p-values for all sizes and specimens show that chalk varies greatly, ranging from 0.08 to 0.63 while the sandstone varies between 0.62 and 0.80. However, comparing only samples of the same size greatly reduces these variations. Here the larger chalk varies between 0.08 and 0.44, the smaller chalk varies between 0.31 and 0.63, the larger sandstone varies between 0.62 and 0.67 and the smaller sandstone varies between 0.73 and 0.80. Thus, the sandstone samples shows very little variation of their p-values. The chalk with a p-value of 0.08 appears to be an anomaly as most of the other larger samples show significantly higher values with the second lowest being over 3.5 times as large.

An explanation for the variation of the p-values for the smaller chalk samples might be the different loading rates used. Backers (2004) saw that a higher loading rate resulted in lower p-values. However, no clear trend is seen here between the loading rate and the p-value for the chalk, the p-value for the sample with the largest loading rate is located in-between the other p-values and not as an extremity. The resulting corrected fracture toughness show no clear trend either. Similarly, one Castlegate from each of the two specimen sizes were tested at different loading rates. The difference between them and the other values is quite small, but it might indicate that a lower loading rate results in an increase of the uncorrected fracture toughness. It should be mentioned that the differences are so small, they are more than likely connected to the nature of the rock themselves. Corrected fracture toughness values show no effect of the loading rates.

Only some of the Castlegate sandstones have stable crack propagation throughout the entire experiment, even a long time after the peak load is reached**.** The specimens where this occurs includes one of the samples with a diameter of 50 mm and all of the specimens with a diameter of 38 mm. Additionally, the peak load occurred at roughly the same clip gage opening for all Castlegate specimens, at displacement of around 0.03-0.04 mm. The peak load differs for the different sample sizes, but the variation within the two sizes are small. The chalks stable crack propagation stopped shortly after reaching their maximum load. Almost immediately

thereafter, most samples failed abruptly and catastrophically. The maximum load occurs between 0.003 and 0.012 mm for all samples, but the scatter is larger here than in sandstone as the relative opening for chalks are much smaller. As with the sandstone, the maximum load varies between the two sizes tested, but there is greater variation within the two specimen sizes of chalk compared to the sandstones. The maximum load of the strongest and weakest of the chalks differs by more than 70 N for the larger specimens while the difference for the smaller specimens is just below 40 N. This is significant compared to how weak these samples are.

The corrected peak load tends to be located before reaching the maximum load, agreeing well with the procedure, where it is stated that the evaluation point typically will lie before the maximum load for tests on small and soft specimens.

To investigate the p-values and its variance, the p-value is calculated for all slopes from the load vs COD data. The sandstones are selected as the results appear to be more consistent with the method, the individual experiments appear to have been correctly reproduced and there seems to be fewer issues with the data. Barker (1979) states that the p-value is not a specimen constant, it varies to some extent with crack length. The plasticity factors calculated herein yields support to this. All samples show varying p-values, where all values are high, from 0.60 to 0.9. The difference between the upper and lower plasticity factors within a sample is at most 0.2, and there is no apparent trend between the location of the points, i.e. early slopes or late slopes, and the size of the plasticity factor. Further, the changes of the p-factor does not occur in a specific overall pattern.

5.1.2 Determined from Load vs LPD

To investigate the difference between following the procedure using LPD data as opposed to COD data, both methods are tested. The results from using load vs LPD data is shown in Figure 5-3 and Figure 5-4 for chalk and sandstone respectively. One thing easily spotted is that there are fewer corrected fracture toughness values for the chalk compared to in Figure 5-1. The same procedure is used in both occasions. However, when the load vs LPD data is used, some samples experience an increase of the subsequent slopes determined from the cycles compared to the initial slope. As a result, the evaluation point occurs later along the curve, in several cases long after the peak load is reached. This is further complicated with the abrupt failure of the chalk often seen to occur not long after the peak load is passed. Because of this, it is not possible to determine the corrected fracture toughness for many of the samples. A possible explanation for the behavior seen, is given later. Further, the results from one sample are left out as the

corrected fracture toughness is calculated as being lower than the uncorrected value. According to Sun et al. (2001) such behavior is unreasonable and therefore the value is left out. For this particular plot, the curve itself is ambiguous in the moments leading up to the first cycle, where the slope of the curve appears to shift several times, making it very difficult to properly determine the corrected fracture toughness. For the sandstone specimens, all values are calculated but one is left out due to it giving a corrected fracture toughness lower than the uncorrected. These samples exhibit some of the same behavior as the chalk, regarding the slope increase. Despite this, there are no problems with the determination of the corrected fracture toughness.

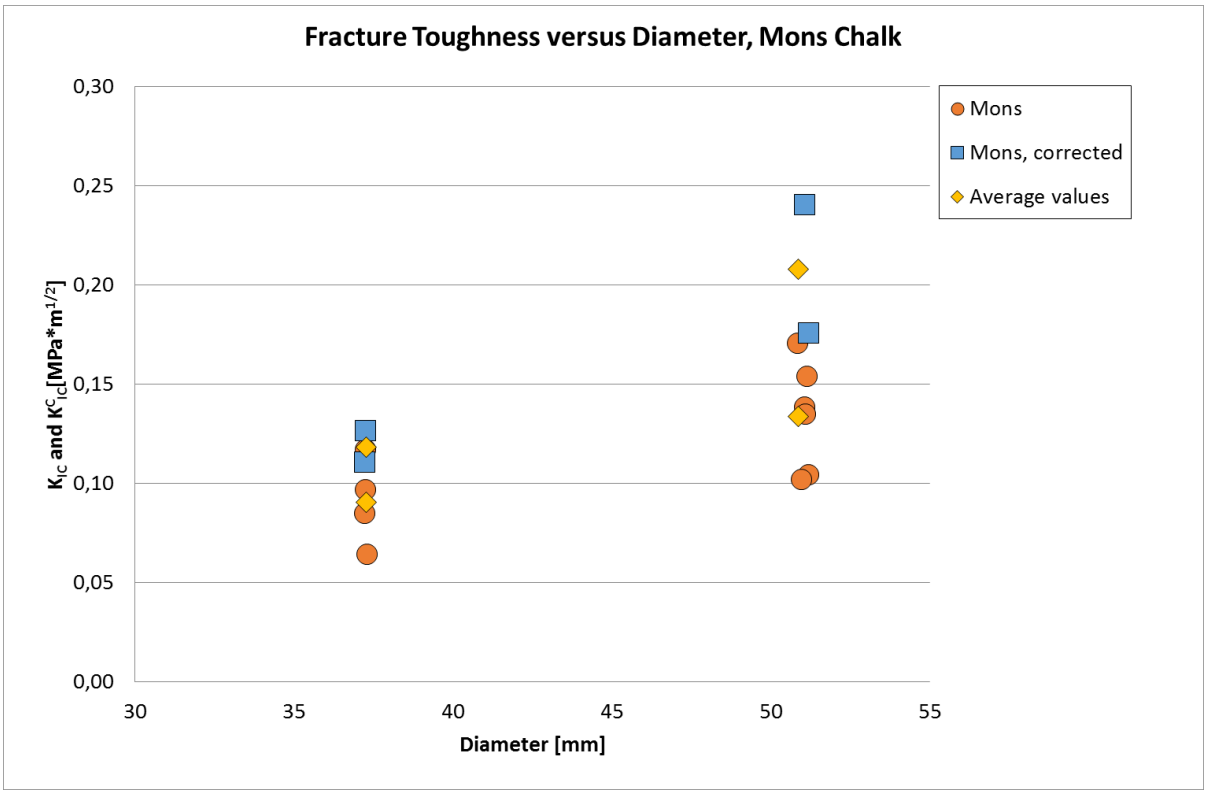

Figure 5-3: Uncorrected and corrected fracture toughness for Mons chalk using load vs LPD data

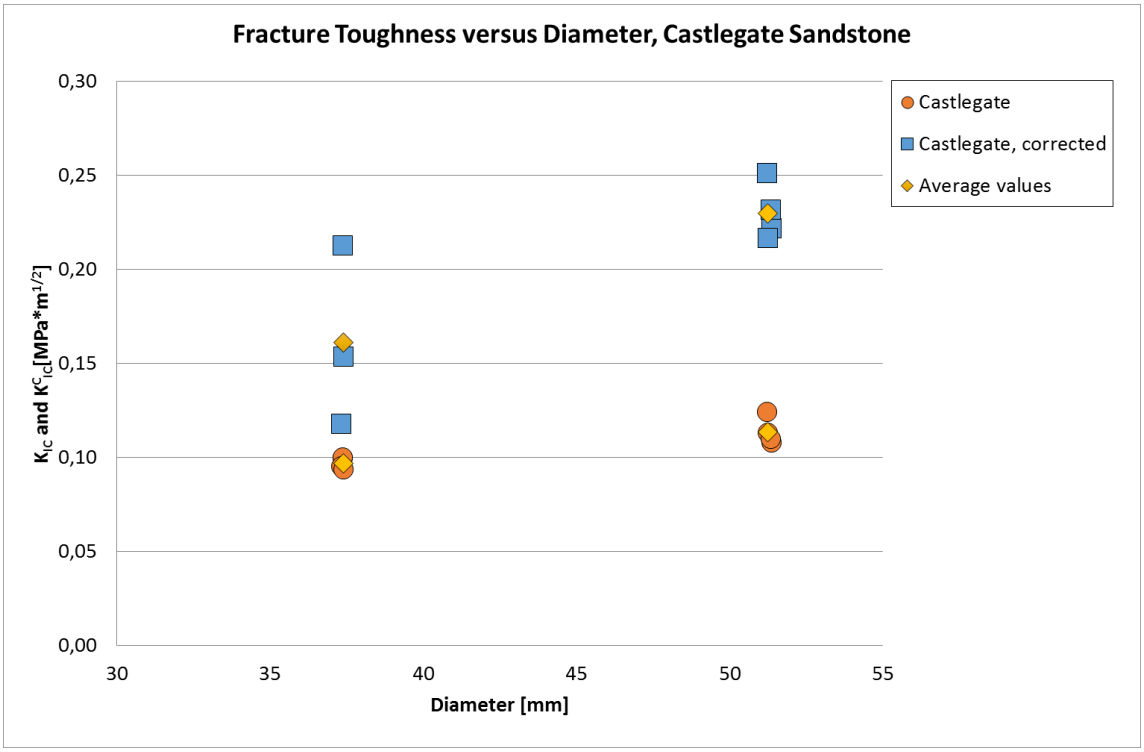

Figure 5-4: Uncorrected and corrected fracture toughness for Castlegate sandstone using load vs LPD data

Table 5-2 shows the mean values for the fracture toughness and the standard deviation for all samples of chalk and sandstone. Included are the mean p-values as well as its standard deviation. The results from one sample are questionable due to abnormal behavior along the load vs LPD curve, but the results are included in the calculation of the values for Table 5-2. The p-values for chalk are based on most samples, and not only the two where a complete determination is possible, as the p-value is calculated based on the two slopes located nearest to the evaluation point. Thus, p-values for chalk are obtained, even though it is not possible to find the corrected fracture toughness for several of the chalk specimens. It is obvious that the p-values deviate from the related dataset for the load vs COD data, seen in Table 5-1. The larger chalk values are generally higher than the corresponding values found using load vs COD, while the smaller chalks are lower. There are no significant differences between the span for the p-value when the two methods are compared for the larger specimens, but the smaller chalk has a substantially lower standard deviation. The mean values for the sandstone are similar, but the standard deviation is larger for the smaller samples, i.e. the opposite of the results from chalk. The corrected fracture toughness values for chalk and sandstone show a scatter similar to the load vs COD data. One difference is the fact that both rocks show signs of a more clear size effect for corrected fracture toughness and not only the chalk. The corrected fracture toughness is clearly higher for the specimens with the largest diameter.

	p	K_{IC}^{C}
Mons, 50 mm	0.57±0.19	0.208±0.046
Mons, 38 mm	0.36±0.01	0.118±0.011
Castlegate, 50 mm	0.67±0.06	0.230±0.015
Castlegate, 38 mm	0.71±0.20	0.161±0.048

Table 5-2: Mode I fracture toughness data from load vs LPD

There appears to be little difference between the two chalk samples with a diameter of 38 mm. As mentioned previously, two different loading rates were used, but as the other two samples did not produce results, it is difficult to relate the differences to the loading rate, as the difference between the two p-values and corrected fracture toughness are very small, close to negligible. The larger chalk also used different loading rates, and here the differences are larger. However, as the results from chalk are seen to vary, it is not possible to relate this to the loading rate. The same is seen for the sandstones where the loading rate is changed; there is little to no difference between the calculated values.

The position of the peak loads resembles the results from load vs COD. The sandstone has a fairly consistent location of the peak load, appearing on the LPD axis at a displacement of 0.065 mm to 0.075 mm for the majority of the samples. A larger scatter is seen in the chalk data. The peak load appears anywhere from 0.01 mm to 0.04 mm along the LPD axis, with a large part of the samples gathered around 0.01 mm to 0.02 mm. A correlation with the loading rate is not seen.

5.2 Fracture Toughness for Mancos Shale

The results for the uncorrected and corrected fracture toughness are seen in Figure 5-5 and Figure 5-6**,** respectively. Both includes the results for specimens with their notch cut parallel and perpendicular to the bedding planes. Each figure only includes one result for each test, with the exception being at zero inclination where multiple samples were tested to see if the gluing method had worked and one extra sample for the case of a perpendicular notch for an inclination of 45°. The reason for the latter was that the first sample had an accident where it was dropped from a height of 15 cm above a table and due to this, the sample might have been altered, affecting the results. Some values are missing in the figures due to the test being inconclusive, i.e. the sample broke where it had been glued together and no determination could be attempted. One exception is done to this. The uncorrected fracture toughness for the specimen with an inclination angle of 90° and the notch cut perpendicular to the bedding. Here the glue broke at around the same maximum load as the parallel notch of the same inclination. Since it was the

glue that failed and not the sample, it is assumed that the sample itself would have at least a similar - if not stronger - peak load and the calculation of the uncorrected fracture toughness is done with the load the glue failed at. However, this value is strictly of no use other than to give a possibly more complete picture of the anisotropy effect. The glue failed on one other occasions as well, but this occurred at such a low load that it is impossible to extract any information from the test.

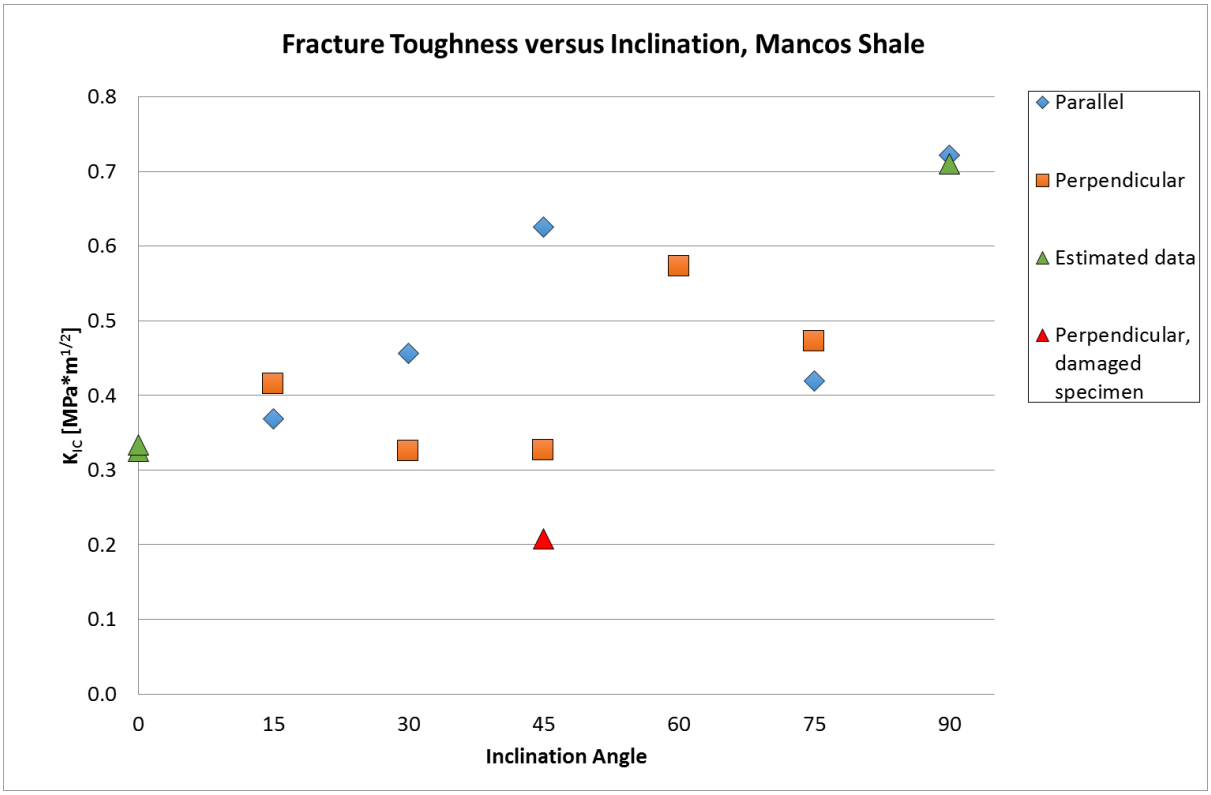

Figure 5-5: Uncorrected fracture toughness for Mancos Shale for notches parallel and perpendicular to bedding. The estimated data at 90° is for a perpendicular specimen

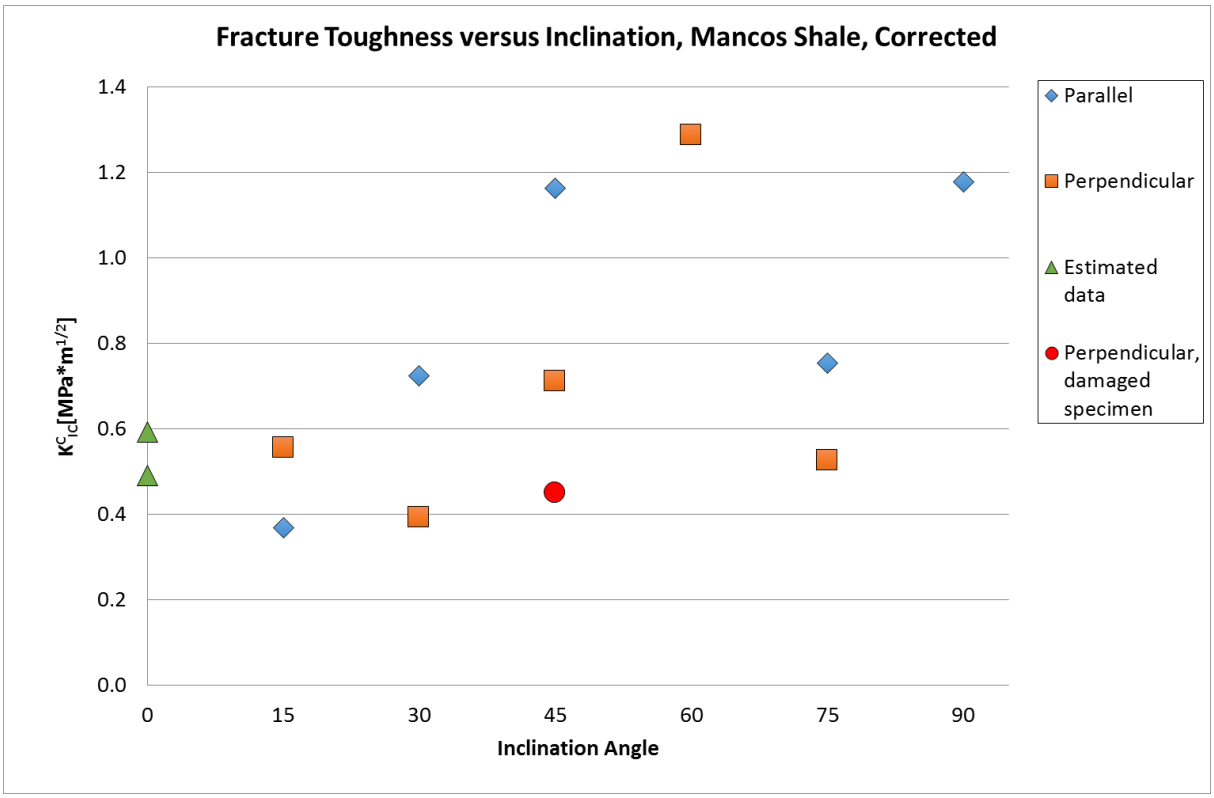

Figure 5-6: Corrected fracture toughness for Mancos shale for notches parallel and perpendicular to bedding

The effect of anisotropy is clearly shown in Figure 5-5 and Figure 5-6, however, to what extent the fracture toughness develops is more difficult to tell, as it could be both increasing and U-shaped. Notches parallel to bedding appears to either increase with inclination angle – except for the specimen with an inclination of 75°, or it can also be U-shaped with a peak load at around 45° and an exceptionally strong specimen at 90°. Both figures show this. Similarly, for notches perpendicular to bedding an U-shape might also exist with a low point at around 30-45° for uncorrected fracture toughness. It can also be that these samples are less affected by the inclination angle prior to reaching an inclination of 45° for uncorrected fracture toughness, and that they then show an increasing tendency. However, such trends are less clear in the corrected fracture toughness data, where the majority of the samples are varying between 0.4 and 0.7 MPa*$m^{1/2}$ with a particularly high value at 60°. A possibility here is that the trend is much more complicated than an U-shape or increasing trend. The trends seen here is not conclusive because several of the experiments were unsuccessful.

Throughout all samples, the specimens have p-values ranging from 0.43 to 0.78 for the perpendicular notches and from 0.49 to 0.70 for the parallel notches. The p-values are generally higher from inclinations of 45° and above, see Figure 5-7. There is no apparent trend regarding the peak load of the different samples.

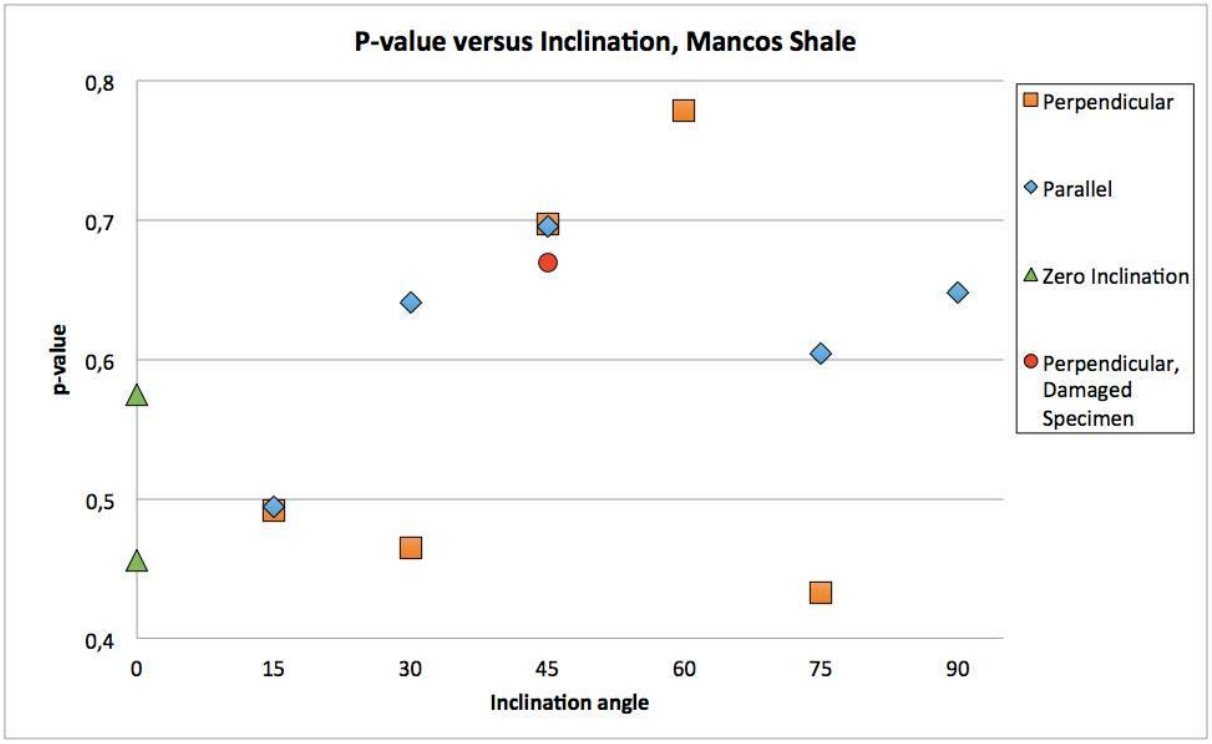

Figure 5-7: Plasticity factor variation for Mancos shale at different inclinations

It appears that on three out of four occasions where both notch types were measured, the trend between uncorrected and corrected fracture toughness is the same, i.e. that the uncorrected and corrected value of a notch parallel to bedding lies above the corresponding values for the sample with a notch perpendicular to bedding and vice versa. The one exception to this occurs at 75°. Here the opposite occurs. The parallel notch is the lower of the two based on the uncorrected fracture toughness, but it is the larger when applying the correction factor. It is possible that there is a correlation between this difference and the fracture patterns. The fracture patterns are investigated later.

Parameters for Mancos shale are not derived using the load vs LPD data. The reason for this is that the data is not good enough, as it produced flat sections at the bottoms of the cycles and the curvature of the reloading sections appears to behave exponentially before it flattens out towards the upper part. Figure 5-8 shows a typical plot for Mancos shale using load vs LPD. Note that some of them behave worse than this, but that this particular plot shows both trends very good.

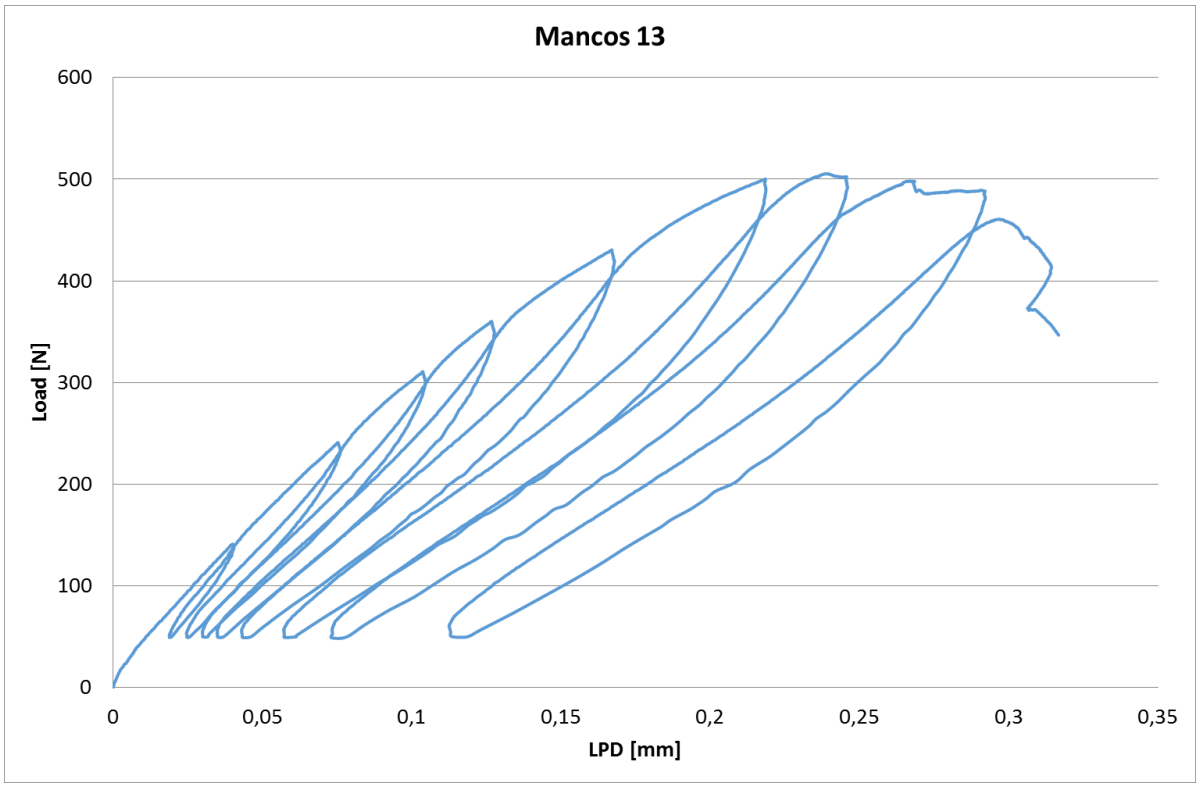

Figure 5-8: Load vs LPD for Mancos 13 shoving some of the difficult trends seen in shale when using load vs LPD

5.3 Fracture Patterns of Mancos Shale

During the CB tests, it became clear that the notches cut perpendicular to the bedding had a different fracture pattern than the ones cut parallel to the bedding. Figure 5-9 and Figure 5-10 shows the fracture patterns from the resulting experiments. The following explanation does not necessarily reflect the order the fractures propagated, but is simply an explanation of the final path seen after the experiments were completed**.** The fractures from notches parallel to bedding leave the chevron notch at the corner tip and then the fractures propagate straight through the sample, across the bedding planes. At times, the fracture briefly follows the boundary between two bedding planes for some samples. In Figure 5-9, part B30, an example of this is seen. The fracture exit the notch inside of a bedding plane, and it realigns itself after a certain distance such that the fracture follows the boundary of two planes, although shortly. The only exception to this is the specimen with an inclination of 75°. Here the fracture leaves the notch not at the corner tips, but in the middle. Other than that, the behavior is the same with the fracture going right through the specimen.

The behavior of the samples with notches perpendicular to bedding deviates strongly from this. The fractures exit the chevron notch either close to the corner tips or along the wall.

It then follows the boundary of two bedding planes. This occurs for all samples from 15° to 60°. At 75°, the behavior resembles the behavior seen for the parallel samples. The fracture exit at the corner tip of the notch, on one side of the specimen the fracture cuts right through the bedding planes, while on the opposite side it appears as the fracture briefly attempts to follow the bedding planes before realigning itself and cut through. Concurrently with this, this particular specimen's p-value is the lowest out of all the Mancos shale tested, resulting in a significantly smaller increase when calculating the corrected fracture toughness.

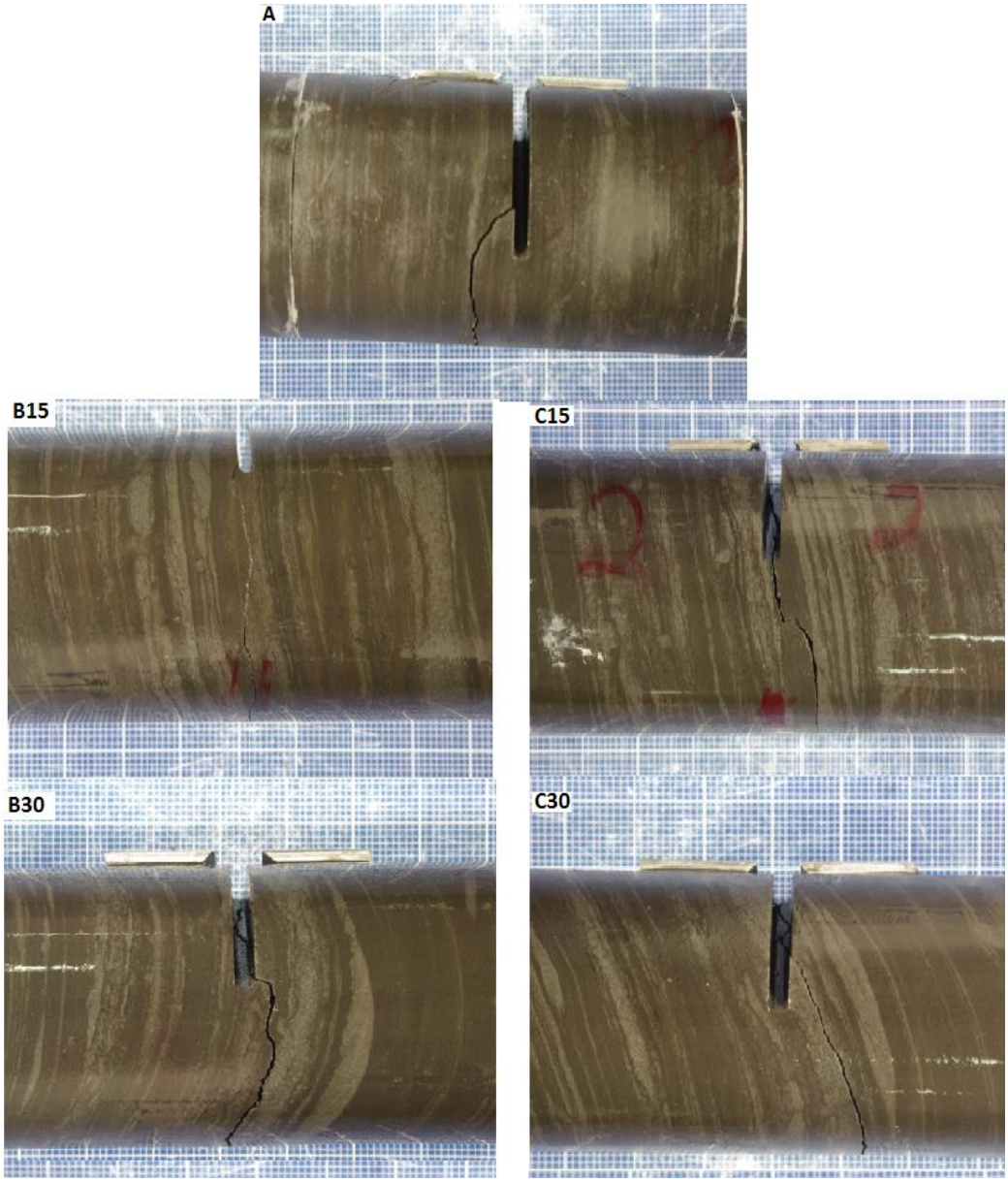

Figure 5-9: Pictures of fracture pattern for Mancos shale for inclinations 0-30°. A: Specimen with 0°, B: notch cut parallel to the bedding planes, C: notch cut perpendicular to the bedding planes. The numbers refers to the inclination

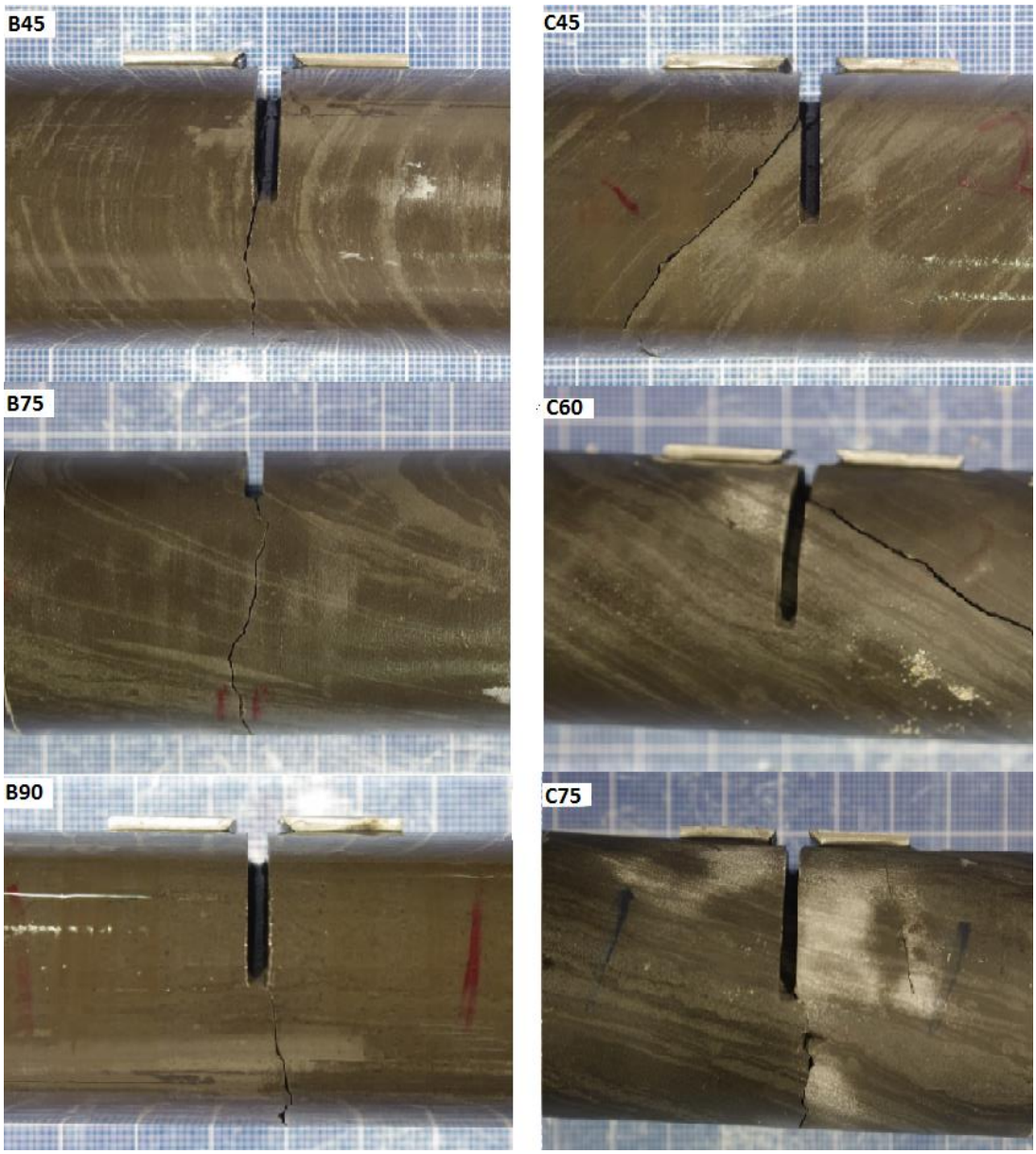

Figure 5-10: Pictures of fracture pattern for Mancos shale for inclinations 45-90°. B: notch cut parallel to the bedding planes, C: notch cut perpendicular to the bedding planes. The number refers to the inclination. Some numbers are missing because of unsuccessful experiments

5.4 Calculated Energy Release rate and Young's Modulus

With equations 2.9 and 4.11, the Young's modulus and corrected energy release rate are calculated. The energy release is calculated for both methods used, i.e. using load vs COD and load vs LPD results. Young's modulus is only calculated for the data from load vs LPD, thus no results are available for the Mancos shale in this case. Table 5-3 summarizes the results for chalk and sandstone for the calculated corrected energy release rate, showing the respective means and standard deviations. The energy release rate matches fairly well between the two methods for chalk specimens of a diameter of 38 mm and sandstone specimens with a diameter

of 50 mm, with both the mean and the standard deviation being relatively close. Chalk, with a diameter of 50 mm, is almost twice as large for load vs LPD compared with load vs COD. However, the data here suffers from few data points. The data for the small sandstone specimens does not match. The results from load vs COD are over twice as high, highlighting the differences seen in the two methods. Generally, the calculated energy release rate show the same results as the corrected fracture toughness data, highlighting the features seen, including size effect. The calculated corrected energy release rate show a clear size effect for the load vs LPD data, where both of the smaller samples clearly have lower energy release rates than the larger samples. For load vs COD, a minor size effect is seen for the chalk with increasing energy release rate for increasing specimen diameter. Sandstone yields somewhat higher values for the smaller samples, but the *relative* difference is not large. Because of the anisotropic properties of the Mancos shale, it is not possible to calculate a corrected energy release rate as the Young's modulus is not known for the different inclinations. The corresponding energy release rate for each specimen is listed in Appendix 11.2.

	G_{IC}^{C} [J/m^2], COD	G_{IC}^{C} [J/m^2], LPD
Mons, 50 mm	4.71±1.28	8.75±3.77
Mons, 38 mm	3.10±1.24	2.78±0.52
Castlegate, 50 mm	24.43±3.75	26.46±3.57
Castlegate, 38 mm	26.76±3.74	13.70±8.01

Table 5-3:Calculated energy release rate based on corrected fracture toughness for chalk and sandstone, using both load vs COD data (left) and load vs LPD (right)

The calculated Young's modulus for chalk and sandstone is listed in Table 5-4. Based on the values given in Table 4-1, the calculated mean value for chalk overestimate the Young's modulus. It should be noted that the standard deviation for both samples is quite high and there appears to be no correlation between the calculated values and the different loading rates used. However, the values for sandstone is slightly underestimated by the small specimens, while the average of the large specimens fits well with the Young's modulus given in Table 4-1. Note that one of the larger specimens gives a somewhat higher Young's Modulus than the rest. This had a slightly lower loading rate. If the result from this is excluded from the average and standard deviation values, the average value become 1.70 +/- 0.21 GPa, which is a slight underestimate. However, this fits well the expected results. According to the Suggested Method, one should expect an underestimate of E due to the nonlinearity behavior of the samples. Loading rate appears to have minimal effect for the smaller sandstone tested at a different rate

than the others. All values are based on all samples, including those that did not result in corrected fracture toughness.

	E [GPa]
Mons, 50 mm	6.65±4.12
Mons, 38 mm	7.75±6.52
Castlegate, 50 mm	2.00±0.62
Castlegate, 38 mm	1.46±0.11

Table 5-4: Calculated Young's modulus for chalk and sandstone

5.5 Fracture Toughness vs Tensile Strength

Concurrently with the work of this thesis, a separate testing program was conducted measuring the direct tensile strength of the same rock types (Jensen, 2016). Initially, it was suggested to determine an empirical correlation between the direct tensile strength and the fracture toughness, but due to the limited amount of rock types tested, this option was not pursued. Instead, correlations found in the literature study, from Zhang et al. (1998), Zhang (2002), Whittaker et al. (1992) and Backers (2004), are applied. Their respective correlations are seen in Table 3-2. Further, as most of these correlations have been found using the tensile strength from Brazilian tests, data from such experiments are also used. The tensile strength data from Brazilian tests is given in Table 4-1 and Figure 4-4 for Mons & Castlegate and Mancos respectively, while the direct tensile strength is given in Appendix 11.3.

Both uncorrected and corrected fracture toughness are used, for the latter both test pools are utilized to see if any of them correlates better than the other. This is done as several of the correlations do not specify if uncorrected or corrected values are used. Backers (2004) correlation is based on corrected fracture toughness. Mancos shale data is only available for the load vs COD. Figure 5-11 and Figure 5-12 show the results for corrected fracture toughness from load vs COD in relation to the direct tensile strength and tensile strength from Brazilian tests respectively. In addition to being the best match, the corrected fracture toughness is more accurate than the uncorrected and the data set from load vs COD is more complete than the set from load vs LPD. For chalk and sandstone, the average values are used for both sizes.

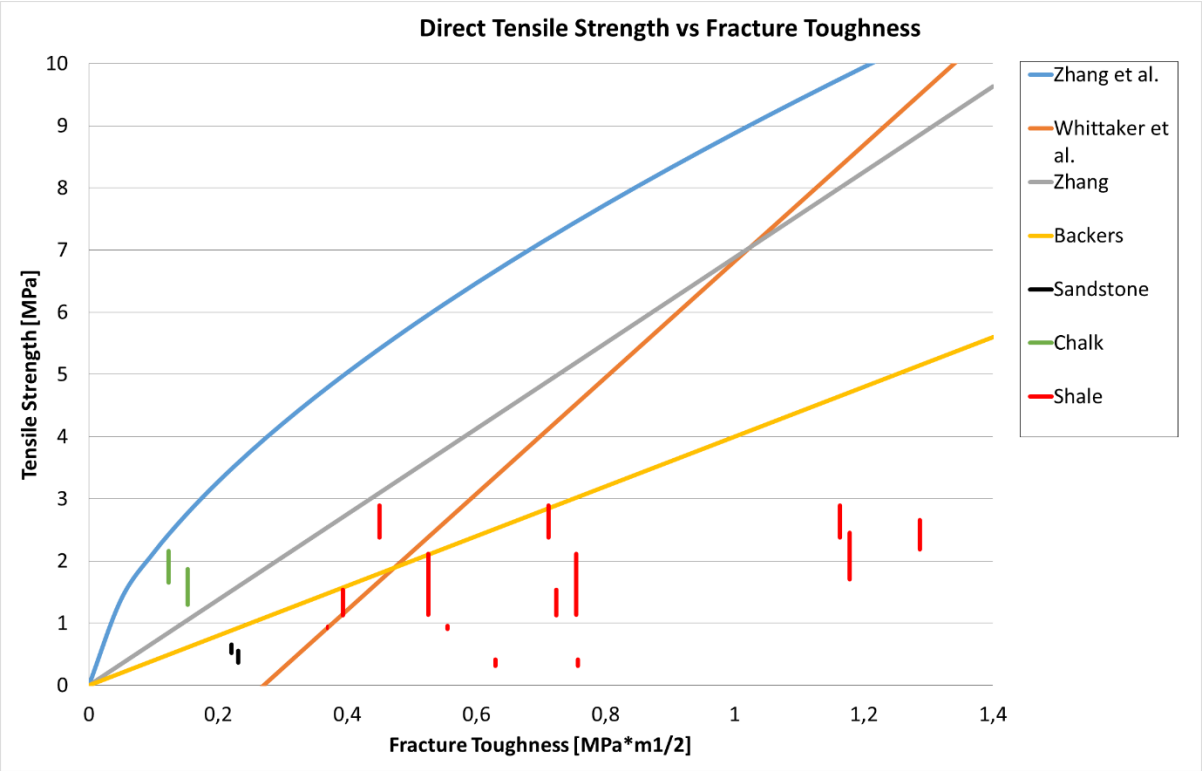

Figure 5-11: Direct tensile strength vs corrected fracture toughness compared with known correlations

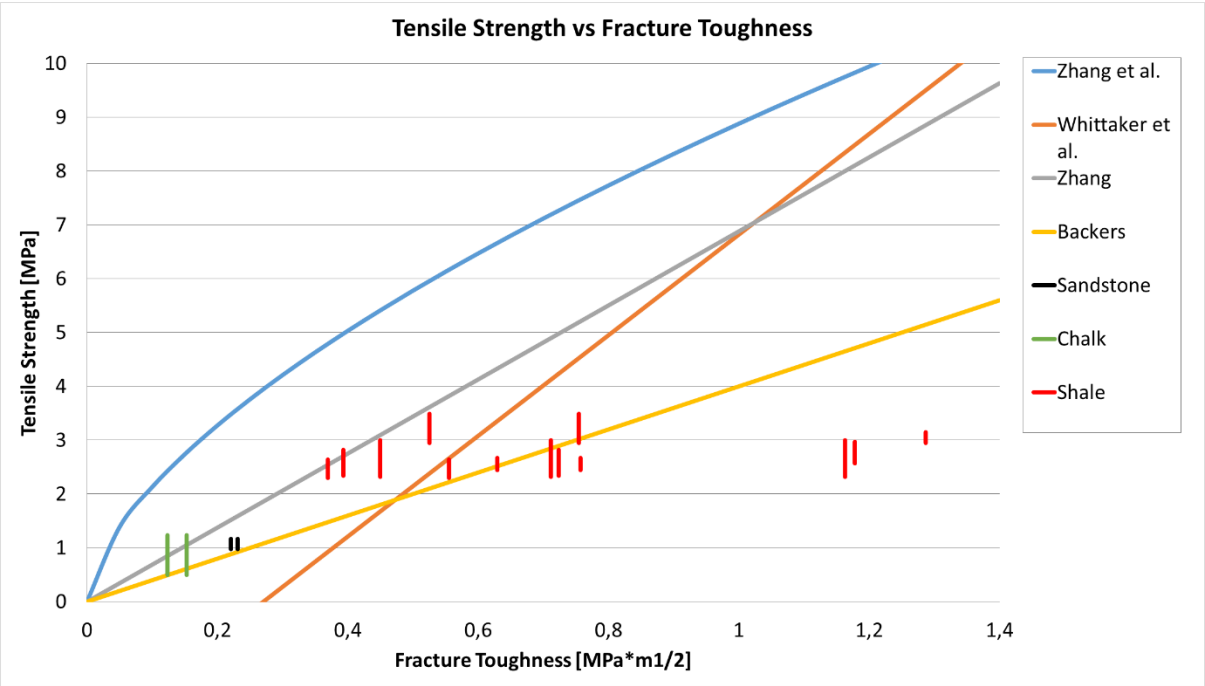

Figure 5-12: Tensile strength from Brazilian tests vs corrected fracture toughness compared with known correlations

On a general basis, the correlations used provide poor matches for all the data obtained. Particularly, the correlations of Whittaker et al. (1992) and Zhang et al. (1998) barely provide any matching values at all, independent of using the direct tensile strength or the tensile strength obtained from Brazilian tests. Both of them highly overestimate the actual values. The correlation of Zhang (2001) and Backers (2004) are better, and both correlates fairly well with chalk and sandstone for both the direct tensile strength and the tensile strength from Brazilian tests. Chalk in particular correlates well using tensile strength from Brazilian tests, both corrected and uncorrected fracture toughness from LPD and COD data. Some matching is achieved for the different inclinations of Mancos shale, and both tensile strength measurements, with more matches occurring when using tensile strength obtained from Brazilian tests. No apparent trends are seen in relation to the inclination angle. None of the fracture toughness values, i.e. uncorrected or corrected by either load vs LPD or load vs COD achieves a better match than the other for chalk and sandstone. Based on the two plots given, it is evident that Backers' correlation matches better than the correlation of Zhang.

A comparison of tensile strength obtained from Brazilian tests show that both uncorrected and corrected fracture toughness increases with increasing tensile strength, but it should be noted that there is a large standard deviation for the chalk data. This is partially shown for the direct tensile strength as well, as both the sandstone and shale data show the same trend. However, chalk does not, where the average direct tensile strength positioned itself between the sandstone and the shale. The testing program behind the direct tensile strength (Jensen, 2016) has not yet determined the discrepancy between these values at the time of writing.

6 Discussion

6.1 Implementation of the Experiment

The experiment followed the procedure outlined by ISRM (Ouchterlony, 1988), where the requirements was followed whenever possible. However, as previously mentioned, some adjustments had to be made. Most of these are related to the preparation of the samples. Firstly, when initially attempting to glue the knife-edges on for COD measurements, it was found that this either resulted in a poor alignment between the two knife-edges or the knife-edges would not stick at all to the samples. The solution to this was to very carefully grind off a little bit of the sample around each of the notches. Something like this is not mentioned in the procedure but it is believed to be negligible to the fracture toughness determination. Further, the notch width requirement could not be met, due to insufficient equipment. Instead, an option was followed where the smallest saw blade available was used. The resulting widths ended up being around 1-1.6 mm too large. This is of course undesirable, but the other option was to not run any experiments at all. The effect of this is not fully determined. According to Kolhe et al. (1998) deviation from notch width requirements can lead to unstable crack growth. Their analysis was done on square samples with a chevron notch under three point loading, a setup very similar to the CB except for square samples instead of round ones. However, looking at the resulting data, stable crack propagation was achieved for several of the samples and most appear to have stable crack growth at least until the peak load has been passed. This is particularly evident for the sandstone samples. Looking at the chalk data it appears that this might have had an effect on these samples as they often fail abruptly around the peak load, typically right after. Another possible explanation for the sudden failure of specimens is the brittleness of the samples. Kundu et al. (2016) states that the brittleness is higher for Mons chalk than for Castlegate sandstone, while Chandler et al. (2013) reports a high brittleness for Mancos shale. Thus, this could be an explanation for why the sandstone has stable crack propagation while the others do not. Nevertheless, the abrupt failure of chalk might mean that the data from these samples is not as good as the others.

The sample preparation for Mancos shale deviated from the others, as it was not possible to obtain samples of the desired length. Therefore, the solution outlined in the procedure was applied. It is believed that the support specimens do not affect the fracture toughness determination of the middle section, but there is no way to know this for sure without testing an intact core piece. The majority of the samples had no problems with the glue, it stuck

properly and inspections of the cores after testing did not reveal any indications of the glue giving in i.e. the support specimen had not moved relative to the middle section, nor was it possible to move it. However, two samples failed as the glue used to attach the support specimen and the middle section yielded. This proves that the glue was not always sufficient and the results obtained using this procedure may have affected the results

The loading frame used experienced a lag effect each time a new cycle was initiated. The length of this lag time depended on the loading rates used, where a slower loading rate resulted in a longer lag time. This meant that the load frame held the current load for a limited amount of time, always less than ten seconds and seldom more than five. This did to some extent complicate the procedure of the experiments, particularly for the chalk when the propagation went from stable to unstable crack growth and the samples would catastrophically fail. Additionally, the loading frame would sometimes increase the load right around the transition from stable to unstable crack growth. This is seen on several of the curves for the chalk specimens, found in Appendix 11.4 and 11.5. The curve starts to decrease, as less load is required to increase the clip-gage opening. However, it might appear as the opening closes faster than the determined load rate and thus the loading applies more load to counteract this, resulting in failure of the specimen and more complicated data.

6.2 Sources of Error

The experimental procedure outlined and followed in this thesis contains many possible sources of errors. The effect of these depends on the severity of the error. Some of them are negligible while others can render the data completely useless. One of the most severe is the calibration of the equipment. As mentioned previously, both the LVDT's and the COD tools were calibrated against known values and thus it is believed that they are correctly calibrated. However, if either of these is calibrated wrong, the corresponding data obtained is useless as it is not a true representation of what occurred. The most severe of these two is the COD tool as it is used both to control the loading frame and in the determination of the fracture toughness. For the latter, the data from the LVDT's is also severe to the thesis. Other measuring tools includes different calipers, used to measure the dimensions of the specimens and the span of the bend fixture. All of these were electrical calipers, with an accuracy to the second decimal point.

The two glues used is an additional source of error. The first glue, an epoxy adhesive, requires two components to be evenly mixed. A new mixture was made for each sample due to

the hardening time and thus it is possible that some of these mixtures have been mixed incorrectly, thereby resulting in a glue that does not provide the necessary adhesion required. This was evident for one sample in particular where it was seen that the knife-edges drifted apart with the COD tool attached, as the two clips on the device pushes outward when attached to the knife-edges. The amount of force they pushed with was enough to drive the knife-edges away. It cannot be ruled out that this has not occurred for other specimens, although to a much less degree where it is not as apparent. Secondly, another glue was used to achieve the correct length of the Mancos shale specimens, detailed above. This is a potential source of error as some samples were seen to not properly hold the specimen together.

The support specimens were subjected to multiple testing as they were reused once. Because of this, the first round of testing might have altered the support samples in some way, possibly affecting the results from the second round. However, there are no indications of this occurring. The behavior of the shale specimens is as expected and there are no apparent trends in the data to suggest they have been altered. Still, it cannot be ruled out. One shale specimen failed inside the support specimen and not along the pre-determined notch, suggesting a preexisting flaw led to failure here and not at the notch. The failure occurred close to the glued surface, with only a few millimeters between the glue and the location of where the sample failed. This might have occurred as a result of the gluing process. No other samples failed like this and inspections of the support specimens did not reveal that anything similar had occurred for the other samples.

A big source of error is related to the calculation of fracture toughness for chalk. The curves were initially made by plotting the load against the COD using the data from Testworks 4. Sandstone yielded good plots, however, the chalk data appears choppy as the curve jumps back and forth as shown in Figure 6-1. A comparison was made with the data from Catman and even though the curves have the same behavior, the latter is much less choppy, providing a relatively smooth line with a better fit for interpretations. It was therefore decided to use the data from Catman, however the data here lags a few seconds behind and the real issue is then to correctly shift the data such that it occurs at the right time. This was done by plotting the two plots on top of each other and finding a good match, in addition to checking several of the data points against each other.

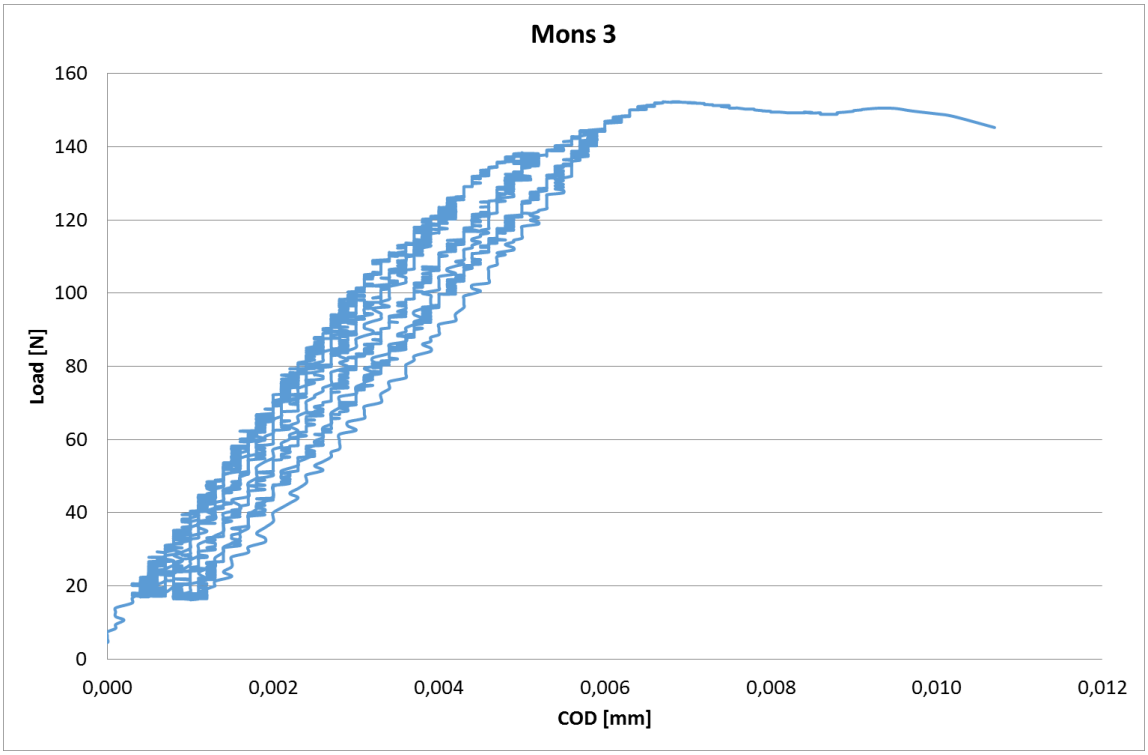

Figure 6-1: Load vs COD for a chalk using readings from Testworks 4. Notice the choppy behavior of the cycles

The experiment was carried out at ambient conditions due to the limitations of the procedure. However, in the future it would be more desirable if the fracture toughness could be determined at conditions more resembling to in-situ, such as tests performed under confining pressure and at elevated temperatures. The literature shows that the mode I fracture toughness is dependent on both of these. Under confining pressure, the fracture toughness has been shown to increase significantly. However, the procedure for determining the fracture toughness under such conditions is not simple, as it requires custom-built equipment to simulate the reservoir conditions (Funatsu et al., 2014, Kuruppu & Seto, 2001). This has been proven successful when using the SCB method with a custom-built pressurized cell where the samples are immersed in an oil bath, making it possible to subject the samples to varying confining pressures. A problem with using a method like this is that it does not properly isolate the sample from the confining pressure and hence it does not prevent the pore pressure from becoming the same as the confining pressure over time, making the effective pressure zero. In SCB tests, this was partially accounted for by spraying the samples with a silicone layer, but this is thought to only slow down this process, not prevent it. A possible solution is to use hollow cylinder tests to include confining pressure in a reliable way, but this does not permit a direct determination of the fracture toughness (Holt, R., personal communication, 2016).

6.3 Determination of the Corrected Fracture Toughness

As previously mentioned, the determination of the corrected fracture toughness was done using both load vs COD data and load vs LPD data for chalk and sandstone. The data was good for sandstone using both methods and fine for chalk using the LPD method. However, the data for chalk using load vs COD proved difficult to analyze, as the data had a strange behavior, including clip gage openings closing more than their initial displacement during unloading. One such example is seen in the figure below. Here slopes are seen to lie above the previous curve prior to leaving the cycle and unloading leads to a displacement less than what it was at the beginning.

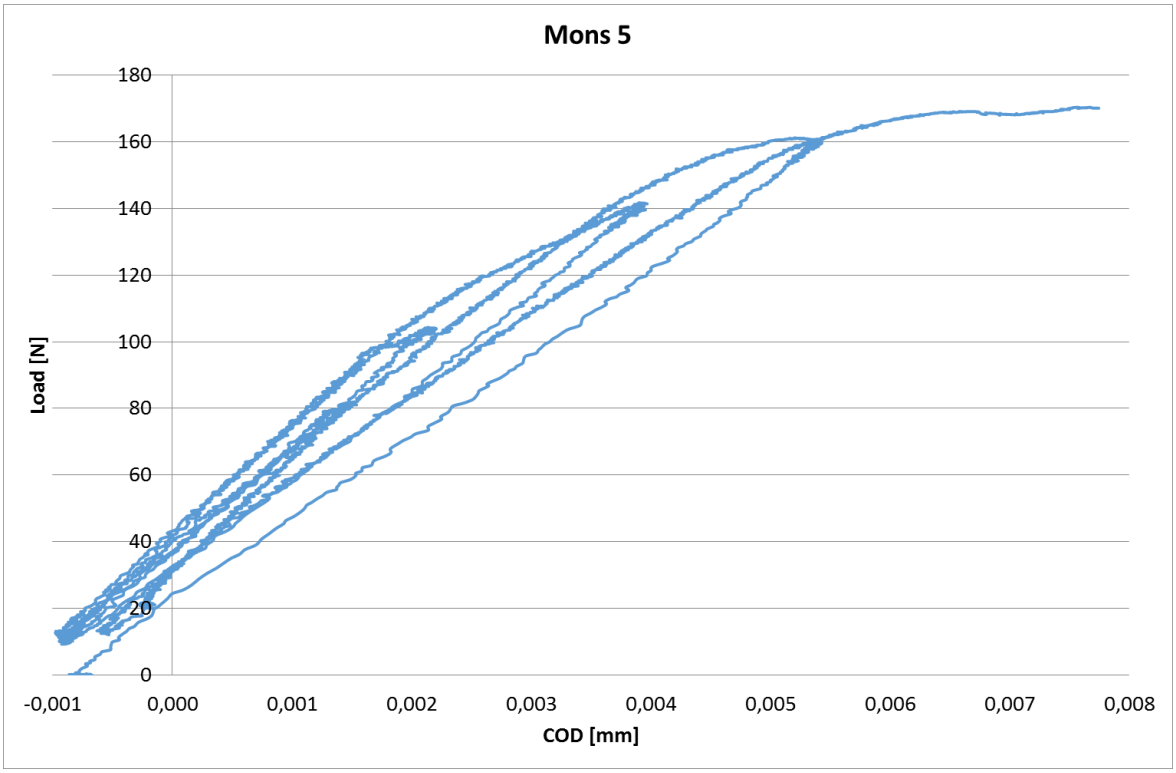

Figure 6-2: Load vs COD for a chalk specimen. Notice the cycles lie above the curve prior to leaving a cycle and that the clip-gage opening displacement at the bottom of the unloading slopes is less than initially

A direct consequence of this is that there are larger uncertainties connected to the determination of the fracture toughness for these specimens than the others, even though the corrected fracture toughness was in fact found for all. Why such behavior occurs has not been determined. It might be because of the high sensitivity of the COD tool, and that it has been affected during the assembly of the specimen, i.e. a temperature increase has occurred on the surface of the COD tool, thereby making it produce abnormal results. However, if this was the reason then such an effect would have been time-limited to a few minutes. The assembly itself takes more time than

this once the clip-gage is attached and the fact that such behavior is seen long into the experiment that last for around 10-15 minutes, suggest this is more than likely not the reason why such behavior is seen. The chalk generally displays a widely different behavior than the sandstones and shales tested. An example of this is given in the figure below. The sudden drop along the curve after the first cycle is seen in both load vs COD and load vs LPD, and it is believed to be because of something that occurs in the sample, such as fracture propagation into a weak zone resulting in an increase of displacement. However, this behavior can also be the result of slippage in the glue. As the knife-edges are somewhat stressed with the clip-gage attached, they might have slipped microscopically, thereby showing an effective opening much larger than it actually is.

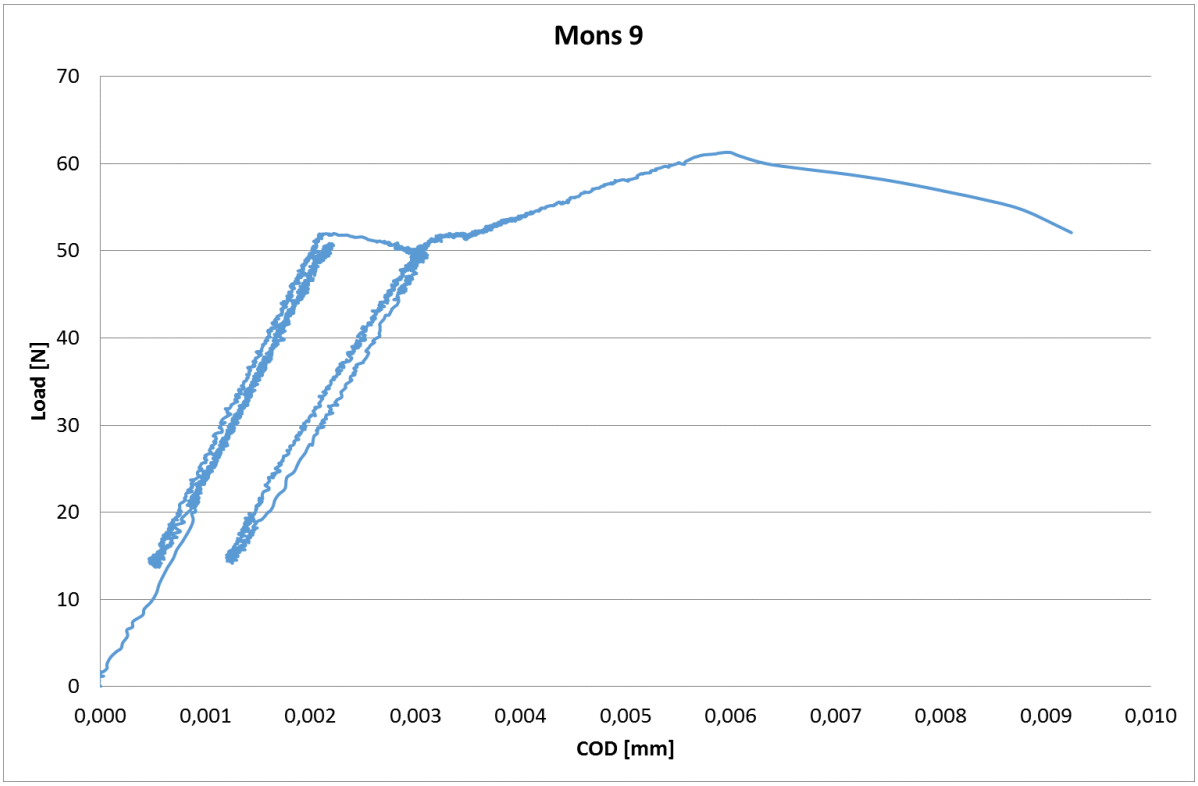

Figure 6-3: Load vs COD plot for Mons 9. Notice the behavior of the curve at around 0.002 mm along the COD axis

The initial slope is based on the curve right after the pre-load. The reason for this is that the data prior to this is somewhat uncertain, as the loading roller does not achieve proper contact immediately. Instead, the loading roller moves closer to the sample, sometimes going down other times up as it tries to establish contact. In addition, there is some time that passes between when the preloading is done and when the actual experiments start.

Several of the plots for load vs LPD show a large displacement at almost zero load before the actual experiments start. This is possibly a result of the LVDT's positioning themselves more correctly when the loading roller first achieves contact with the specimen. Looking at the LPD vs time for these samples it is seen that this is not a persistent effect that affects the final curve as it is only seen prior to reaching the pre-load.

One thing that is seen for all data using LPD data is the fact that the first few slopes determined from the cycles are larger than the initial slope. This is believed to occur because of stiffness effects in the sample and it highly affects the data as the evaluation point is moved compared to the load vs COD data. Stiffness effect is the result of the initial loading. The applied load will lead to closure or collapse of some of the pre-existing cracks in the specimen. During unloading of the sample, these cracks are not reopened. When reloading then occurs, the resulting slope increases, as the sample is now stiffer. For the subsequent slopes, such behavior might not occur and the slope will decrease as the majority of the pre-existing cracks have already collapsed.

Based on the results from each determination, the information given by ISRM and on the set-up itself, it is believed that the results from the load vs COD determination gives the most correct values for the rocks tested, and this is why they have been focused on during the analysis. There are a number of reasons for this. Firstly, the p-values for sandstone show little variation and the location of the evaluation point occurs ahead of the peak load for both sandstone and chalk. According to ISRM, the latter is something one should expect for soft, weak rocks while the former is something one should always expect. It should be emphasized that the p-values for chalk show a larger scatter but this is possibly a result of the curves that are hard to interpret and odd behavior of the samples. Secondly, the data from the clip-gage is believed to be more accurate, partially due to the unstable saddle arrangement the LVDTs use.

The calculated values for both the uncorrected and corrected fracture toughness is within the anticipated magnitude. Bearing in mind that the specimens tested are considered weak to very weak, it seems fitting that the corresponding fracture toughness is so low. The increase from uncorrected to corrected is somewhat large, due to the large plasticity factors, but it is in line with numbers seen in the literature for other rocks (Backers, 2004). Even though the load vs COD data is considered more accurate, the numbers obtained from using load vs LPD is also within the expected values.

6.4 Size Effect

The fracture toughness is assumed to be a material property, and therefore expected to be roughly the same for specimens of different sizes. However, a size effect is typically observed, seen in the uncorrected fracture toughness here and by others (Scavia et al., 1995, Ayatollahi & Akbardoost, 2014). For sufficiently large samples, it is assumed the fracture toughness will stay constant. Fracture toughness is dependent on the specimen size mostly because of the presence of the fracture process zone around the crack tip. The larger the fracture process zone is relative to the specimen, the more dependent the fracture toughness is on the size of the specimen. This explains why sufficiently large samples are independent of size; the fracture process zone is usually small compared to the specimen size. An investigation of the fracture process zone would therefore be interesting. Backers (2004) used acoustic emissions to investigate the size of the fracture process zone. Similarly, Ohno et al. (2014) used acoustic emissions to investigate the fracture process zone in square concrete specimens from three point bending**.** Backers also investigated the fracture process zone through crack density measurements from scanning electron microscopy. Unfortunately, neither of these options were used in this thesis, and hence it is not possible to investigate any correlations here. Further, a proper investigation of the size effect based on the data obtained is not possible, as only two specimen sizes have been tested.

It is indicated that the corrected fracture toughness is a size independent parameter in the ISRM method. This is partially seen here as the corrected fracture toughness of sandstone exhibits sign of size independence as the two values are fairly close, based on the load vs COD data. The chalk on the other hand does not show this. Matsuki et al. (1991) states that samples with large non-linearity in the stress-strain diagram shows a correlation between the specimen diameter and corrected fracture toughness. More work is needed in this field before any conclusions can be drawn.

6.5 Irregularities in the Mons Chalk

The fact that there is more scatter for the chalk is possibly related to the yellow/ gold irregularities seen in the sample. For some, but not all of the specimens tested, these irregularities appears randomly across the fractured surface. Figure 6-4 shows an example of this. Here the irregularity appears both close to the notch tip and on the lower left half of the sample. The irregularity in the lower left half is quite long. It is highly possible that this affects the fracture toughness, but it is difficult to say to what extent for two reasons. The first relates to the amount seen directly on the fractured surface. The amount visible on the surface varies

from specimen to specimen and there are no measurements of the amount. Secondly, it is quite possible that more yellow irregularities lie right beneath the surface, not visible to the naked eye. Several of the samples show no irregularities on the fractured surface, but clearly show these along the sides of the sample. Further, comparing the peak loads and fracture toughness, both uncorrected and corrected, there are no trends as specimens on both end of the scale contains these irregularities. However, this does not rule out that they had an effect on the samples tested. Testing of these irregularities have been conducted in the past at SINTEF Petroleum, but they did not reach a conclusion of what this was.

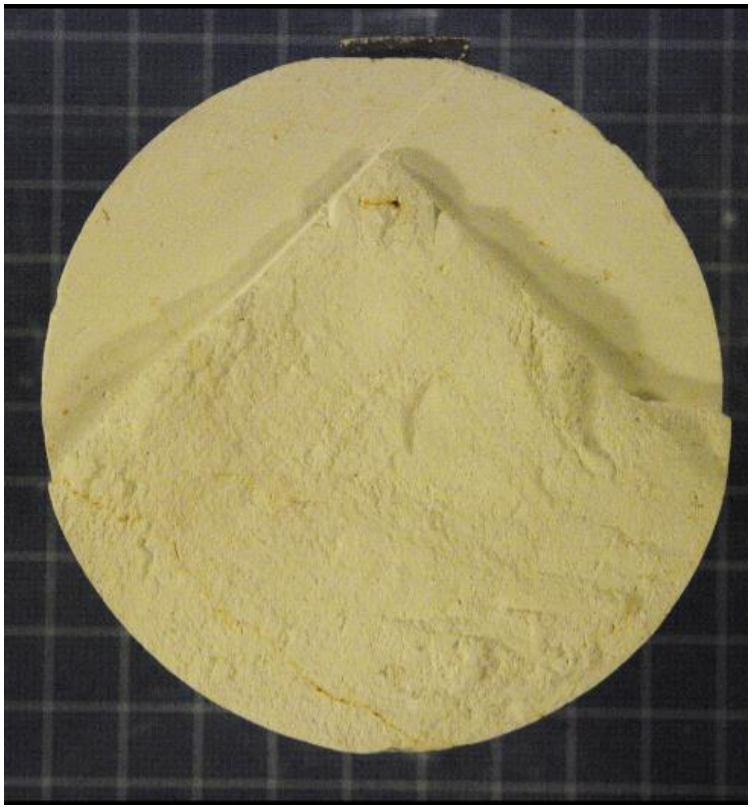

Figure 6-4: Picture of a chalk sample. Yellow/ gold irregularities is seen close to the notch tip and on the lower left half of the sample

6.6 Fracture Toughness vs Tensile Strength

In chapter 3.4, several reasons are given for why a relationship between the fracture toughness for mode I and the tensile strength exist. Additionally, one can intuitively agree that such a relationship exist when it is assumed that tensile failure is the result of coalescence of tensile microcracks (Kemeny, 1993). Further, it is generally agreed that extension of cracks begins in the plane orthogonal to the greatest tension, and hence the tensile strength is one of the controlling factors for fracture toughness, regardless of the mode. This points to an inherent relationship between these two parameters. Such a relationship was established in Backers

(2004), but an attempt at finding a new relationship was not made here due to the limited rock types tested. Instead, a match was attempted between the data and known correlations.

The results from the fracture toughness vs tensile strength comparison is not surprising, due to a number of reasons. The rocks tested are considered weak to very weak, while none of the correlations used are specifically designed for such rocks. Instead, these correlations are focused on a broad range of different rock types. Much of the fracture toughness data has also been obtained from a selection of different methods, and not just the Suggested Methods. The tensile strength data used for these correlations are either only taken from Brazilian tests (Backers, 2004), or from a broad range of different methods. As both the tensile strength and fracture toughness is known to vary depending on the method used, it is of no surprise that an overall good match was not found. The fact that Backers' correlation achieved one of the better fits is also not unreasonable as the testing methods used there focused on only one test type for fracture toughness (CB) and one test type for the tensile strength (Brazilian tests). Correlations are more than likely to achieve a better consensus if the methods used are limited to only one testing method for each. Further, correlations might achieve a higher accuracy if they tend to focus on similar rocks, i.e. weak rocks only, or maybe even finding a correlation that fits for one particular rock. The latter is not the best option, as the work required would be tremendous. The former option is therefore better as it requires less work, and it might yield better results as the rocks used are more similar to each other.

6.7 Mancos Shale

The fracture pattern seen from the tests on Mancos Shale is consistent with the fact that fractures tend to follow the way that requires the least amount of work. Concurrently with this, the specimens are designed so that the fracture is initiated at the apex of the chevron and follows the symmetry designed by the notch. The boundary between two bedding planes is typically the weakest zone of the rock, and shale easily splits along this plane. For the specimens with a notch cut perpendicular to the bedding planes, the fracture therefore tends to follow this boundary, as this requires the least amount of work. It is easier for the fracture to follow the zone of weakness between two bedding planes, than it is to cut through the planes. However, for the notches cut parallel to bedding it is not possible to follow the planes, as the notch is oriented in such a way that the fracture propagates perpendicular to them. The amount of work needed to propagate through the sample is much lower than the work needed to realign the fracture and have it follow the bedding planes.

One specimen is seen to deviate from the behavior of the rest of the samples with perpendicular notches, the one with an inclination of 75°. As explained earlier, the fracture propagated through the sample and not along two bedding planes. Two possibilities for this seem more likely than others. One possibility is that there was some kind of weakness in the specimen along the fracture path that let the fracture propagate *through* the bedding planes. Another option is that the inclination is too severe, so it would require more work to follow the bedding planes as opposed to propagate through them. It is unfortunate that the specimen with an inclination of 90° for the same notch orientation was unsuccessful, as it would have shed further light on the trends seen here. If the 75° and 90° had behaved in the same manner it would most likely have indicated that there is a limit for the inclination angle in which the fracture would rather propagate through a specimen than following the bedding planes. What is seen here about the behavior of shale is highly relevant for planning and execution of well paths and hydraulic fracturing operations in shale.

Relating this to the fracture toughness values seen is somewhat more difficult, partially due to the limited amount of tests on each inclination. Intuitively, one would perhaps assume that the fracture toughness is larger for the parallel notches than the perpendicular notches, and the corrected fracture toughness data hints to this, as this is the larger value on three of the four occasions both notch orientations are calculated. However, each specimen might have weaknesses, such as pre-exiting cracks, in the area were the fracture is induced, thereby making the particular specimen weaker.

When the inclination angle is increased, mixed mode fractures between mode I and mode II occur due to the shear displacements between the laminations as the fractures align with the anisotropic features; the bedding planes of the rock. This is most evident for the specimens with notches cut perpendicular to the bedding planes. Similar observations were made by Ghamgosar et al. (2015). They reported, based on CCNBD specimens with bedding planes, that for increasing inclination angles the failure went from brittle to ductile behavior. The results here points to similar behavior, as the plasticity factor is generally higher for the specimens of higher inclination.

6.8 Fracture Toughness vs Specimen Properties.

Comparing the corrected fracture toughness results with the specimens properties show several interesting trends. It is seen that higher values of unconfined compressive strength and bulk density results in higher fracture toughness values while a higher porosity resulted in lower fracture toughness. These results are in agreement with Backers (2004) and Whittaker et al. (1992). Backers' analysis was done with the corrected fracture toughness. The Young's modulus does not match with the trends seen in other literature, where the Young's modulus is positively correlated with the fracture toughness. The chalk is seen to highly deviate from this trend. Considering that only three rock types are tested, this is not surprising. In Backers' results it is seen that some of his data mismatches greatly with the correlations he has determined. However, time did not allow for a more thorough investigation of these relationships, nor a discussion into why such relationships exist.

7 Conclusion

Mode I (tensile) fracture toughness testing has been performed on Mons chalk, Castlegate sandstone and Mancos shale using the Chevron Bend method. Non-linearity behavior is accounted for through determination of the plasticity factor p. Size effect is investigated on Mons chalk and Castlegate sandstone, and anisotropy is investigated on Mancos shale. It is found that the uncorrected fracture toughness for specimens of chalk and sandstone exhibit a size effect, where the fracture toughness increases with specimen size. Accounting for non-linearity behavior, the corrected fracture toughness is independent of size for sandstone while the size effect is still present for chalk. Applying the correction factor gives more accurate fracture toughness values, but the scatter in the sample set is increased. The fracture toughness of Mancos shale, both uncorrected and corrected, is shown to be related to the inclination of the bedding planes, but to what extent is not properly determined as both U-shaped and increasing tendencies are seen. For notches perpendicular to bedding, an even more complex trend is seen in the corrected fracture toughness data, but a complete picture is not determined due to several unsuccessful experiments. The general increase in the plasticity factor indicates mixed mode fracturing. The fractures tended to follow the bedding planes whenever possible, instead of propagating right through the specimens.

The fracture toughness values found, determined at ambient conditions, are typically very low, agreeing with their classification as weak to very weak rocks, and the values are in the same magnitude as other published fracture toughness values. The determined corrected fracture toughness is 0.153, 0.124, 0.221 and 0.231 MPa*$m^{1/2}$ for Mons chalk of diameter 50 and 38 mm, and Castlegate sandstone of diameter 50 and 38 mm, respectively. A much larger variation is seen in the Mancos shale, where the corrected fracture toughness is between 0.370 and 1.287 MPa*$m^{1/2}$.

One of the primary areas where fracture toughness is used is in modeling of rock mechanics related situations, such as hydraulic fracturing. Its use here depends on the particular code, but it is often used as a fracture criterion for both fracture initiation and propagation. Thus, the results found here is relevant for simulation of these rock types, primarily for benchmarking results in model development and to improve current models. Also, what is seen here about the behavior of shale is highly relevant for planning and execution of well paths and hydraulic fracturing operations in shale.

8 Future Work

Much of the work done within this thesis was done with a limited amount of time, knowledge and resources. The completed investigation reveals several interesting relationships, but it barely scratches the surface of the possibilities. For future work, some suggestions or topics of interest are given.

- Investigate the possibility of performing fracture toughness measurements under in-situ conditions, either with modifications done to the equipment used here or with a more suitable testing method.
- Perform testing on a broader selection of samples, with the focus being on the relationship between tensile strength and fracture toughness. Such work could be relevant for the ongoing development of MDEM at SINTEF. This could also be tied into the relationship fracture toughness has with other rock properties.
- Future work should be done with the correct notch width and a possible investigation into the effect of the notch width itself.
- The results from testing of Mancos shale show an anisotropy effect, but it is limited by the amount of samples tested. More testing should be done to determine the correct behavior.
- Future testing should be accompanied by acoustic emission recording to monitor the fracture initiation and propagation to allow for a better understanding of what is actually happening in the rock when exposed to increasing tension
- Address the size effect by testing a broader range of specimen sizes. Such work could conclude if there is a clear size effect for both the uncorrected and corrected fracture toughness.
- Automate the system based on the numbers used here. Typical values for sandstone and chalk has been derived, thus it is possible to develop a system than can use other loading rates to allow for investigation of a larger span and the effect of this. Nevertheless, an automated system is more likely to produce even better reproducibility of sample testing.

9 Nomenclature & Abbreviations

γ_s = Specific surface energy

ε = Strain

Θ = Angle, chevron angle

ν = Poisson's ratio

σ = Stress

σ_a = Applied stress

σ_f = Fracture initiation stress in tension

σ_{ij} = Stress tensor

σ_t = Tensile strength

a = (Half) crack length, major semi-axis of an elliptical crack

A = Crack surface area

a_0 = Chevron tip position

A_{min} = Dimensionless factor

B = Constant in scale effect law

BCM = Boundary collection method

BEM = Boundary element method

CB = Chevron bend

CCNBD = Cracked chevron notched Brazilian disc

COD = Clip-gage opening displacement

D = Diameter

DDM = Displacement discontinuity model

E = Young's modulus

E' = Effective Young's modulus

F = Load

$\bar{F}$ = Average load

F_1 = Load at the intersection between the first finalized line and the curve

F_1' = Load at a specific point along the first finalized line

F_2 = Load at the intersection between the second finalized line and the curve

F_c = Corrected peak load

F_e = Load at a calculated point between F_2 and F_1'

FEM = Finite element method

F_H = Load at low point on reloading part of the cycle

f_{ij} = Geometric stress factor

F_L = Load at high point where COD/ LPD starts to decrease

F_{max} = Maximum load

FPZ = Fracture process zone

g_0 = Dimensionless factor

G_I = Strain energy release rate

G_I = Strain energy release rate for mode I

G_{IC} = Critical strain energy release rate for mode I

G_{IC}^C = Calculated critical energy release rate for mode I

h = Height of specimen flanks

HCCD = Hollow center cracked disc

ISRM = International Society for Rock Mechanics

K = Stress intensity factor

K_0 = Stress intensity factor threshold for subcritical crack growth

K_I = Stress intensity factor for mode I

K_{IC} = Critical stress intensity factor or fracture toughness, mode I

K_{IIC} = Critical stress intensity factor or fracture toughness, mode 2

K_{II} = Mode II stress intensity factor

K_{III} = Mode III stress intensity factor

K_k = Stress intensity factor, subscript k refers to the mode

K_{IC}^C = Corrected fracture toughness, mode I

LEFM = Linear elastic fracture mechanics

LPD = Load point displacement

LVDT = Linear variable differential transducer

MDEM = Modified discrete element method

p = Plasticity correction factor

Q = Constant in scale effect law

r = Radial distance, distance from crack tip

r^2 = Coefficient of determination

S = Span

s_c = Slope

SCB = Semi-circular bend

$s_{int.\ slope}$ = Initial tangent slope

SNBD = Straight Brazilian notched disc

SR = Short rod

t = Notch width

U = Total energy of infinite cracked plate

U_c = Elastic strain energy released as a result of the newly introduced crack length and relaxation of above and below the crack

UCS = Unconfined compressive strength

U_p = Change in potential energy

U_s = Change in the elastic surface energy as a result of the new crack surface being formed

U_t = Total initial elastic strain energy of a stressed and uncracked plate

W = Work done by any external forces

x_2 = Displacement between F_2 and unloaded state

x_l = Displacement of two matching loaded states along the linearized unloading lines

x_u = Residual displacement in unloaded state

Y = Geometry factor

ΔF = Load difference between the low point and the point located directly vertically beneath it on the unloading part of the cycle

10 References

Abe, H., Mura, T., & Keer, L. M. (1976). 'Growth Rate of a Penny-shaped Crack in Hydraulic Fracturing of Rocks'. *Journal of Geophysical Research*, 81, pp. 5335-5340.

Al-Shayea, N. A., Khan, K., & Abduljauwad, S. N. (2000). 'Effects of Confining Pressure and Temperature on Mixed Mode (I-II) Fracture Toughness of a Limestone Rock'. *International Journal of Rock Mechanics and Mining Sciences*, 37(4), pp. 629-643.

Amrollahi, H., & Baghbanan, A. (2009). 'Effects of grain size distribution on K_{IC} using CCNBD and HCCD specimens'. Presented at the *ISRM Regional Symposium – EUROCK 2009*, Cavtat, Croatia, 29-31 October 2009, pp. 209-213.

Atkinson, B. K. (1984). 'Subcritical crack growth in geological materials'. *Journal of Geophysical Research*, 89, pp. 4077-4114.

Ayatollahi, M. R., & Akbardoost, J. (2012). 'Size effects on fracture toughness of quasi-brittle materials – A new approach'. *Engineering Fracture Mechanics*, 92, pp. 92-100.

Backers, T. (2004). 'Fracture Toughness Determination and Micromechanics of Rock Under Mode I and Mode II Loading'. PhD Thesis, University of Potsdam, Germany.

Barker, L. M. (1977). 'A simplified method for measuring plane strain fracture toughness'. *Engineering Fracture Mechanics*, 9(2), pp. 361-369.

Barker, L. M. (1979). 'Theory for determining K_{IC} from small, non-LEFM specimens, supported by experiments on aluminum'. *International Journal of Fracture*, 15(6), pp. 516-536.

Bazant, P. (1984). 'Size Effect in Blunt Fracture: Concrete, Rock, Metal'. *Journal of Engineering Mechanics*, 110(4), pp. 518-535.

Bearman, R. A. (1999). 'The use of the point load test for the rapid estimation of the Mode I fracture toughness'. *International Journal of Rock Mechanics and Mining Sciences*, 36, pp. 257-263.

Chandler, M., Meredith, P., & Crawford, B. (2013). 'Experimental Determination of the Fracture Toughness and Brittleness of Mancos Shale, Utah'. *Geophysical Research Abstracts*, 15. Available at: http://www.ucl.ac.uk/earth-sciences/research/shale-gas-hub/documents/abstracts/chandler-egu-2013. Accessed 24 June 2016.

Chavez, A. A., Otegui, J. L., Sánches, M., Morris, W., & Bianchi, G. L. (2015). 'Field and experimental brittleness (toughness) determination of Vaca Muerta Shale'. Presented at the *49th US Rock Mechanics/ Geomechanics Symposium*, San Francisco, California, U.S.A., 28 June - 1 July.

Chudnovsky, A., Zhang, H., Wong, G., & Dudley, J. W. (2012). 'Scaling Problem in Heterogeneous Rock Fracture'. Presented at the *46th US Rock Mechanics/ Geomechanics Symposium*, Chicago, Illinois, USA, 24-27 June.

Fischer-Cripps, A. C. (2007). '*Introduction to Contact Mechanics*', 2nd ed., Springer.

Fjær, E., & Nes, O.-M. (2013). 'Strength Anisotropy of Mancos Shale'. Presented at the *47th U.S. Rock Mechanics/ Geomechanics Symposium,* San Francisco, California, U.S.A., 23-26 June.

Fowell, R. J. (1995). 'Suggested Method for Determining Mode I Fracture Toughness Using Cracked Chevron Notched Brazilian Disc (CCNBD) Specimens'. *International Journal of Rock Mechanics and Mining Sciences & Geomechanical Abstracts*, 32(1), pp. 57-64.

Funatsu, T., Kuruppu, M., & Matsui, K. (2014). 'Effects of temperature and confining pressure on mixed mode (I-II) and mode II fracture toughness of Kimachi sandstone'. *International Journal of Rock Mechanics and Mining Sciences,* 67, pp. 1-8.

Funatsu, T., Shimizu, N., Kuruppu, M., &Matsui, K. (2015). 'Evaluation of Mode I Fracture Toughness Assisted by the Numerical Determination of K-Resistance'. *Journal of Rock Mechanics and Rock Engineering,* 48(1), pp .143-157.

Funatsu, T., Takashi, T., & Kuruppu, M. (2012). 'Effect of Anisotropy on Fracture Toughness of Sandstone by SCB Specimen'. Presented at the *ISRM Regional Symposium – 7th Asian Rock Mechanics Symposium,* Seoul, Korea, 15 – 19 October 2012, pp. 413-418.

Ghamgosar, M., Williams, D. J., & Erarslan, N. (2015). 'Effect of Anisotropy on Fracture Toughness and Fracturing of Rocks'. Presented at the *49th US Rock Mechanics/ Geomechanics Symposium,* San Francisco, California, U.S.A., 28 June - 1 July.

Griffth, A. A. (1921). 'The phenomenon of rupture and flow in solids'. *Philosophical Transactions of the Royal Society of London, Series A,* 221, pp. 163-198.

Inglis, C. E. (1913). 'Stresses in a plate due to the presence of cracks and sharp corners'. *Transactions, Institute Naval Architects,* 60, pp. 219-230.

Irwin, G. R. (1948). 'Fracture Dynamics'. *Fracturing of metals,* American Society of Metals, pp. 147-166.

Irwin, G. R. (1957). 'Analysis of Stresses and Strains Near the End of a Crack Traversing a Plate'. *Journal of Applied Mechanics*, 24, pp. 361-364.

Issa, M. A., Issa, M. A., Islam, M. S., & Chudnovsky, A. (2000).' Size effects in concrete fracture – Part II: Analysis of test results'. *International Journal of Fracture,* 102(1), pp. 25-42.

Jensen, S. (2016). 'Experimental Study of Direct Tensile Strength in Sedimentary Rocks'. Master thesis, Norwegian University of Science and Technology, Norway.

Kataoka, M., & Obara, Y. (2015). 'Anisotropy in fracture toughness of sedimentary and crystalline rocks estimated by semi-circular bend test'. Presented at the *ISRM Regional Symposium – EUROCK 2015,* Salzburg, Austria, 7-10 October 2015, pp. 695- 700.

Kataoka, M., Obara, Y., & Kuruppu, M. (2011). 'Estimation of fracture toughness of anisotropic rocks by SCB test and visualization of fracture by means of X-ray CT'. Presented at the *12th ISRM Congress*, Beijing, China, 16-21 October 2011, pp. 667-670.

Kataoka, M., Obara, Y., & Kuruppu, M. (2015). 'Estimation of Fracture Toughness of Anisotropic Rocks by Semi-Circular Bend (SCB) Tests Under Water Vapor Pressure'. *Journal of Rock Mechanics and Rock Engineering*, 48(4), pp. 1353-1367.

Kemeny, J. M. (1993). 'The micromechanics of deformation and failure in rocks'. In Paşamehmetğu et al. (eds). Assessment and prevention of failure phenomena in rock engineering, Balkema, Rotterdam, pp. 23-33.

Khanna, A., & Kotousov, A. (2015). 'Controlling the Height of Multiple Hydraulic Fractures in Layered Media'. *SPE Journal*, 21(1), pp. 1-8.

Kolhe, J., Chung-Yuen, H., & Zehnder, A. T. (1998). 'Effects of finite notch width on the fracture of chevron-notched specimens'. *International Journal of Fracture*, 94, pp. 189-198.

Kundu, S., Striosz, A., & Pradhan, S. (2016). 'A simple Discrete-Element-Model of Brazilian Test'. Available at: http://arxiv.org/pdf/1503.08757.pdf. Accessed 23 June, 2016.

Kuruppu, M. D., Obara, Y., Ayatollahi, M. R., Chong, K. P., & Funatsu, T. (2014). 'ISRM Suggested Method for Determining the Mode I Static Fracture Toughness Using Semi-Circular Bend Specimen'. *Journal of Rock Mechanics and Rock Engineering*, 47, pp. 267-274.

Kuruppu, M. D., & Seto, M. (2001). 'Determination of fracture toughness of rock under in-situ conditions using semi-circular specimen'. Available at: http://www.gruppofrattura.it/ocs/index.php/ICF/ICF10/paper/viewFile/4556/6564. Accessed 7 July, 2016.

Lawn, B. (1993). '*Fracture of brittle solids*'. Cambridge University press, Cambridge

Macdonald, K. C., Scheirer, D. S., & Carbotte, S. M. (1991). 'Mid-Ocean Ridges: Discontinuities, Segments and Giant Cracks'. *Science, New Series*, 253, pp. 986-994

Martin, A. N. (2000). 'Crack Tip Plasticity: A Different Approach to Modelling Fracture Propagation in Soft Formations'. Presented at the *2000 SPE Annual Technical Conference and Exhibition*, Dallas, Texas, U.S.A., 1-4 October.

Matsuki, K., Hasibuan, S. S., & Takahashi, H. (1991). 'Specimen size requirements for determining the inherent fracture toughness of rocks according to the ISRM suggested methods'. *International Journal of Rock Mechanics and Mining Sciences & Geomechanical Abstracts*, 28(5), pp. 365-374.

Nasseri, M. H. B., & Mohanty, B. (2008). 'Fracture toughness in anisotropy granitic rocks', *International Journal of Rock Mechanics and Mining Sciences*, 45, pp. 167-193.

Nasseri, M. H. B., Grasselli, G., Mohanty, B., Wirth, J., & Braun, M. (2007). 'Experimental relationship between fracture toughness and fracture roughness in anisotropic granitic rocks'. Presented at the *1st Canada – U.S. Rock Mechanics Symposium*, Vancouver, Canada, 27-31 May.

Nasseri, M. H. B., Rezanezhad, F., & Young, R. P. (2011). 'Analysis of fracture damage zone in anisotropic granitic rock using 3D X-ray CT scanning techniques'. *International Journal of Fracture*, 168, pp. 1-13

Ohno, K., Uji, K., Ueno, A., & Ohtsu, M. (2014). 'Fracture process zone in notched beam under three-point bending by acoustic emission'. *Construction and Building Materials*, 67, pp. 139-145.

Orowan, E. (1949). 'Fracture and strength of solids'. *Reports on Progress in Physics*, 12 (1), pp. 185-232.

Ouchterlony, F. (1986). 'A Core Bend Specimen With Chevron Edge Notch For Fracture Toughness'. Presented at the *27th U.S. Symposium on Rock Mechanics*, Tuscaloosa, Alabama, U.S.A., 23-25 June.

Ouchterlony, F. (1986). 'A core bend specimen with chevron edge notch for fracture toughness measurements'. Presented at the *27th U.S. Symposium on Rock Mechanics*, Tuscaloosa, Alabama, U.S.A., 23-25 June.

Ouchterlony, F. (1989). 'On the Background to the Formulae and Accuracy of Rock Fracture Toughness Measurements Using ISRM Standard Core Specimens'. *International Journal of Rock Mechanics and Mining Sciences & Geomechanical Abstracts*, 26(1), pp. 13-23.

Ouchterlony, F. (1989). 'On the background to the formulae and accuracy of rock fracture toughness measurements using ISRM standard core specimens'. *International Journal of Rock Mechanics and Mining Sciences & Geomechanical Abstracts*, 26(1), pp. 13-23

Ouctherlony, F. (1988). 'Suggested methods for determining the fracture toughness of rock'. *International Journal of Rock Mechanics and Mining Sciences & Geomechanics Abstract*, 25(2), pp. 71-96.

Papanastasiou, P. (1999). 'The effective fracture toughness in hydraulic fracturing'. *International Journal of Fracture*, 96, pp. 127-147.

Papanastasiou, P., & Atkinson, C. (2015). 'The Brittleness Index in Hydraulic Fracturing'. Presented at the *49th US Rock Mechanics/ Geomechanics Symposium*, San Francisco, California, U.S.A., 28 June- 1 July.

Scavia, C., Re, F., Zaninetti, A., & Crivelli, R. (1995).'Effects of specimen size on rock fracture mechanics parameters'. Presented at the *8th ISRM Congress*, Tokyo, Japan, 25-29 September.

Settari, A. (1988). 'Quantitative Analysis of Factors Influencing Vertical and Lateral Fracture Growth'. *SPE Production Engineering*, 3(3), pp. 310-322.

Shen, B., & Rinne, M. (2007). 'A fracture mechanics code for modelling sub-critical crack growth and time dependency'. Presented at the *1st Canada - U.S. Rock Mechanics Symposium*, Vancouver, Canada, 27-31 May.

Shen, B., & Stephansson, O. (1993). 'Modification to the G-criterion of crack propagation in compression'. *International Journal of Engineering Fracture Mechanics*, 47(2), pp. 177-189.

Shen, B., Siren, T., & Rinne, M. (2014). 'Modelling Fracture Propagation in Anisotropic Rock Mass'. *Journal of Rock Mechanical Engineering*, 48, pp. 1067-1081.

Shlyapobersky, J. (1985). 'Energy Analysis of Hydraulic Fracturing'. Presented at the *26th U.S. Symposium on Rock Mechanics*, Rapid City, South Dakota, 26-28 June.

Shlyapobersky, J., Issa, M. A., Issa, M. A., Islam, M. S., Dudley, J., Shulkin, Y., & Chudnovsky, A. (1998). 'Scale Effects on Fracture Growth Resistance in Poroelastic Materials'. Presented at the *1998 SPE Annual Technical Conference and Exhibition*, New Orleans, Louisiana, U.S.A., 27-30 September.

Shoji, T., Hayashi, K., Kojima, T., Ito, T., Takahashi, H., & Abe, H. (1985). 'Growth Behavior of Hydraulically Created Crack and its Size Evaluation Using Well Logging Data – Crustal Rock Fracture Mechanics Approach'. *Geothermal Resource Council Transactions*, 9, pp. 579-584.

Sih, G. C. (1976). 'Fracture toughness concept'. *Properties related to fracture toughness, ASTMSTP 605*, pp. 3-15.

Simpson, N. D. J. (2013). 'An analysis of tensile strength, fracture initiation and propagation in anisotropic rock (gas shale) using Brazilian tests equipped with high speed video and acoustic emission'. Master thesis, Norwegian University of Science and Technology, Norway.

Simpson, N. D. J., Stroisz, A., Bauer, A., Vervoort, A., & Holt, R. M. (2014). 'Failure Mechanics of Anisotropic Shale during Brazilian Tests'. Presented at the *48th U.S. Rock Mechanics/ Geomechanics Symposium*, Minneapolis, Minnesota, U.S.A., 1-4 June.

Sun, Z., Chen, F., & Xu, J. (2001). 'Comments on chevron bend specimen for determining fracture toughness of rock'. *Transactions of Nonferrous Metals Society of China*, 11(4), pp. 609-612.

Thiercelin, M. (1989). 'Fracture Toughness and Hydraulic Fracturing'. *International Journal of Rock Mechanics and Mining Sciences & Geomechanical Abstracts*, 26, pp. 177-183.

Thiercelin, M., Jeffrey, R. G., & Ben Naceur, K. (1989). 'Influence of Fracture Toughness on the Geometry of Hydraulic Fractures'. *SPE Production Engineering*, 4(4), pp. 435-442.

Ulusay, R. (2014). '*The ISRM Suggested Methods for Rock Characterization, Testing and Monitoring 2007-2014'*. Springer.

Ulusay, R., & Hudson, J. A. (2007). '*The Complete ISRM Suggested Methods for Rock Characterization, Testing and Monitoring 1974-2006'*. Elsevier.

Van Dam, D. B., Papanastasiou, P., & de Pater, C. J. (2002). 'Impact of Rock Plasticity on Hydraulic Fracture Propagation and Closure'. *SPE Production & Facilites*, 17(3), pp. 149-159.

Walle, L. E., & Papamichos, E. (2015). 'Acidizing of Hollow Cylinder Chalk Specimens and its Impact on Rock Strength and Wormhole Network Structure'. Presented at the *49th U.S. Rock Mechanics/ Geomechanics Symposium,* San Francisco, California, U.S.A., 28 June – 1 July.

Wang, H. Y., Marongiu-Porcu, M., & Economides, M. J. (2014). 'Poroelastic versus Poroplastic Modeling of Hydraulic Fracturing'. Presented at the *SPE Hydraulic Fracturing Technology Conference*, Woodlands, Texas, U.S.A., 4-6 February.

Weng, X. (2014). 'Modeling of complex hydraulic fractures in naturally fractures formation'. *Journal of Unconventional Oil and Gas Resources*, 9, pp. 114-135.

Whittaker, B. N., Singh, R. N., & Sun, G. (1992). *'Rock Fracture Mechanics: Principles, Design and Application'*, 1st ed., Elsevier.

Yu, Y., Zhang, Z. X., Yu, J., & Liao, G. H. (1998). 'Energy dissipation and damage characters in rock direct tensile destruction'. *Chinese Journal of Rock Mechanics and Engineering*, 17(4), pp. 386-392.

Zhang, Z. X, Kou, S. Q., Lindqvist, P. A., & Yu, Y. (1998). 'The relationship between the fracture toughness and tensile strength of rock'. Strength theories: applications, development & prospects of the 21st century, Science Press, Beijing/ New York.

Zhang, Z. X. (2002). 'An empirical relation between mode I fracture toughness and the tensile strength of rock'. *International Journal of Rock Mechanics & Mining Sciences*, 39, pp. 401-406.

Zhang, Z. X., Kou, S.Q., Jiang, L.G., & Lindqvist, P.A. (2000). 'Effects of loading rate on rock fracture: fracture characteristics and energy partitioning'. *International Journal of Rock Mechanics and Mining Sciences*, 37(5), pp. 745-762.

Zhang, Z. X., Kou, S.Q., Yu, J., Yu, Y., Jiang, L.G., & Lindqvist, P.A. (1999). 'Effects of loading rate on rock fracture'. *International Journal of Rock Mechanics and Mining Sciences*, 36, pp. 597-611.

Zhao, X. L., & Riegiers, J.-C. (1993). 'Determination of In-Situ Fracture Toughness'. *International Journal of Rock Mechanics and Mining Sciences & Geomechanical Abstracts*, 30(7), pp. 837-840.

11 Appendix

11.1 Risk Assessment

Since this master thesis involved work in a lab, safety precautions needed to be taken. Prior to gaining access, a safety course provided by NTNU was completed. A tour was given of the lab area, with focus on highlighting potential hazards, location of first aid and safety equipment and protocols to follow in the case of an emergency. Below is a table of the potential hazards specifically related to the work done in this thesis, as well as actions taken to limit these risks to a minimum.

Hazards	**Safety measures**
Pinch point hazard due to loading frames present in the laboratory area	Awareness of hazards related to the equipment and proper training was given. The loading frames had built in safety barriers and at all times, hands and feet were kept away from ongoing experiments.
Harmful chemicals was present in the lab	Stored in enclosed cabinets, with information present related to proper handling and safety precautions. No access permission was given to the student.
Spill hazard resulting in slippery floor as a result of using inert oil when dealing with Mancos shale.	Use lid on the buckets when moving the samples. Avoid spill when sample is taken out of the bucket by using a rag or cloth specifically made for oil cleanup. If some inert oil is spilled on the floor, clean up immediately.
Quick hardening glue can cause harm to skin and eyes etc.	Use goggles and gloves at all times when dealing with glue. If contact with skin, apply hot, running water immediately to cleanse the skin, before the glue hardens.

Table 11-1: Risk assessment of potential dangers in the lab

11.2 Specimen Information and Test Results

Below is specimen information and test results for the specimens tested. Note that some numbers are missing due to some experiments being unsuccessful. MC: Mons chalk, CS: Castlegate sandstone, MS: Mancos shale, D: diameter, L: length, S: support span, a_0: initial notch depth, t: notch width, COD rate: clip-gage opening rate, K_{IC}: uncorrected fracture toughness, p: plasticity factor, K_{IC}^{C}: corrected fracture toughness, G_{IC}^{C}: calculated corrected critical energy release rate, E: Calculated Young's modulus, par: parallel, per: perpendicular.

			Dimensions						Results/ Analysis				
Id.	**Inc.**	**Notch Place.**	**D**	**L**	**S**	**a_0**	**t**	**COD rate**	**Max. Load**	**K_{IC}**	**p**	**K_{IC}^{C}**	**G_{IC}^{C}**
			[mm]	[mm]	[mm]	[mm]	[mm]	[mm/min]	[N]	[Mpa*m$^{1/2}$]	[ ]	[Mpa*m$^{1/2}$]	[J/m^2]
MC1	-	-	50.87	200.41	169.3	7.9	2.5	0.03	185.2	0.170	-	-	-
MC2	-	-	51.21	192.41	169.3	7.8	2.5	0.001	115.8	0.104	0.39	0.156	4.78
MC3	-	-	51.08	186.89	169.3	7.8	2.5	0.003	152.3	0.138	0.29	0.181	6.49
MC4	-	-	51.12	180.03	169.3	7.8	2.5	0.003	148.7	0.134	0.08	0.136	3.65
MC5	-	-	51.17	200.53	169.3	7.8	2.5	0.003	170.4	0.154	-	-	-
MC6	-	-	50.99	201.55	169.3	7.8	2.5	0.003	111.4	0.102	0.44	0.141	3.91
MC7	-	-	37.26	153.51	124.5	5.0	2.5	0.003	84.6	0.117	0.46	0.123	3.00
MC8	-	-	37.27	153.45	124.5	5.0	2.5	0.0006	70.0	0.097	0.31	-	-
MC9	-	-	37.25	153.45	124.5	5.0	2.5	0.001	61.3	0.085	0.63	0.149	4.39
MC10	-	-	37.31	153.53	124.5	5.0	2.6	0.001	46.7	0.064	0.55	0.098	1.91
CS1	-	-	51.24	200.37	169.3	7.8	2.5	0.003	138.1	0.124	0.65	0.210	22.04
CS2	-	-	51.40	200.71	169.3	7.7	2.8	0.006	121.6	0.108	0.62	0.206	21.14
CS3	-	-	51.26	200.55	169.3	7.8	2.7	0.006	126.3	0.113	0.67	0.243	29.45
CS4	-	-	51.36	200.96	169.3	7.7	2.6	0.006	123.4	0.110	0.66	0.224	25.08
CS5	-	-	37.39	153.12	124.5	5.0	2.6	0.006	72.7	0.099	0.80	0.248	30.71
CS6	-	-	37.39	153.12	124.5	5.0	2.6	0.006	73.2	0.100	0.75	0.222	24.50
CS7	-	-	37.35	153.28	124.5	5.0	2.7	0.006	69.4	0.095	0.77	0.241	29.07
CS8	-	-	37.42	153.15	124.5	5.0	2.6	0.03	68.7	0.093	0.73	0.214	22.78
MS1	-	-	39.96	154.19	133.3	7.3	2.3	0.006	286.3	0.414	0.57	0.757	-
MS4	-	-	39.93	146.18	133.4	7.3	2.2	0.006	294.0	0.427	0.46	0.630	-
MS5	15	par.	38.28	155.12	127.5	3.4	2.3	0.006	326.3	0.369	0.49	0.370	-
MS6	15	per.	38.23	155.19	127.5	3.4	2.4	0.006	365.3	0.415	0.49	0.555	-
MS7	30	par.	38.20	154.74	127.5	3.4	2.4	0.006	400.4	0.457	0.64	0.724	-
MS8	30	per.	38.28	155.15	127.5	3.4	2.4	0.006	287.8	0.326	0.47	0.393	-
MS9	45	par.	38.25	155.51	127.5	3.4	2.3	0.006	551.3	0.626	0.70	1.163	-
MS10	45	per.	38.29	147.86	127.5	3.4	2.4	0.006	184.0	0.208	0.67	0.450	-
MS11	45	per.	38.23	144.64	127.5	3.4	2.2	0.006	286.7	0.326	0.70	0.712	-
MS13	60	per.	38.26	152.60	127.5	3.4	2.2	0.006	505.5	0.573	0.78	1.287	-
MS14	75	per.	38.20	153.63	127.5	3.4	2.2	0.006	414.1	0.472	0.43	0.526	-
MS15	75	par.	38.25	141.24	127.5	3.4	2.2	0.006	369.7	0.420	0.60	0.755	-
MS16	90	par.	38.25	153.61	127.5	3.4	2.2	0.006	636.5	0.722	0.65	1.178	-

Table 11-2: Specimen information and test results for all specimens tested using load vs COD

		Results/ Analysis					
Id.	**COD rate**	**Max. Load**	K_{IC}	p	K_{IC}^{C}	G_{IC}^{C}	E
	[mm/min]	[N]	[Mpa*$m^{1/2}$]	[ ]	[Mpa*$m^{1/2}$]	[J/m^2]	[GPa]
MC1	0.03	185.2	0.170	-	-	-	-
MC2	0.001	115.8	0.104	0.49	0.175	6.08	6.50
MC3	0.003	152.3	0.138	0.67	0.240	11.41	11.58
MC4	0.003	148.7	0.134	0.29	-	-	9.82
MC5	0.003	170.4	0.154	0.77	-	-	3.66
MC6	0.003	111.4	0.102	0.65	-	-	1.70
MC7	0.003	84.6	0.117	-	-	-	17.12
MC8	0.0006	70.0	0.097	0.37	0.126	3.15	7.25
MC9	0.001	61.3	0.085	0.36	0.110	2.41	3.51
MC10	0.001	46.7	0.064	-	-	-	3.12
CS1	0.003	138.1	0.124	0.73	0.251	31.40	2.89
CS2	0.006	121.6	0.108	0.71	0.222	24.47	1.46
CS3	0.006	126.3	0.113	0.59	0.216	23.31	1.84
CS4	0.006	123.4	0.110	0.67	0.231	26.66	1.80
CS5	0.006	72.7	0.099	0.56	-	-	1.40
CS6	0.006	73.2	0.100	0.88	0.213	22.52	1.42
CS7	0.006	69.4	0.095	0.52	0.117	6.88	1.63
CS8	0.03	68.7	0.093	0.87	0.153	11.70	1.39

Table 11-3: Test results for load vs LPD. Note that the specimen information is not given again. Shale is not included as it was not determined using this method

11.3 Tensile Strength Data

Number of Samples Tested	Average Diameter [mm]	Average Length [mm]	Average Tensile Strength [MPa]	Standard Deviation
9	38.20	77.52	1.907	±0.253
6	50.30	101.98	1.583	±0.286

Table 11-4: Direct tensile strength for Mons chalk (Jensen, 2016)

Number of samples tested	Average diameter [mm]	Average Length [mm]	Average Tensile Strength [MPa]	Standard Deviation
3	37.37	76.59	0.461	±0.094
4	51.34	102.71	0.589	±0.066

Table 11-5: Direct tensile strength for Castlegate sandstone (Jensen, 2016)

Inclination Angle [°]	Number of Samples Tested	Average Diameter [mm]	Average Length [mm]	Average Tensile Strength [MPa]	Standard Deviation
0	4	38.15	77.04	0.314	±0.102
15	3	38.28	74.67	0.908	±0.048
30	4	38.28	76.94	1.128	±0.409
45	3	38.27	77.01	2.378	±0.514
60	3	38.27	77.48	2.423	±0.235
75	2	38.30	74.85	1.625	±0.489
90	3	38.28	77.02	2.079	±0.374

Table 11-6: Direct tensile strength for Mancos shale (Jensen, 2016)

11.4 Plot for Load vs COD

Below are the plots given for load vs COD data. The plots are cut off where the sample fails such that is possible to see the cycles and interesting trends.

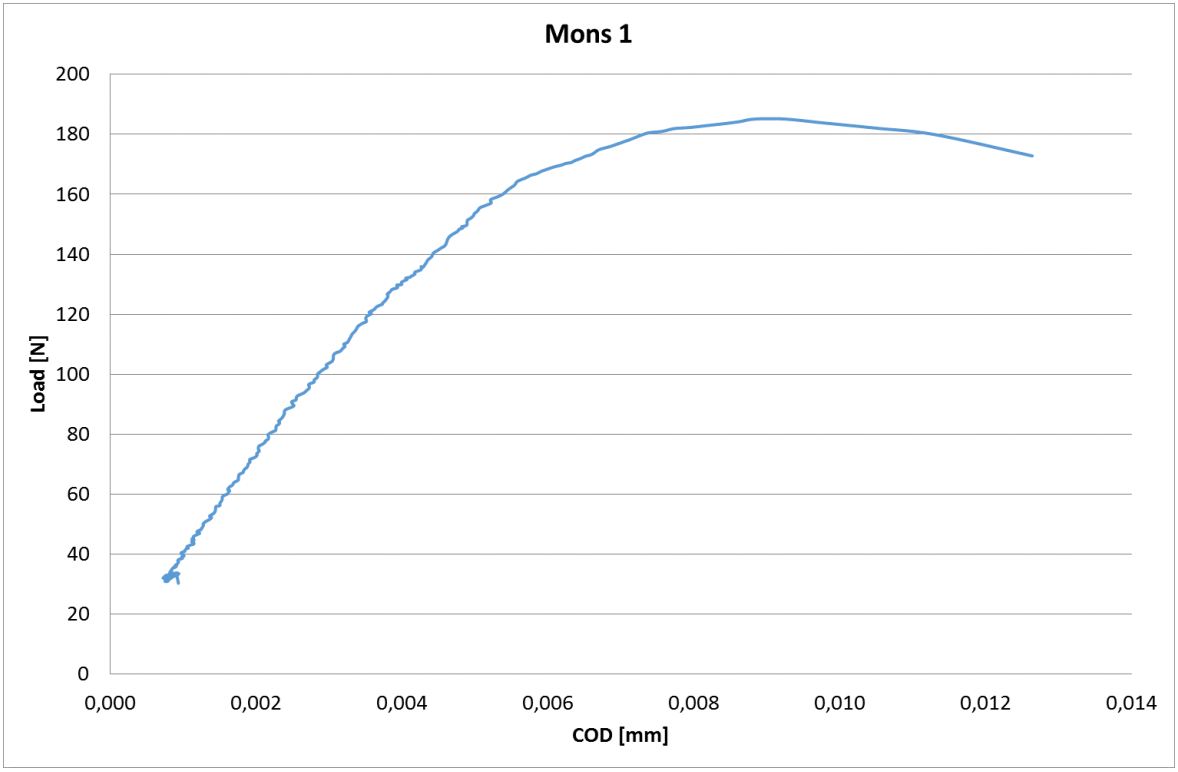

Figure 11-1: Load vs COD for Mons 1. Diameter is 50.87 mm. Note that no cycles were run in this test. Some data is missing at the beginning since the Catman was started late

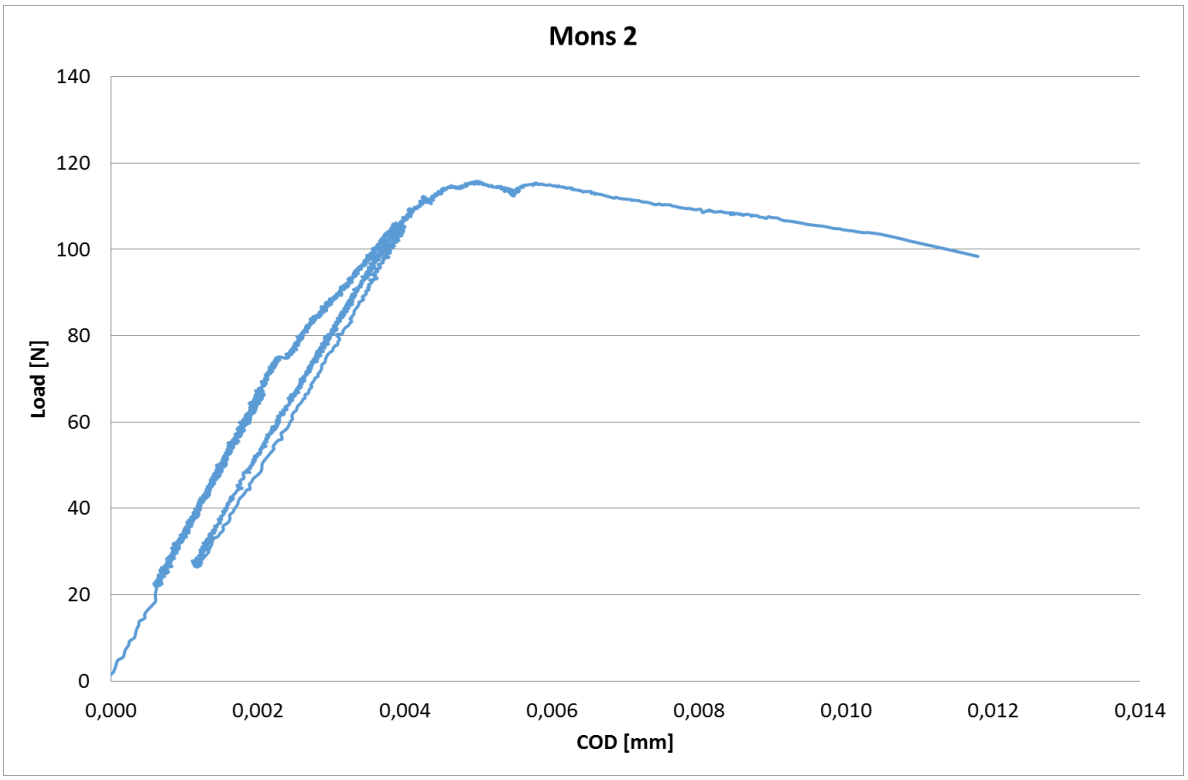

Figure 11-2: Load vs COD for Mons 2. Diameter is 51.21 mm

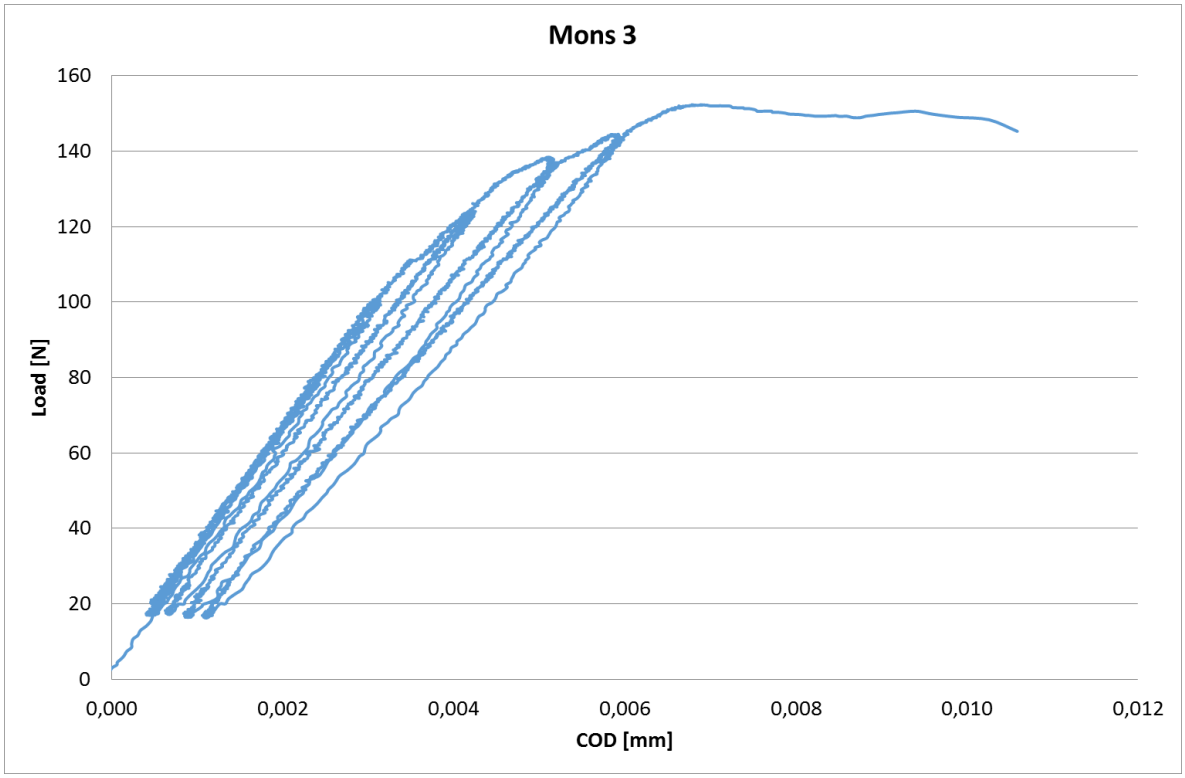

Figure 11-3: Load vs COD for Mons 3. Diameter is 51.078 mm

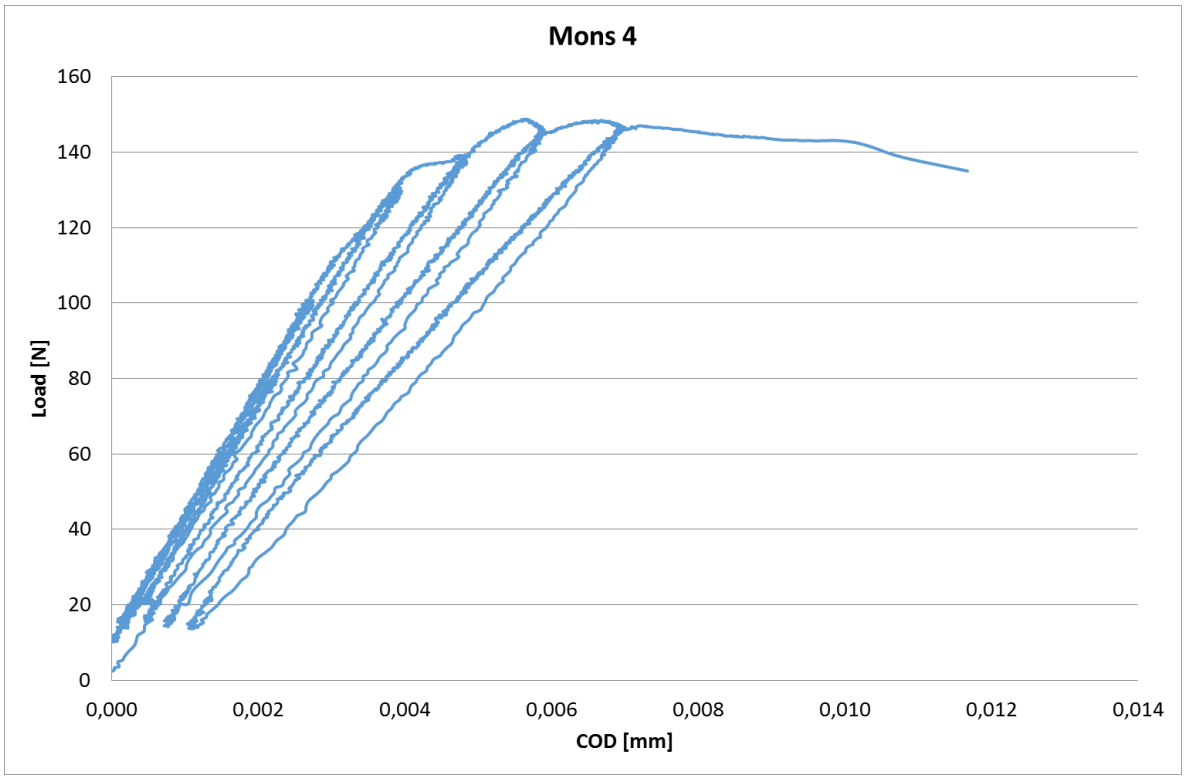

Figure 11-4: Load vs COD for Mons 4. Diameter is 51.12 mm

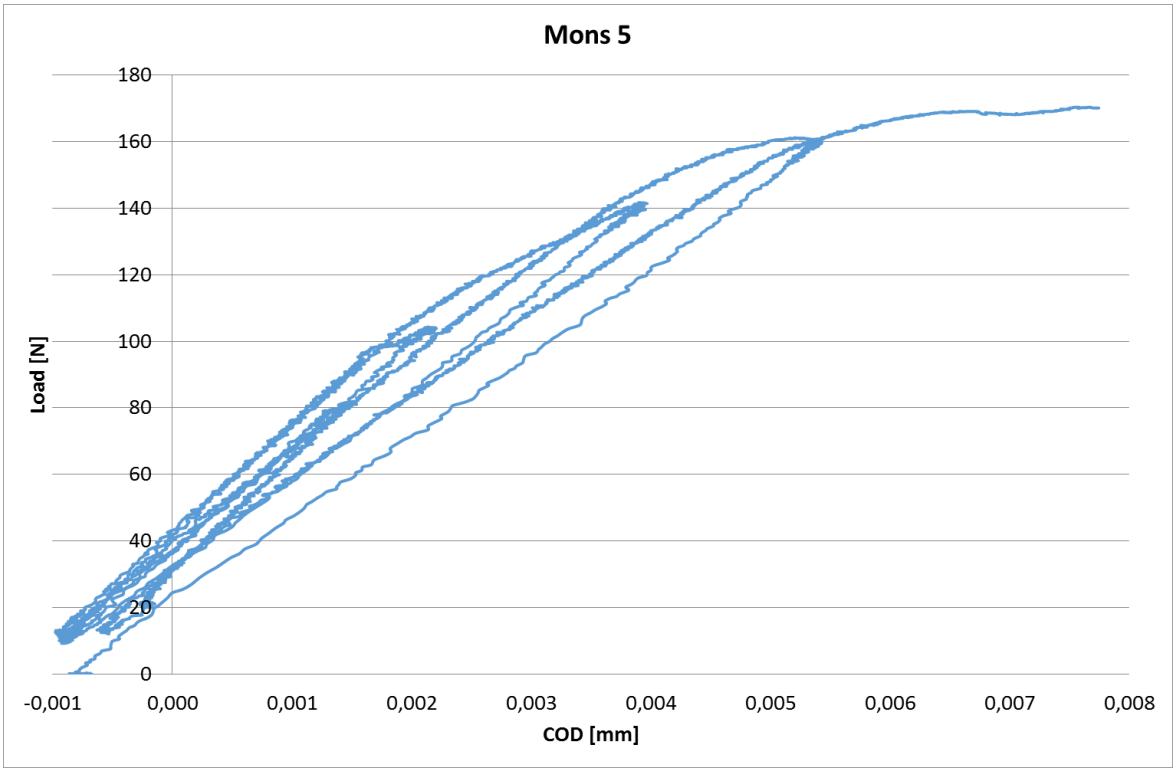

Figure 11-5: Load vs COD for Mons 5. Diameter is 51.17 mm

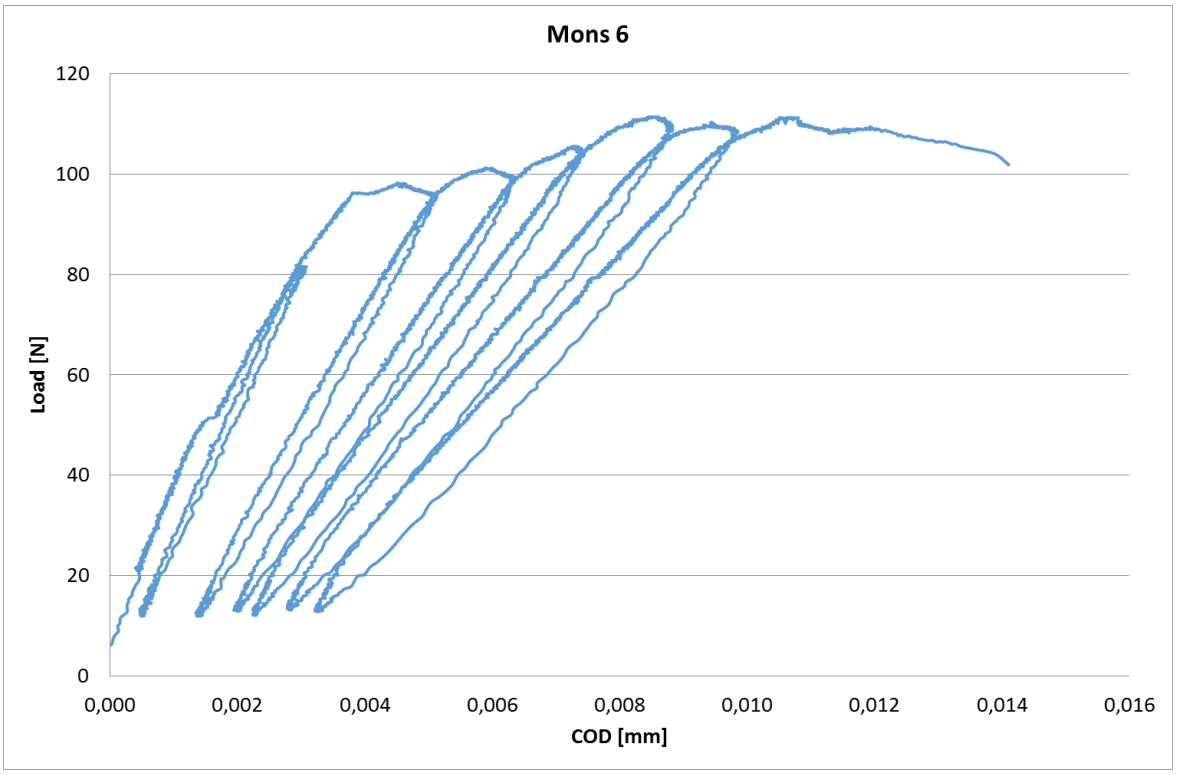

Figure 11-6: Load vs COD for Mons 6. Diameter is 50.99 mm

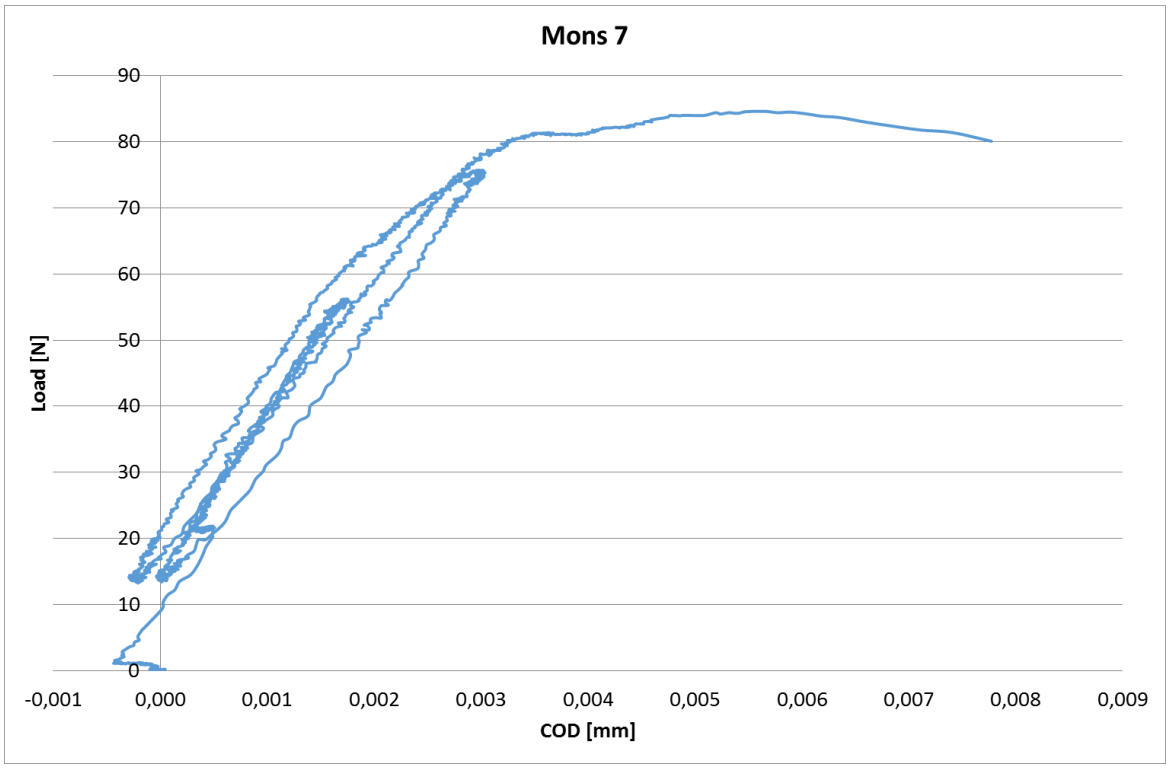

Figure 11-7: Load vs COD for Mons 7. Diameter is 37.26 mm

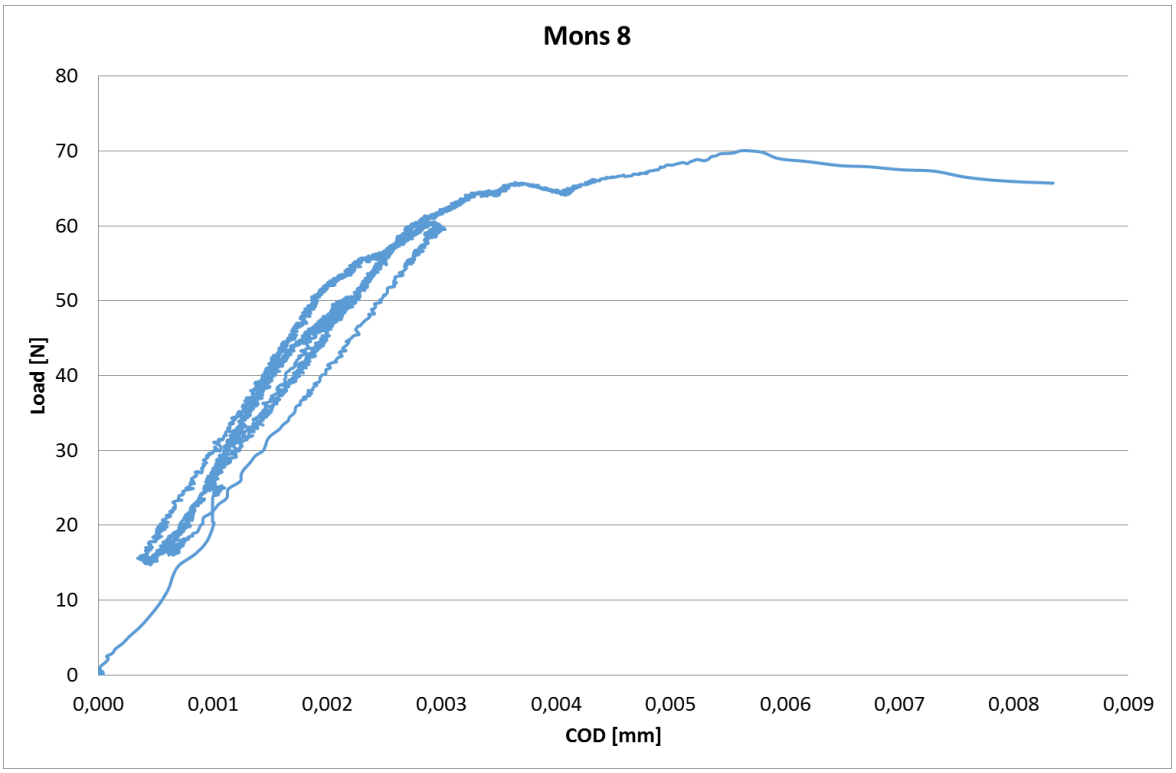

Figure 11-8: Load vs COD for Mons 8. Diameter is 37.27 mm

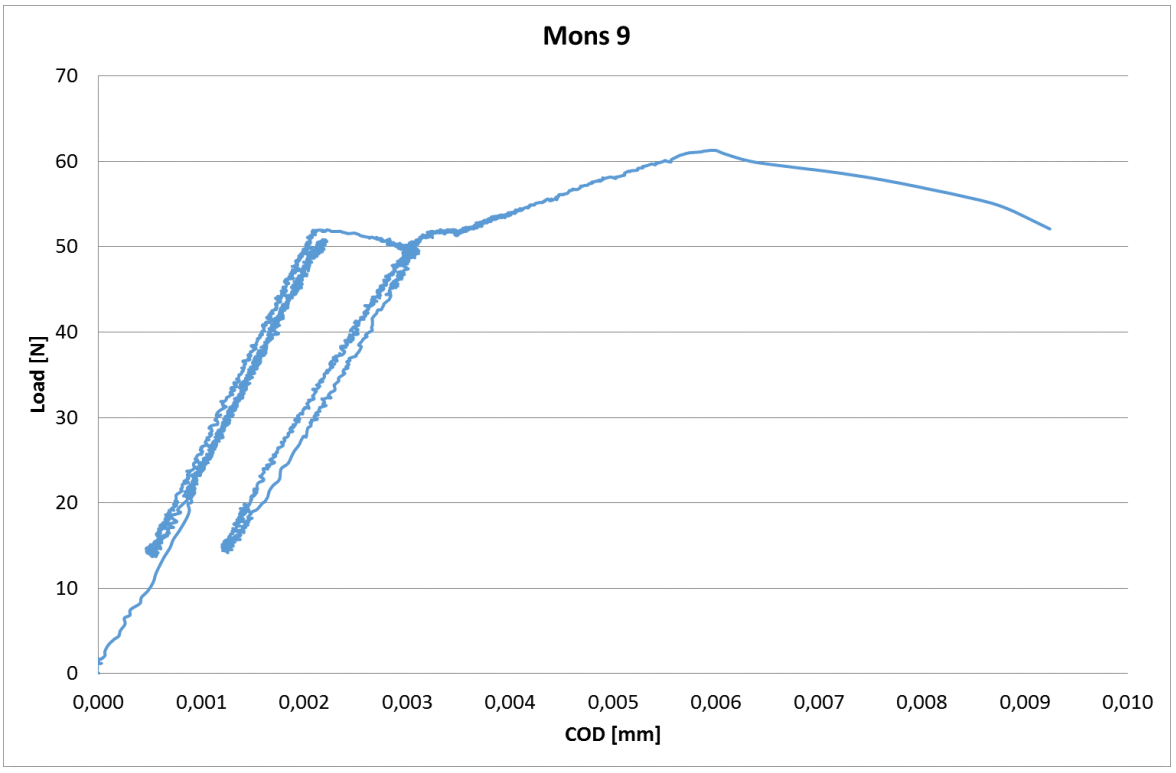

Figure 11-9: Load vs COD for Mons 9. Diameter 37.25 mm

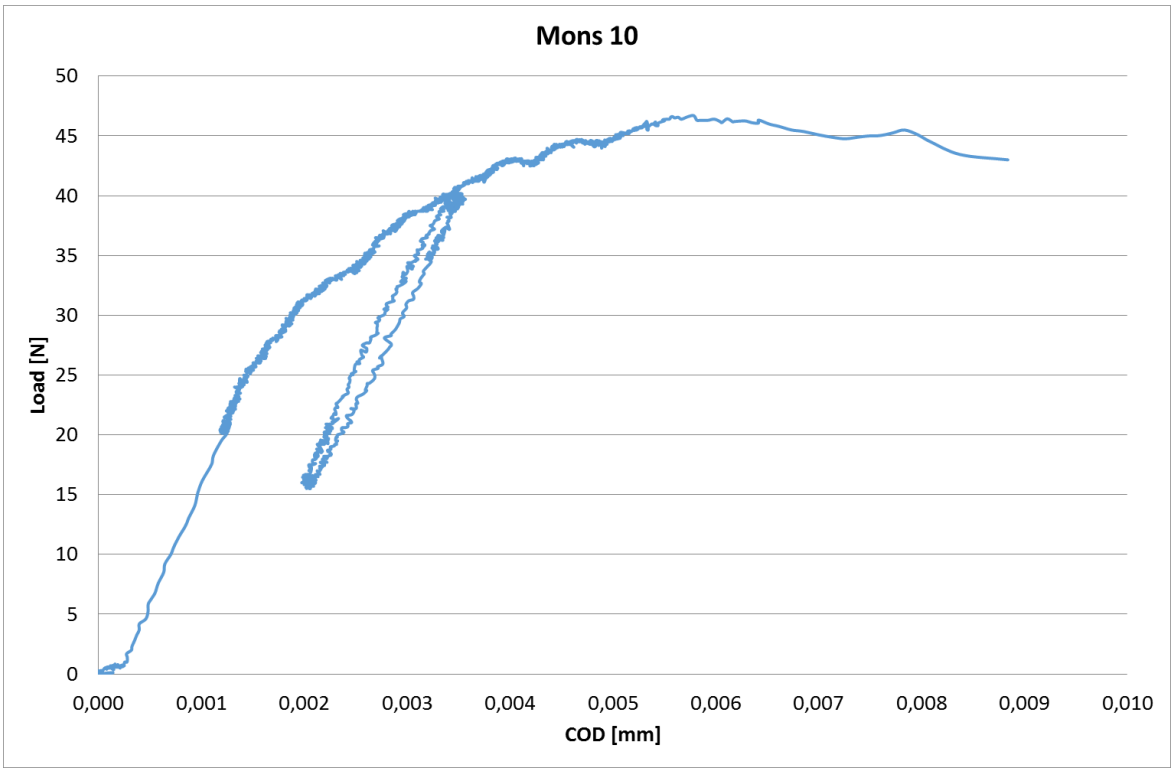

Figure 11-10: Load vs COD for Mons 10. Diameter 37.31 mm

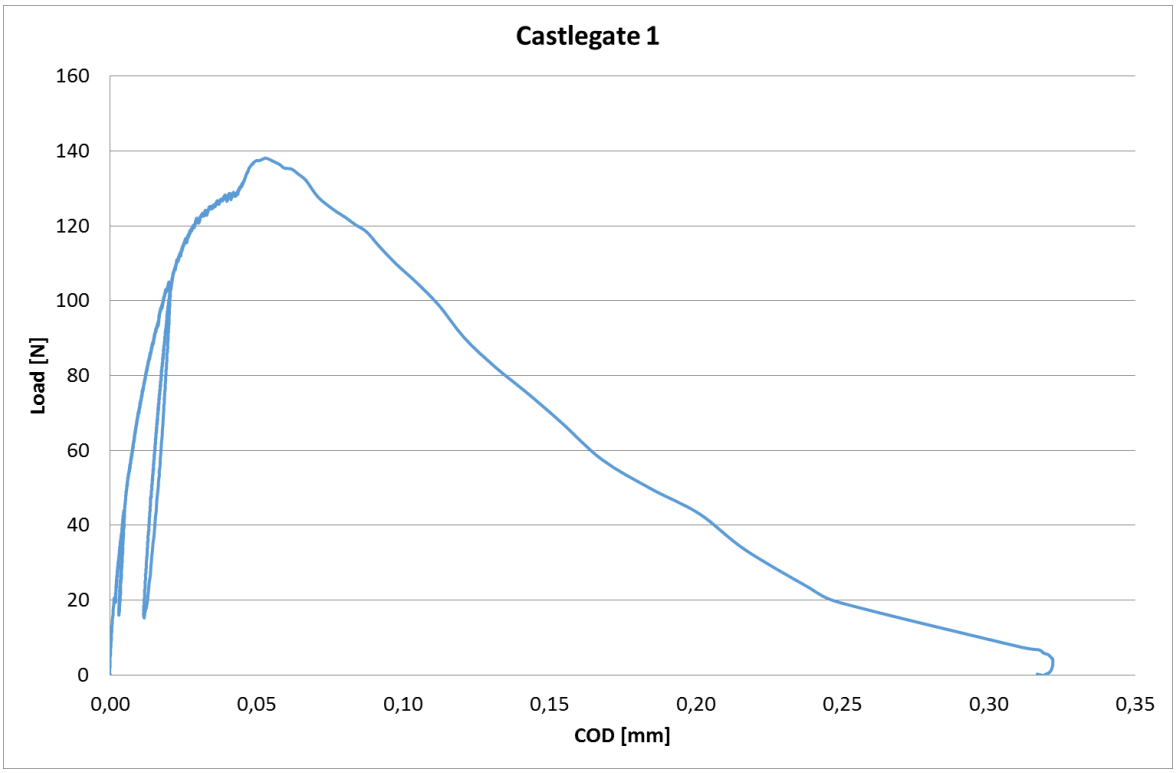

Figure 11-11: Load vs COD for Castlegate 1. Diameter is 51.24 mm

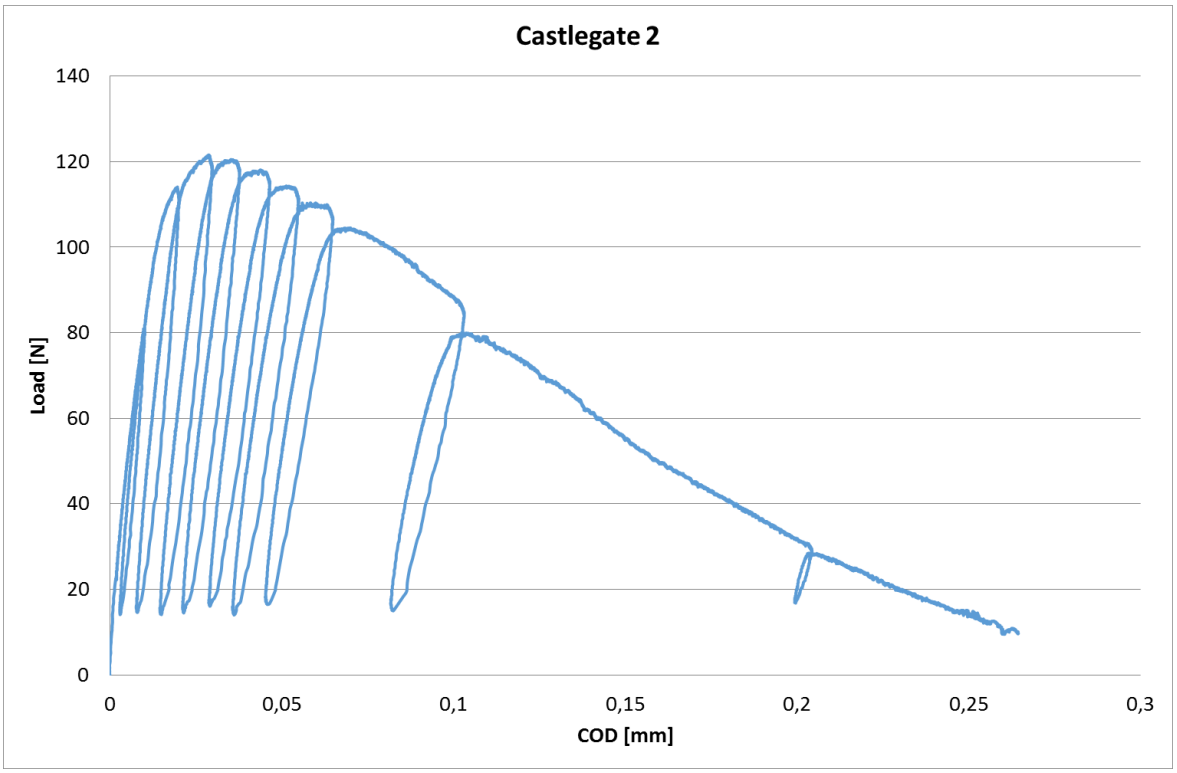

Figure 11-12: Load vs COD for Castlegate 2. Diameter is 51.40 mm

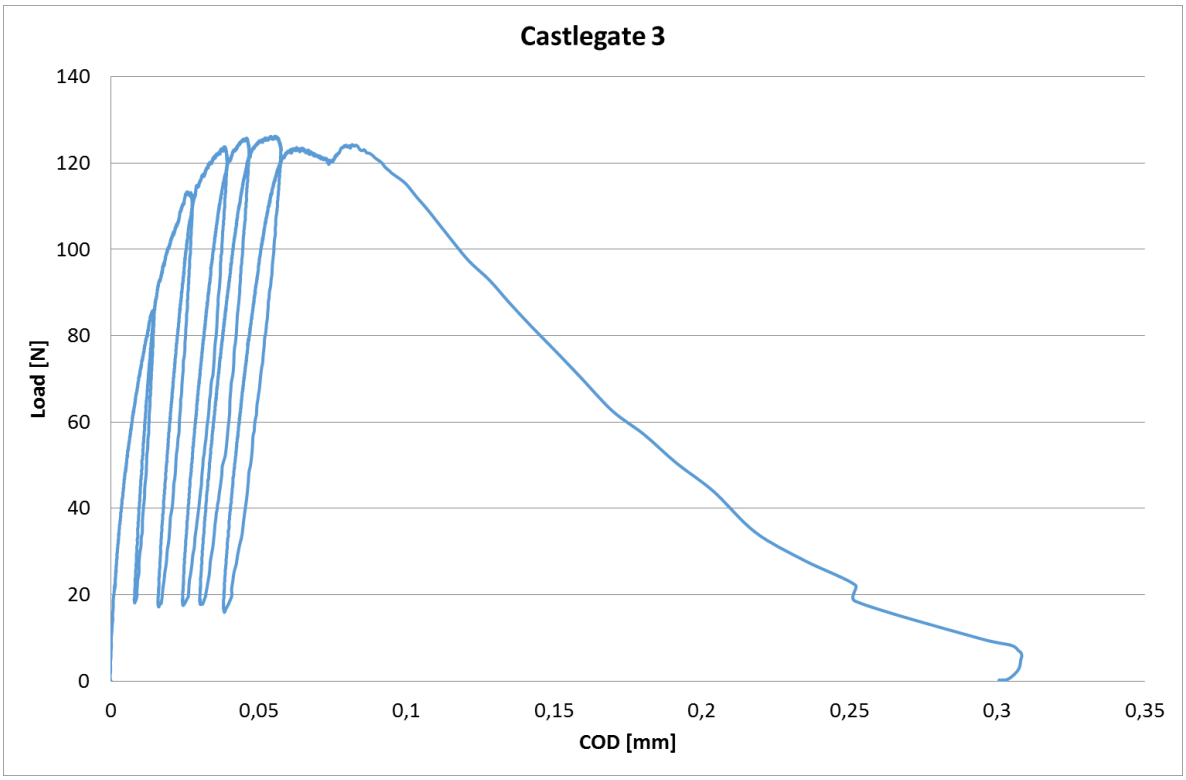

Figure 11-13: Load vs COD for Castlegate 3. Diameter is 51.26 mm

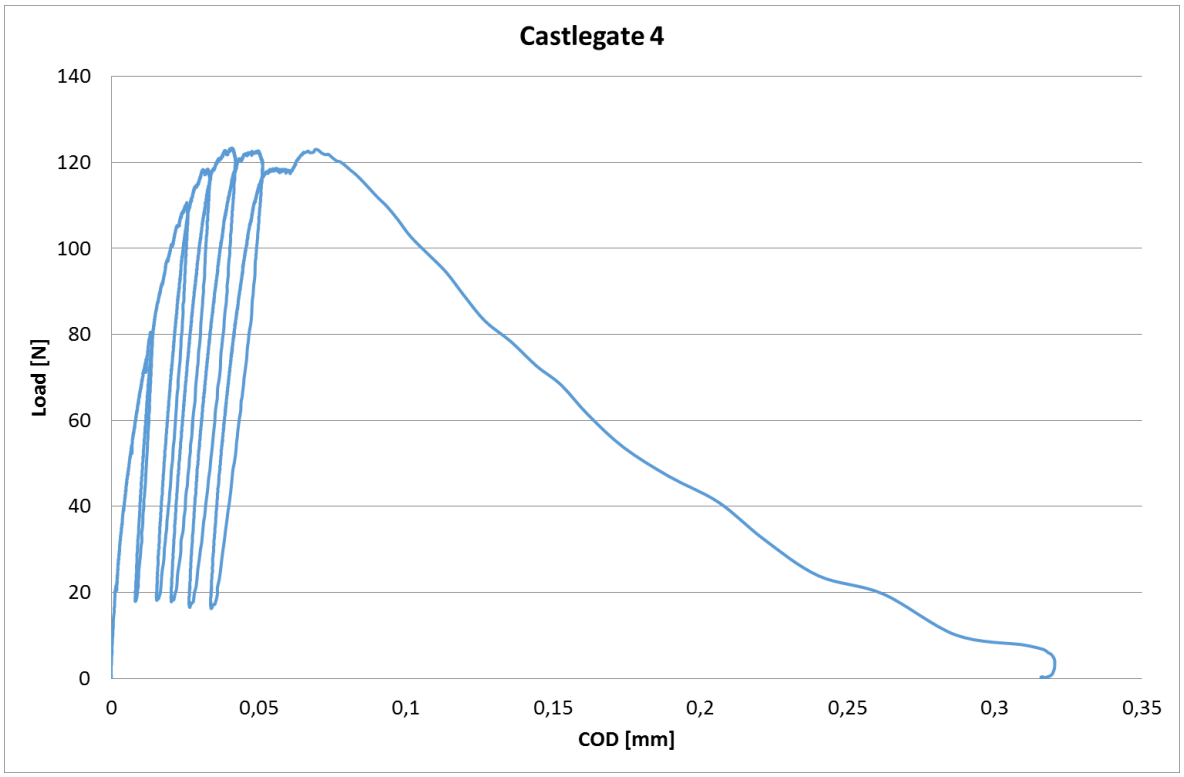

Figure 11-14: Load vs COD for Castlegate 4. Diameter is 51.36 mm

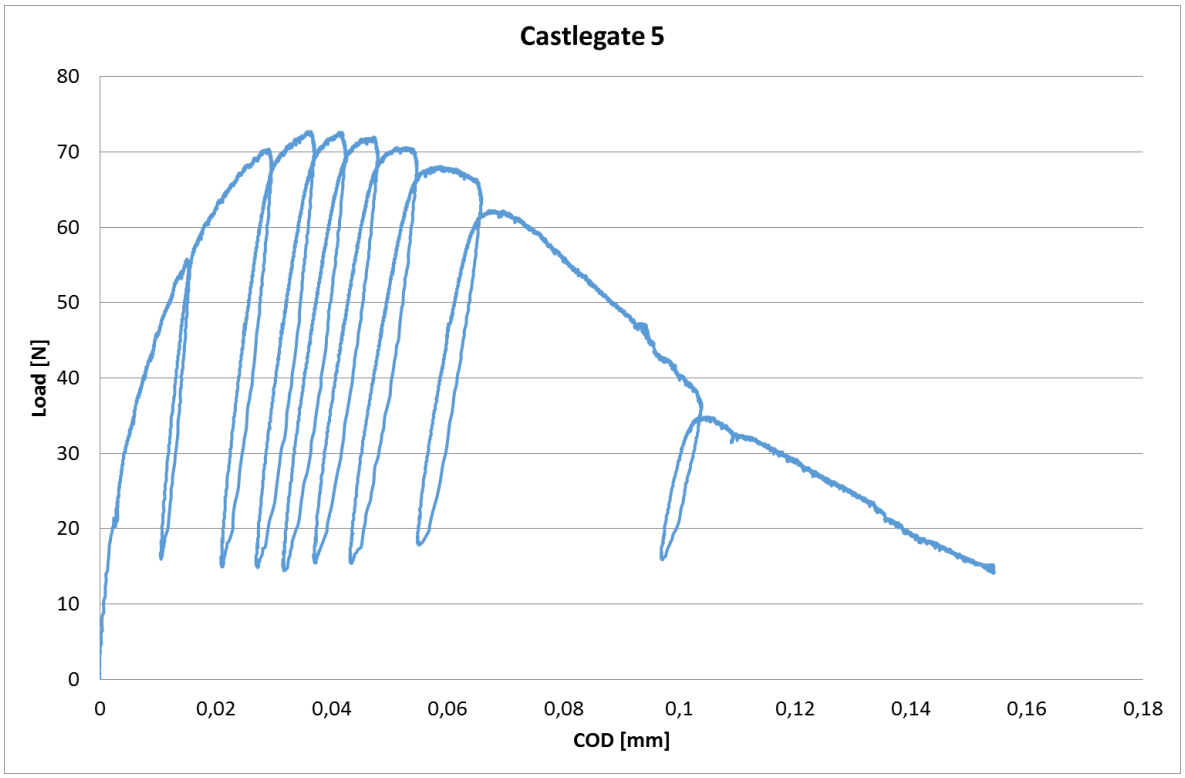

Figure 11-15: Load vs COD for Castlegate 5. Diameter is 37.39 mm

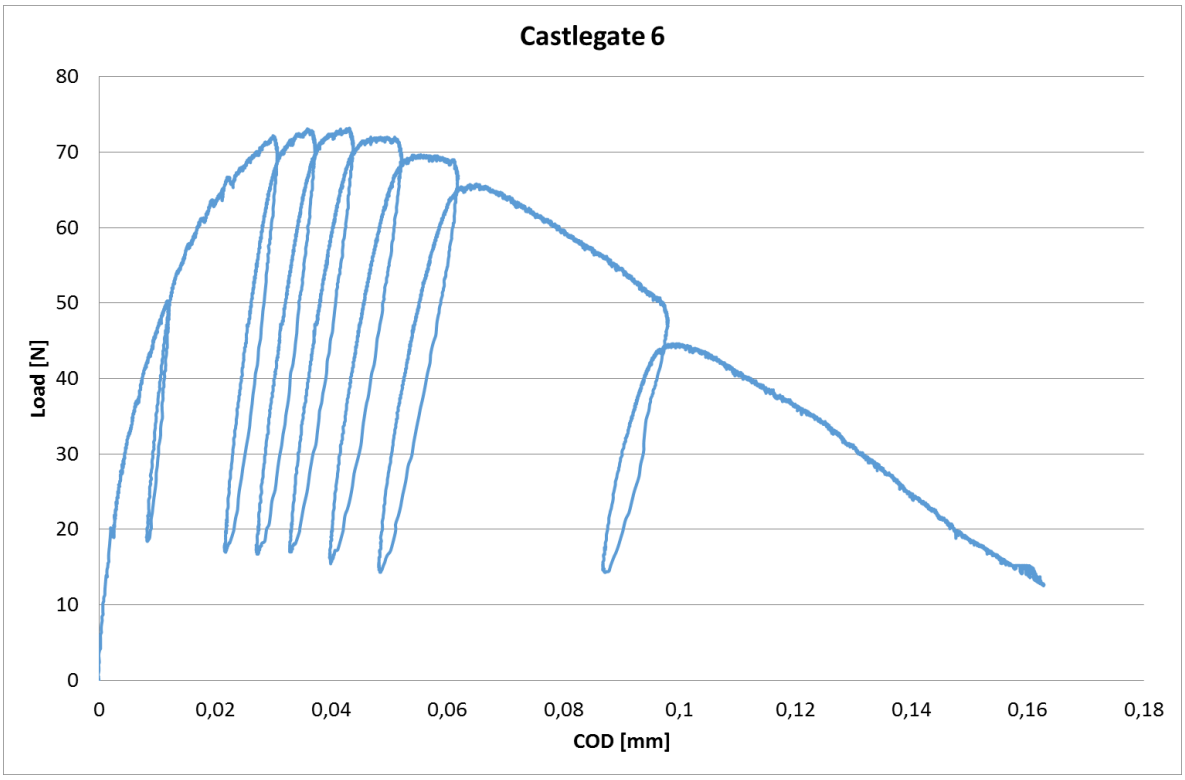

Figure 11-16: Load vs COD for Castlegate 6. Diameter is 37.39 mm

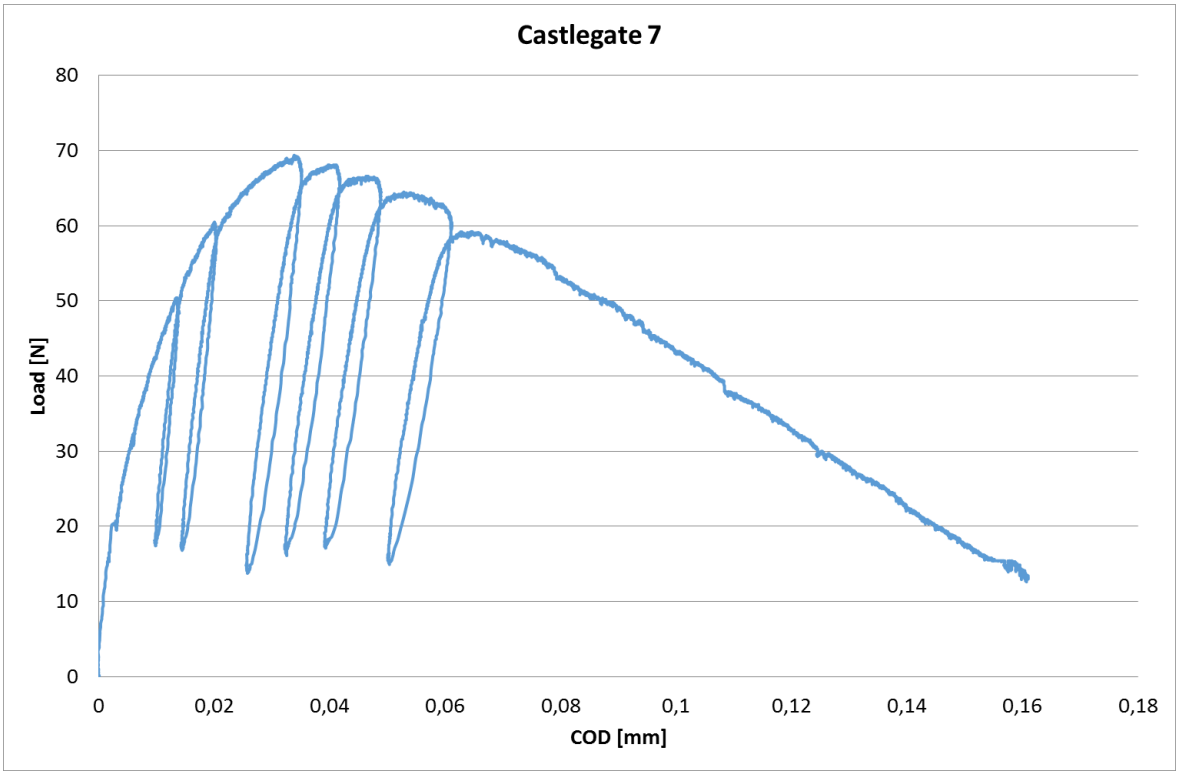

Figure 11-17: Load vs COD for Castlegate 7. Diameter is 37.35 mm

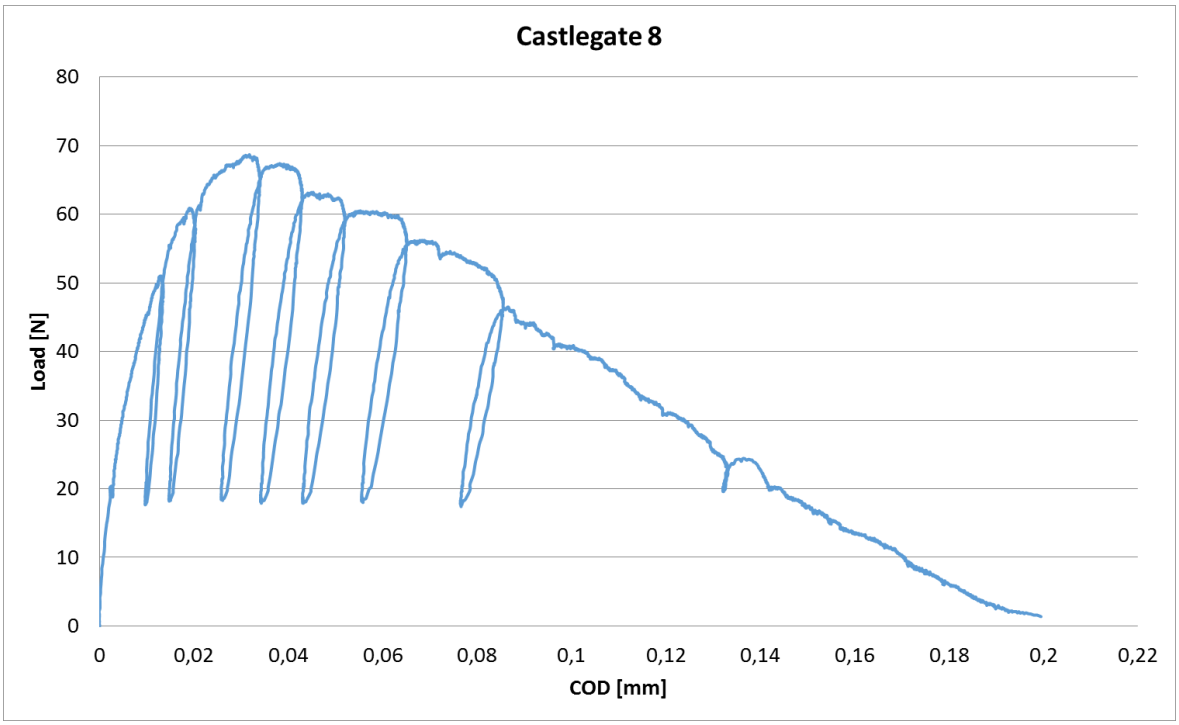

Figure 11-18: Load vs COD for Castlegate 8. Diameter is 37.42 mm

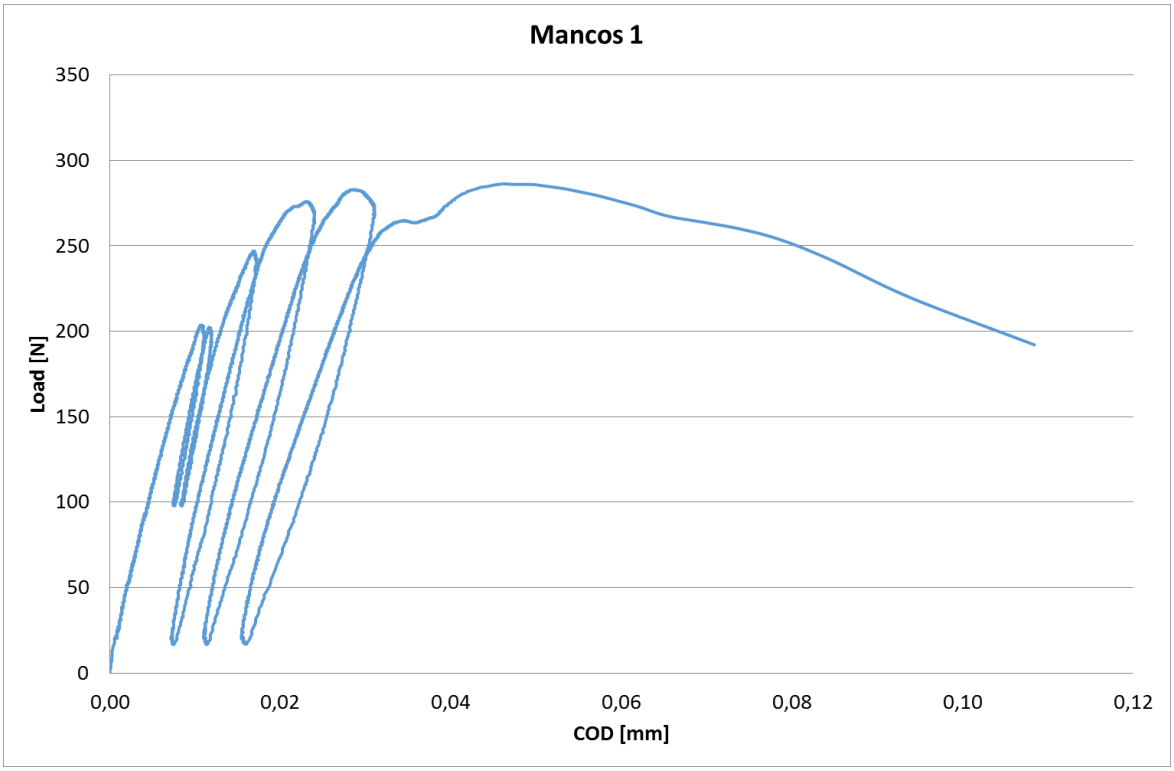

Figure 11-19: Load vs COD for Mancos 1. Diameter is 39.96 mm. Inclination is 0°

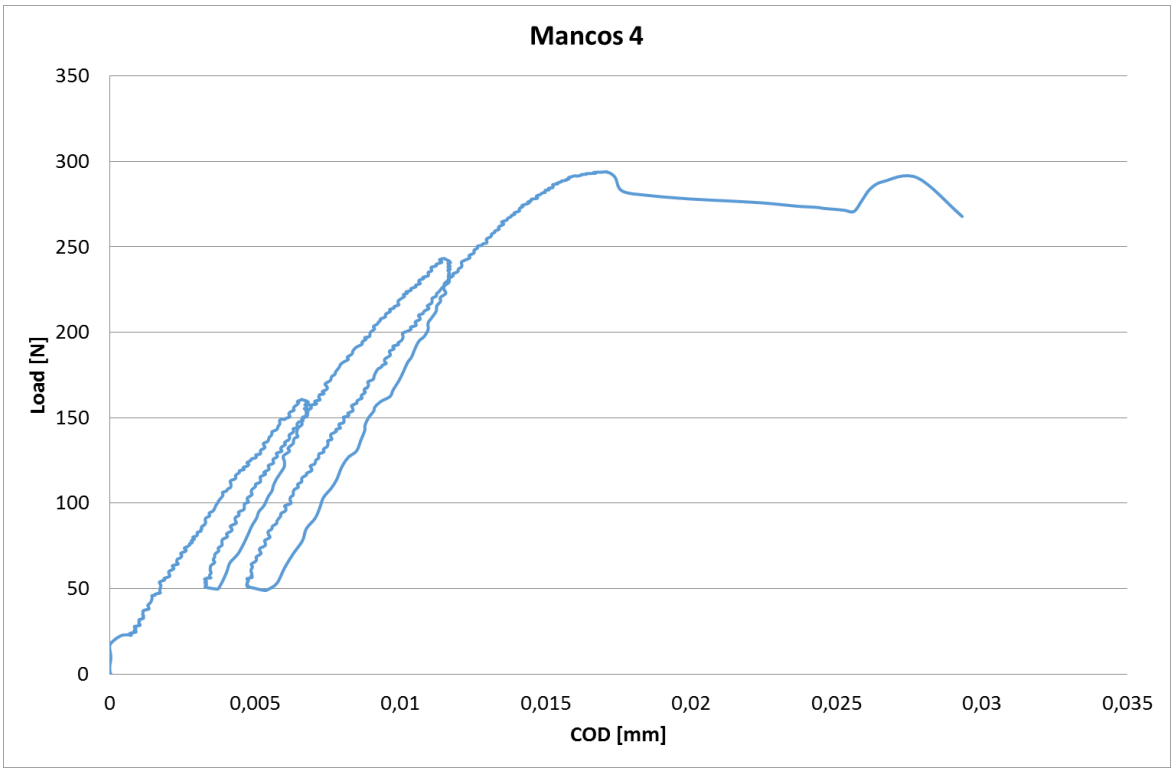

Figure 11-20: Load vs COD for Mancos 4. Diameter is 39.93 mm. Inclination is 0°

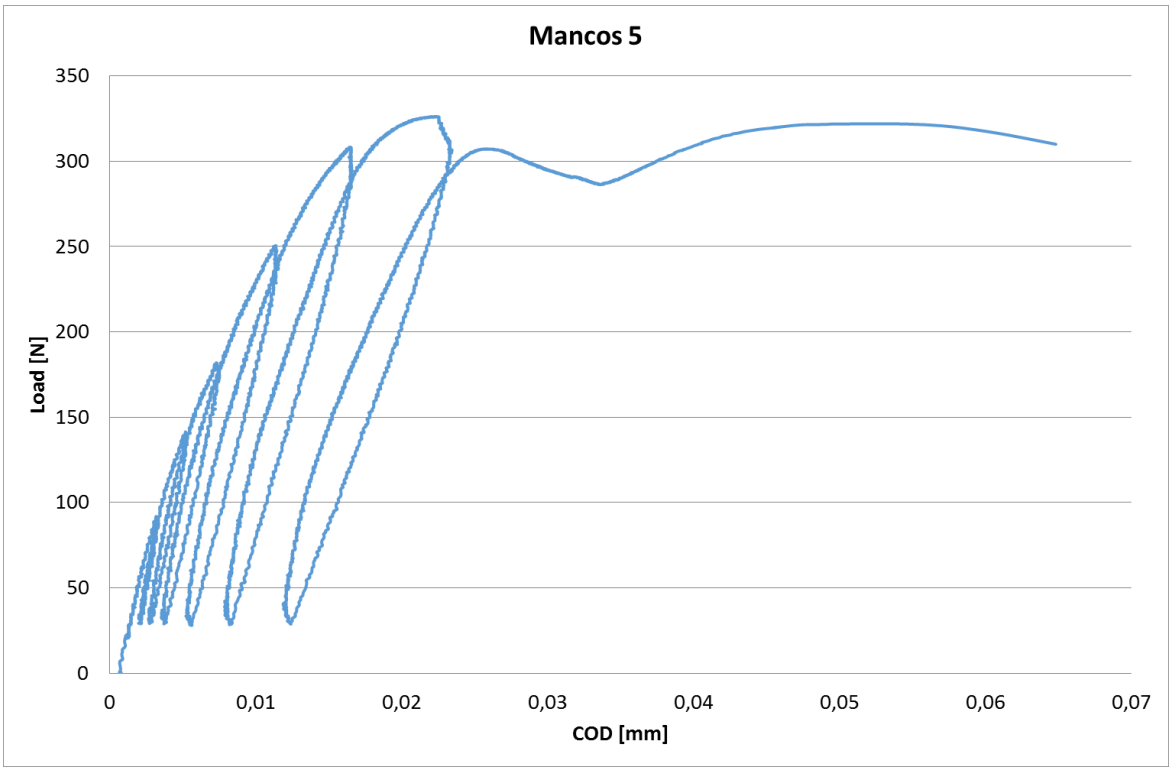

Figure 11-21: Load vs COD for Mancos 5. Diameter is 38.28 mm. Inclination is 15°. Notch is parallel to bedding

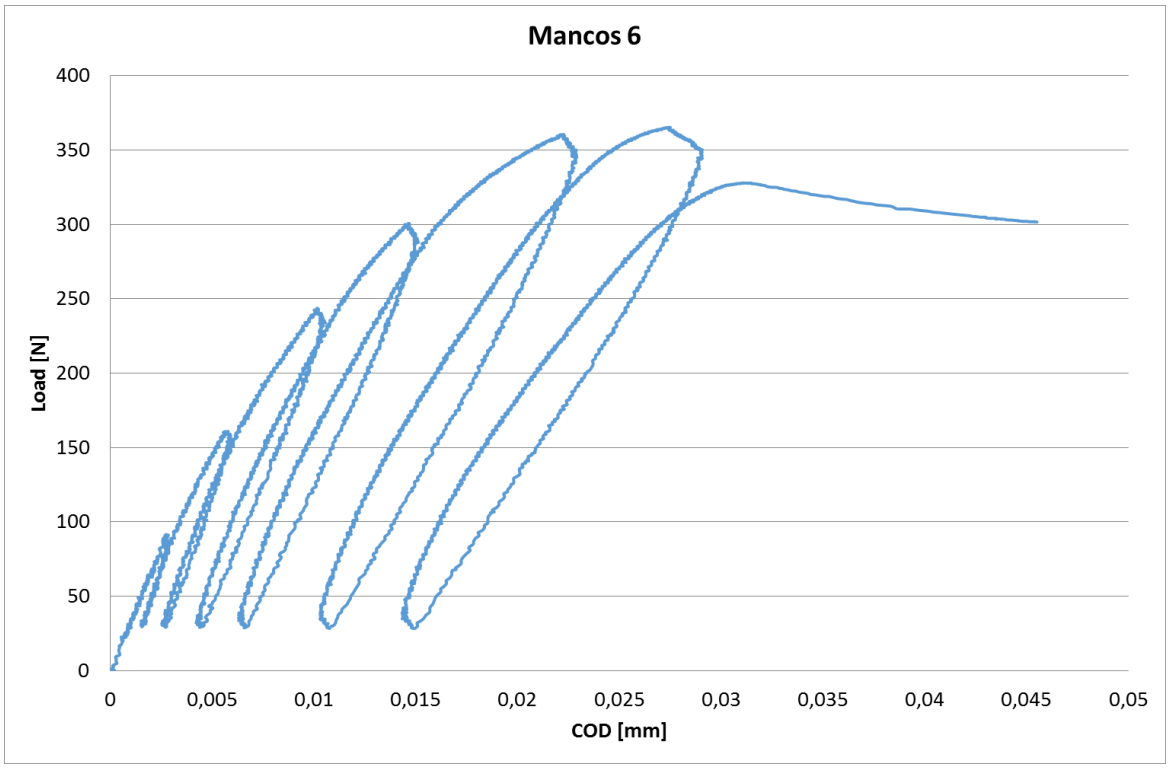

Figure 11-22: Load vs COD for Mancos 6. Diameter is 38.23 mm. Inclination is 15°. Notch is perpendicular to bedding

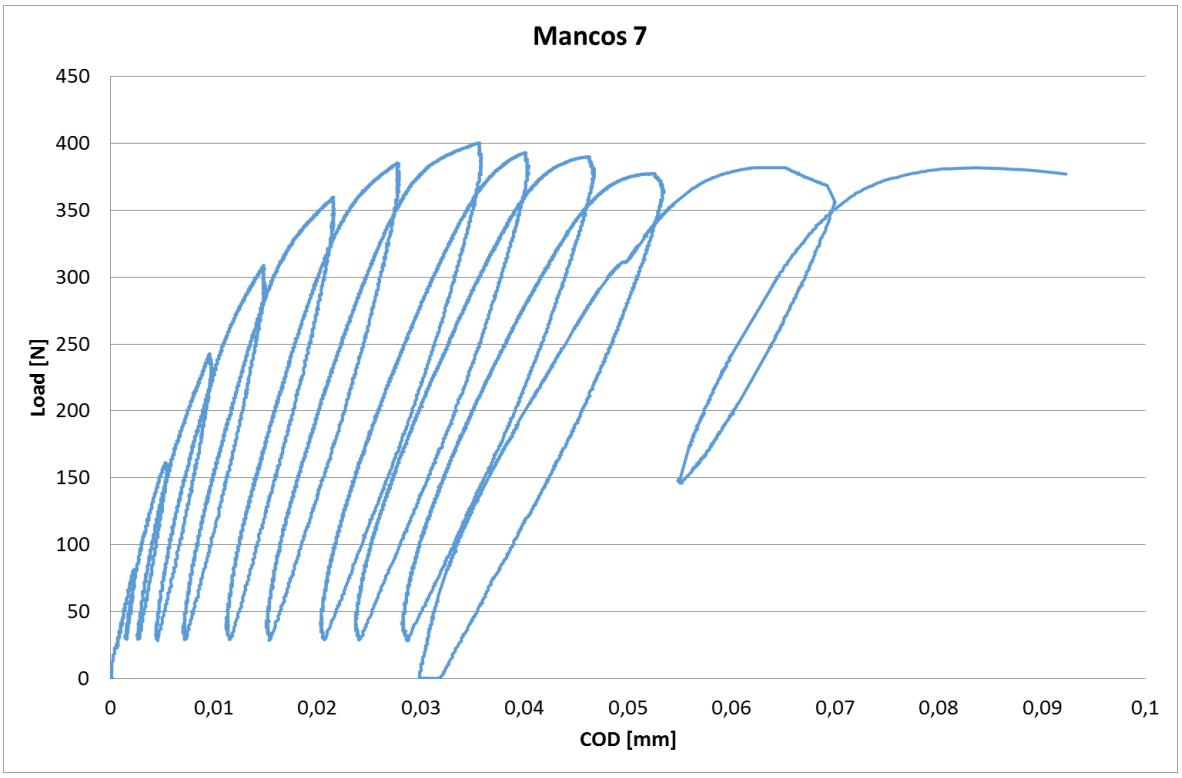

Figure 11-23: Load vs COD for Mancos 7. Diameter is 38.20 mm. Inclination is 30°. Notch is parallel to bedding

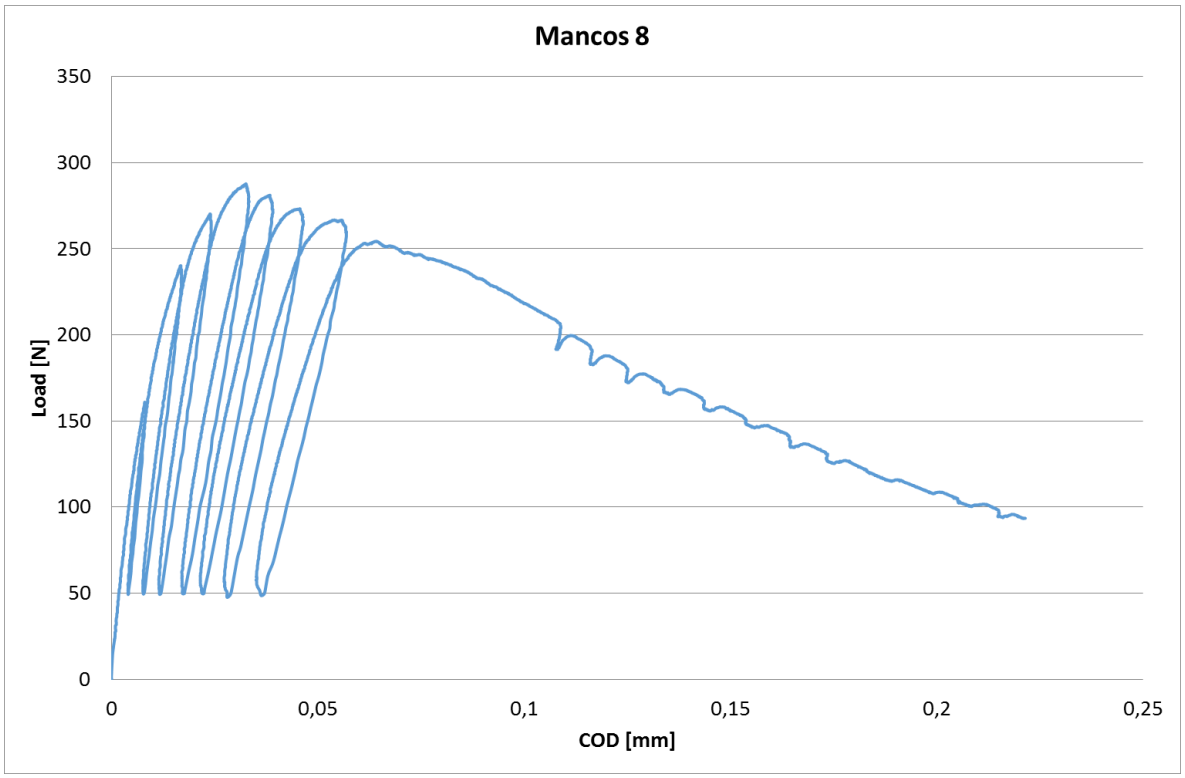

Figure 11-24: Load vs COD for Mancos 8. Diameter is 38.28 mm. Inclination is 30°. Notch is perpendicular to bedding

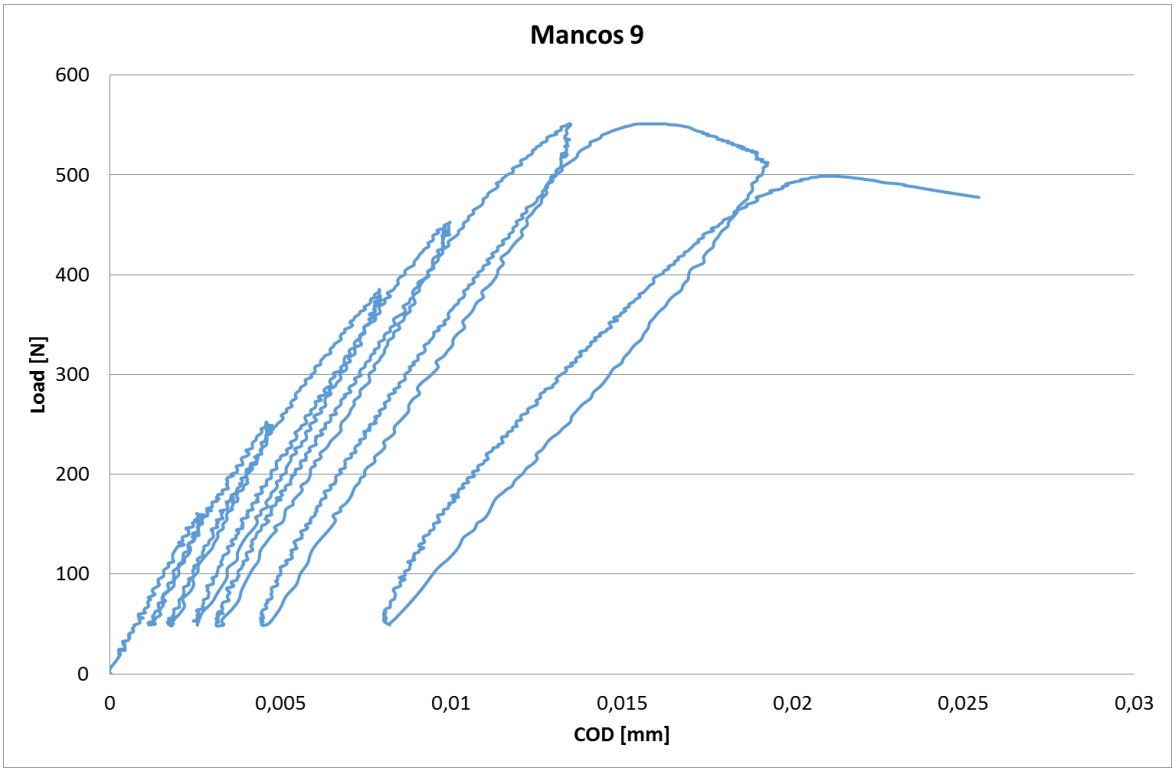

Figure 11-25: Load vs COD for Mancos 9. Diameter is 38.25 mm. Inclination is 45°. Notch is parallel to bedding

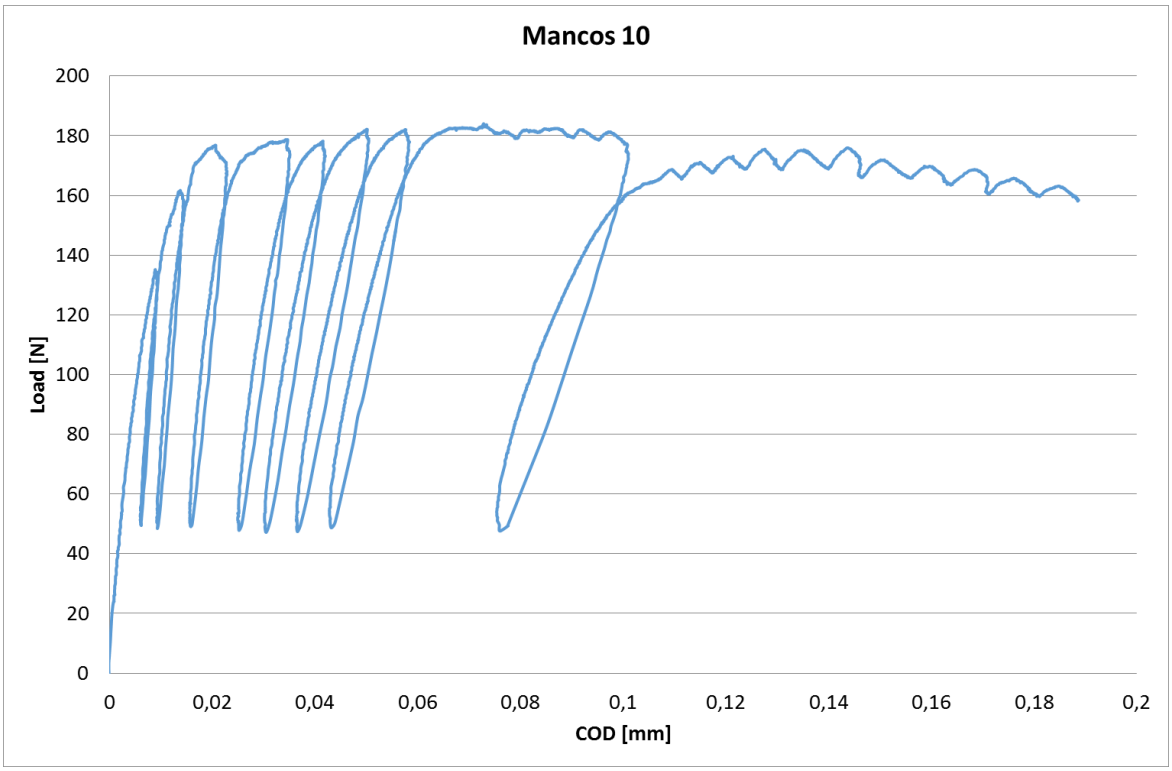

Figure 11-26: Load vs COD for Mancos 10. Diameter is 38.29 mm. Inclination is 45°. Notch is perpendicular to bedding

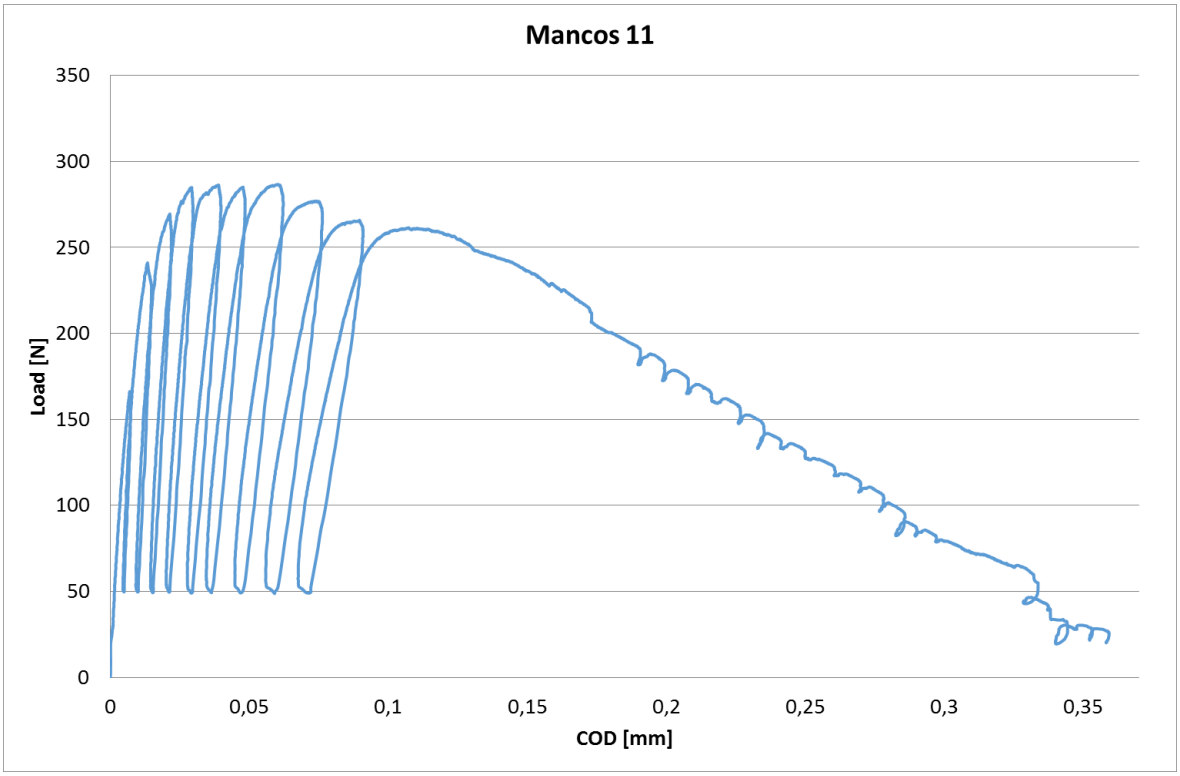

Figure 11-27: Load vs COD for Mancos 11. Diameter is 38.23 mm. Inclination is 45°. Notch is perpendicular to bedding

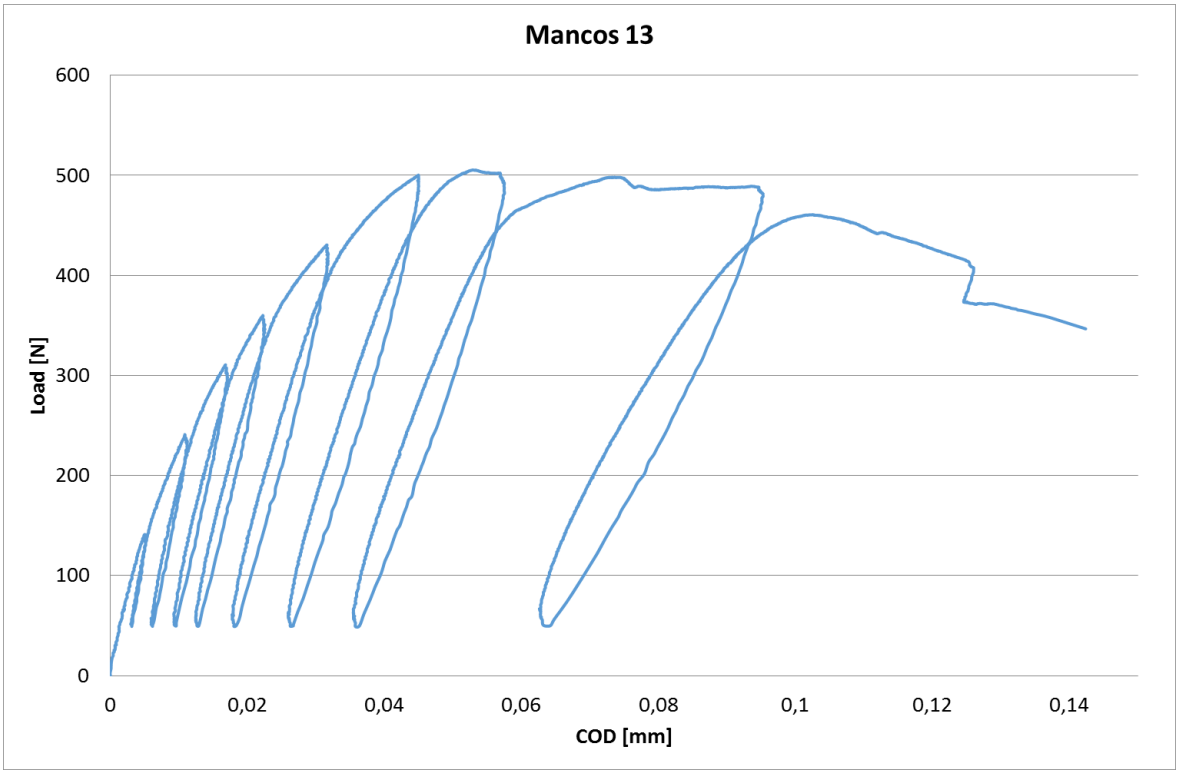

Figure 11-28: Load vs COD for Mancos 13. Diameter is 38.26 mm. Inclination is 60°. Notch is perpendicular to bedding

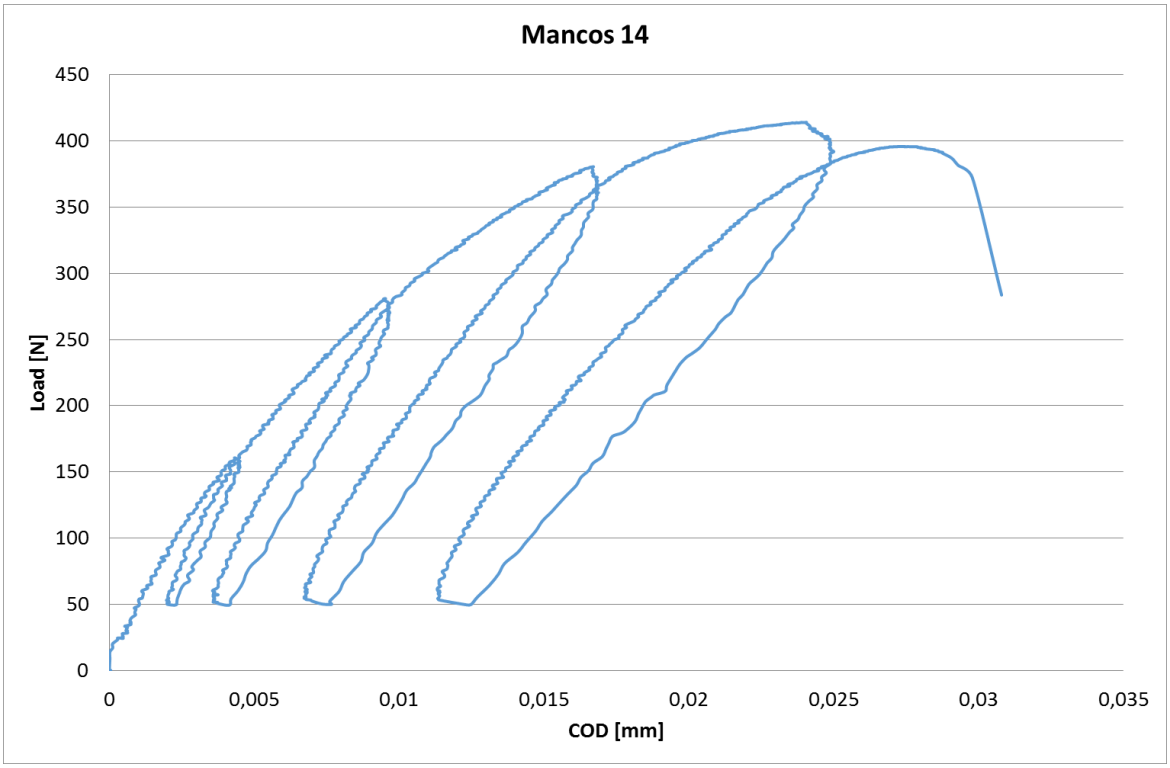

Figure 11-29: Load vs COD for Mancos 14. Diameter 38.20 mm. Inclination is 75°. Notch is perpendicular to bedding

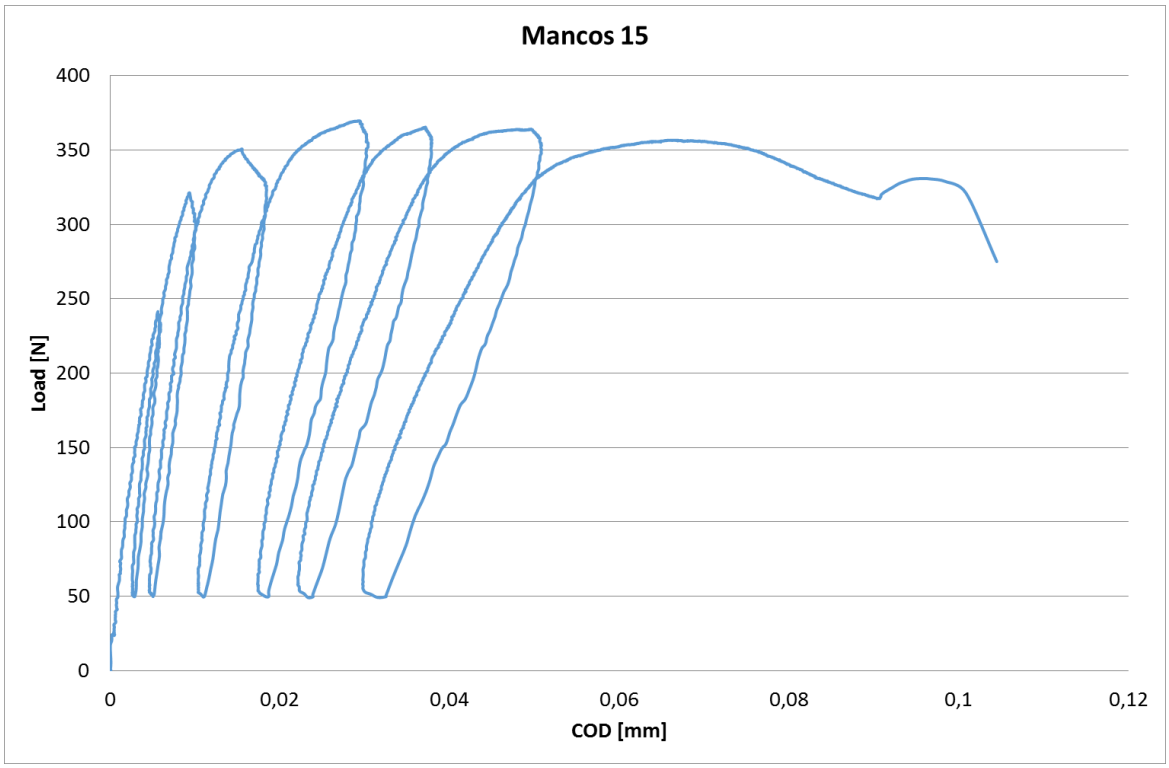

Figure 11-30: Load vs COD for Mancos 15. Diameter is 38.25 mm. Inclination is 75°. Notch is parallel to bedding

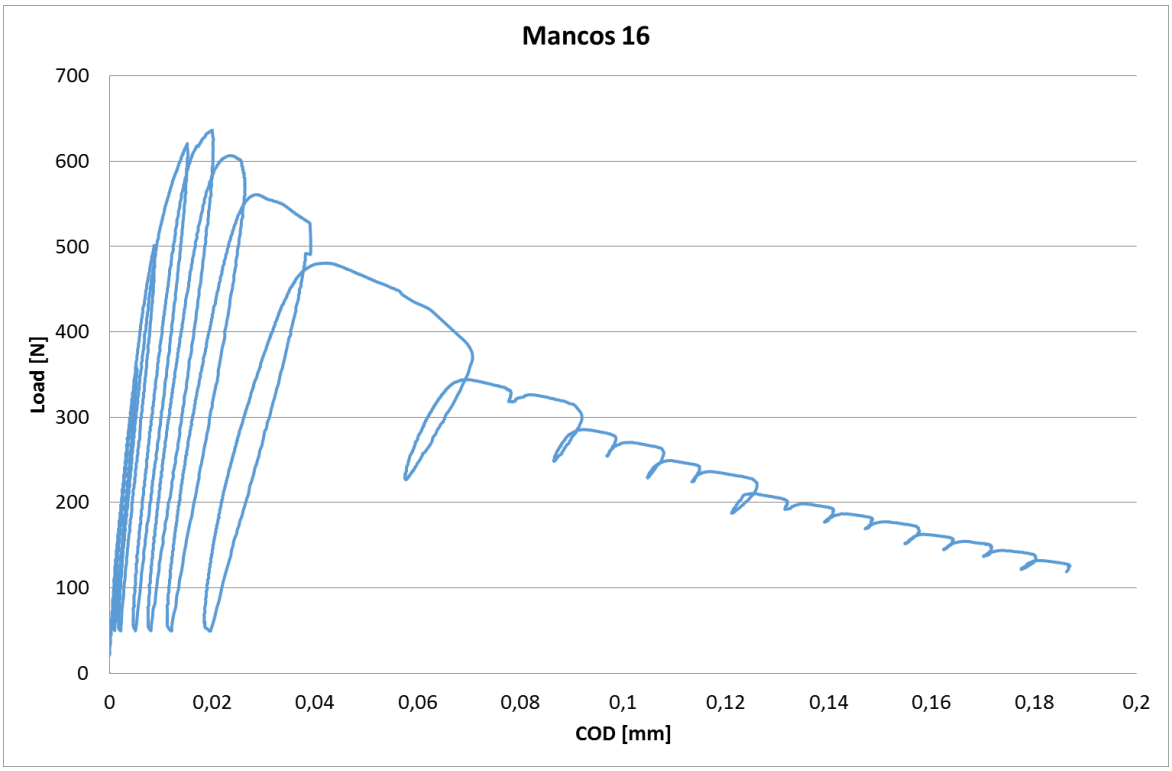

Figure 11-31: Load vs COD for Mancos 16. Diameter is 38.25 mm. Inclination is 90°. Notch is parallel to bedding

11.5 Plot for Load vs LPD

Below are the plots given for load vs COD data. The plots are cut off where the sample fails such that is possible to see the cycles and interesting trends.

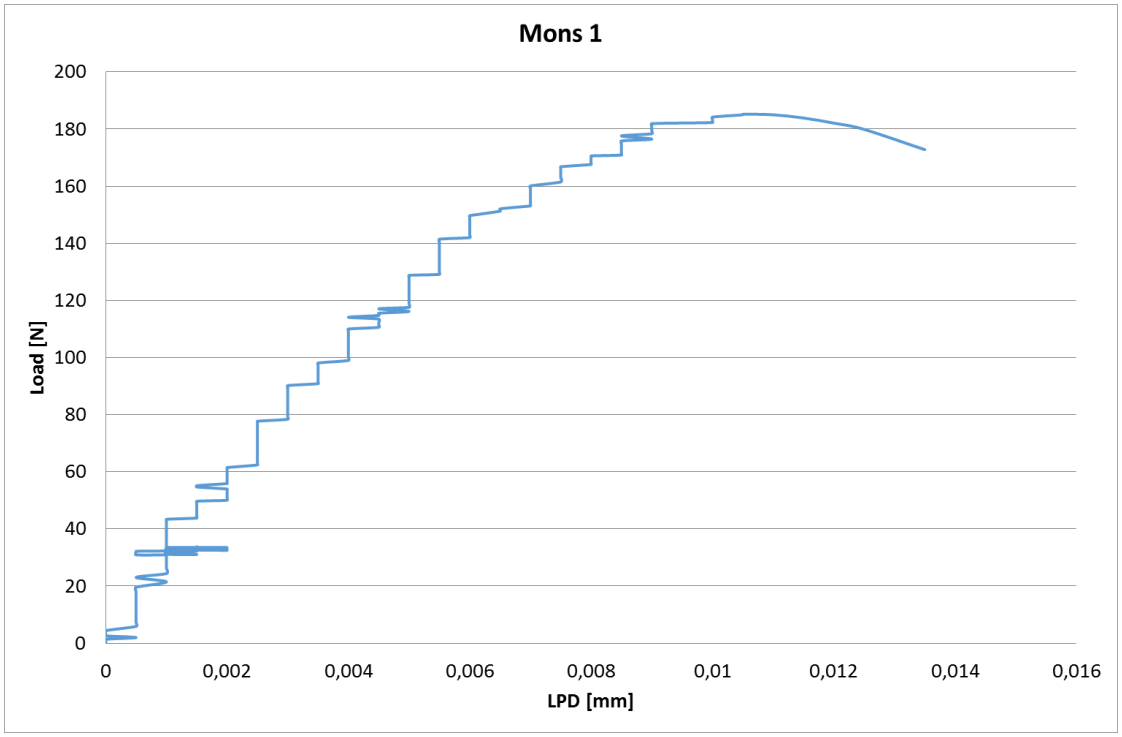

Figure 11-32: Load vs LPD for Mons 1. Diameter is 50.87 mm. Note that no cycles were run in this test

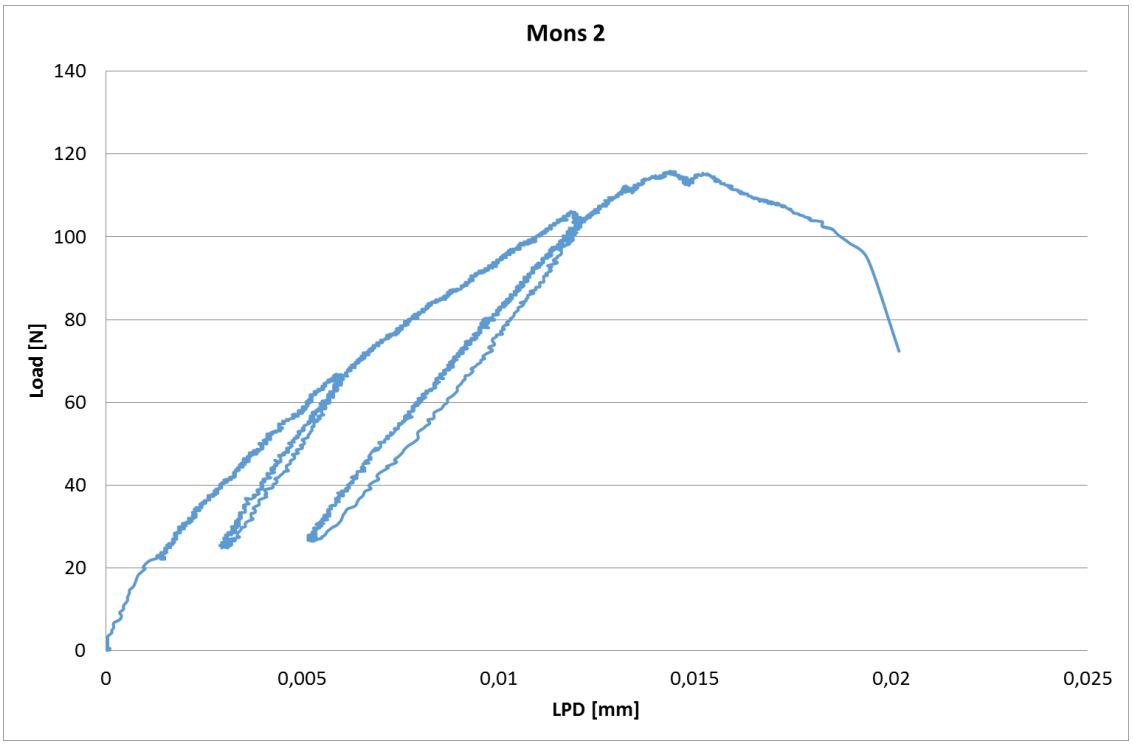

Figure 11-33:Load vs LPD for Mons 2. Diameter is 51.21 mm

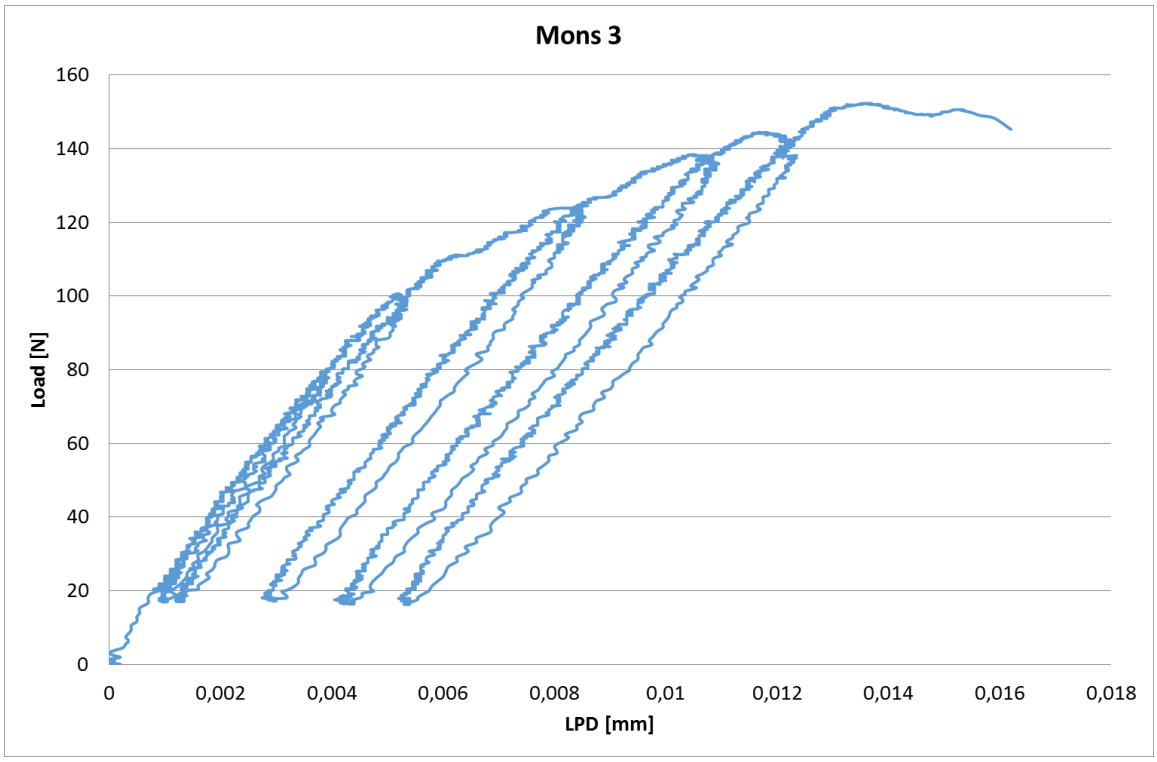

Figure 11-34: Load vs LPD for Mons 3. Diameter is 51.08 mm

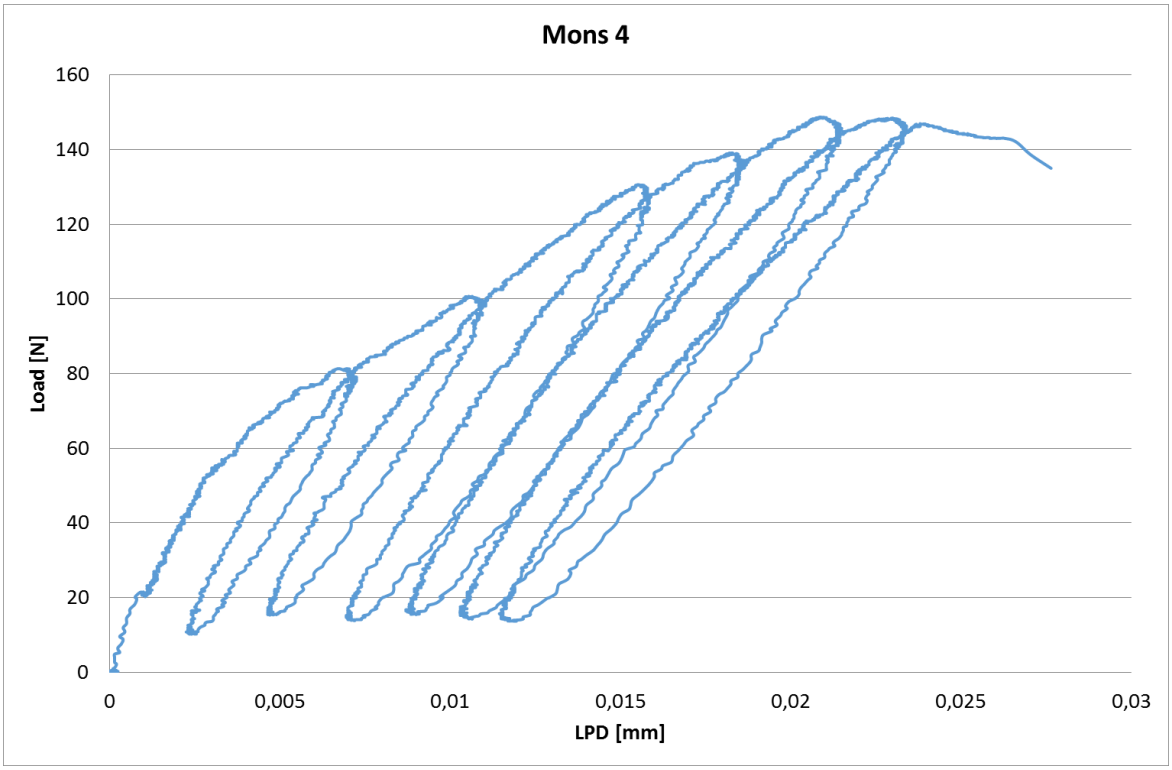

Figure 11-35: Load vs LPD for Mons 4. Diameter is 51.12 mm

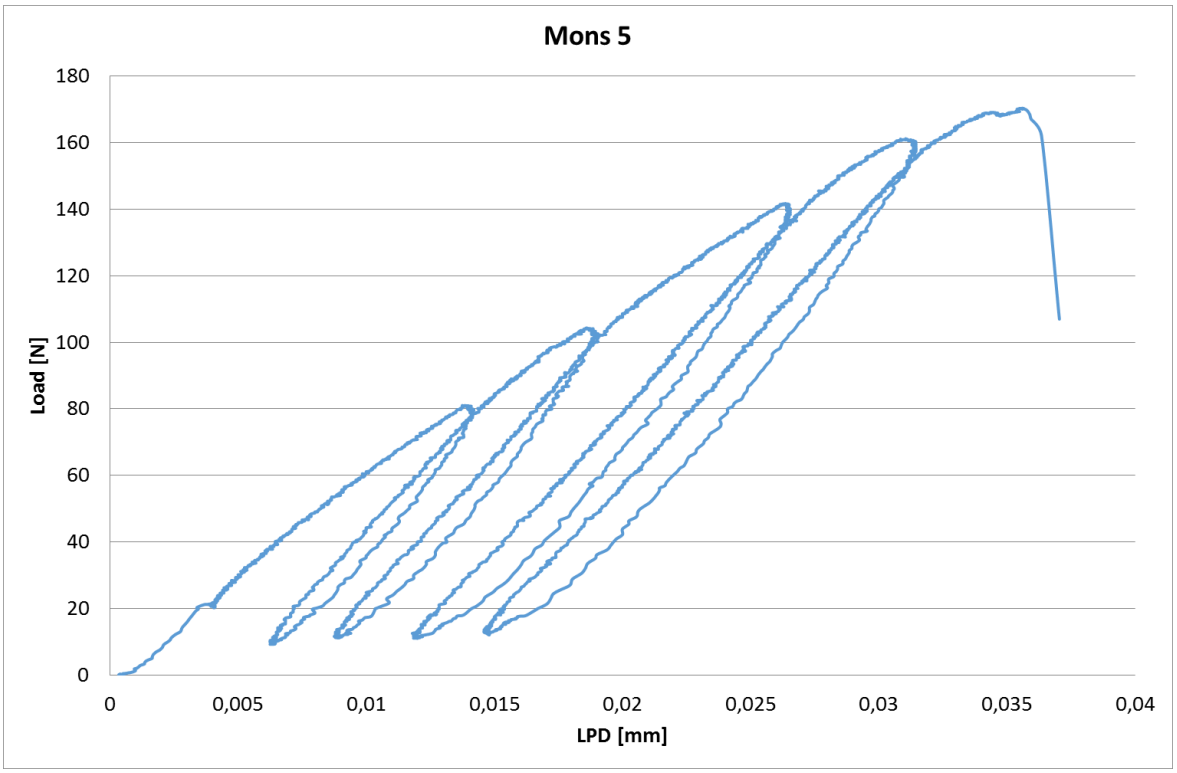

Figure 11-36: Load vs LPD for Mons 5. Diameter is 51.17 mm

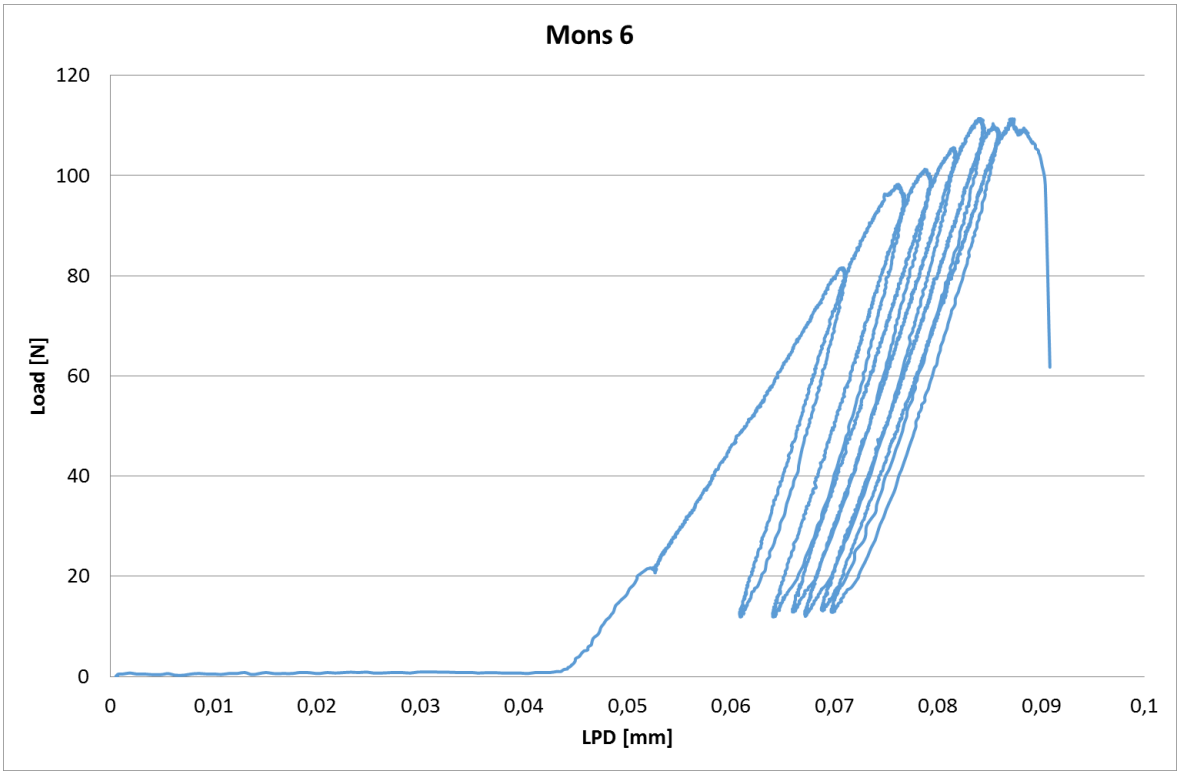

Figure 11-37: Load vs LPD for Mons 6. Diameter is 50.99 mm

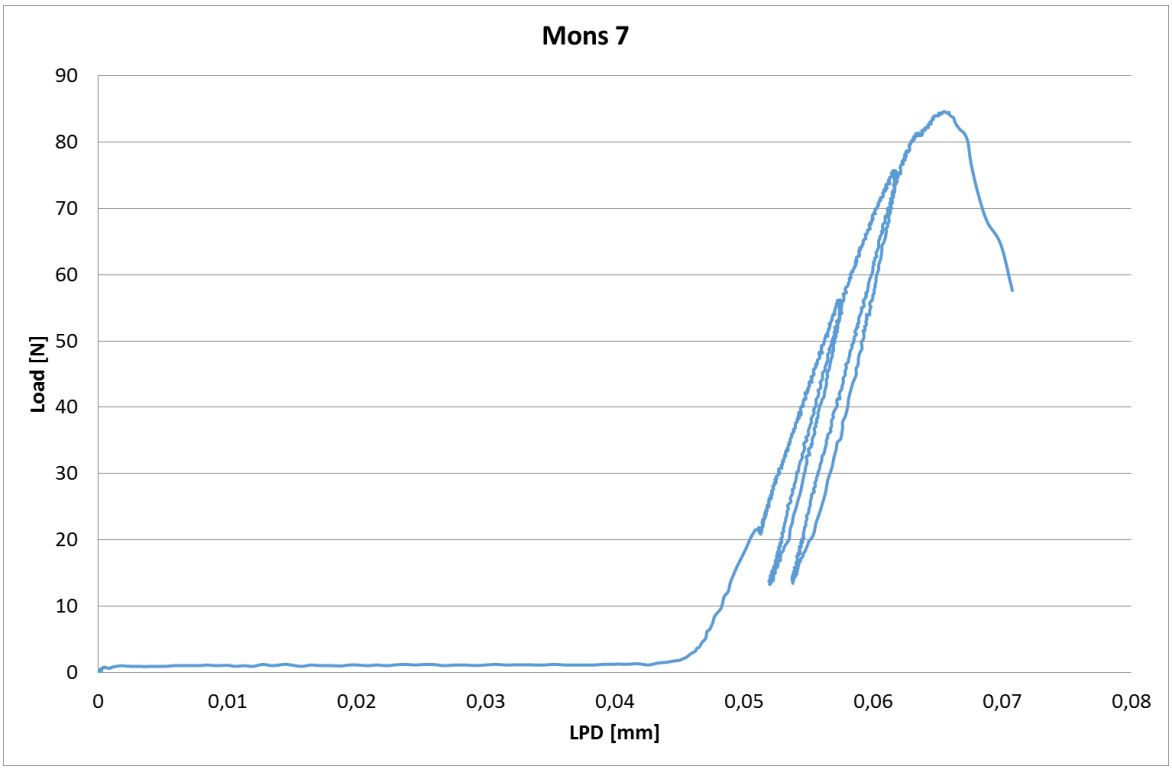

Figure 11-38: Load vs LPD for Mons 7. Diameter is 37.26 mm

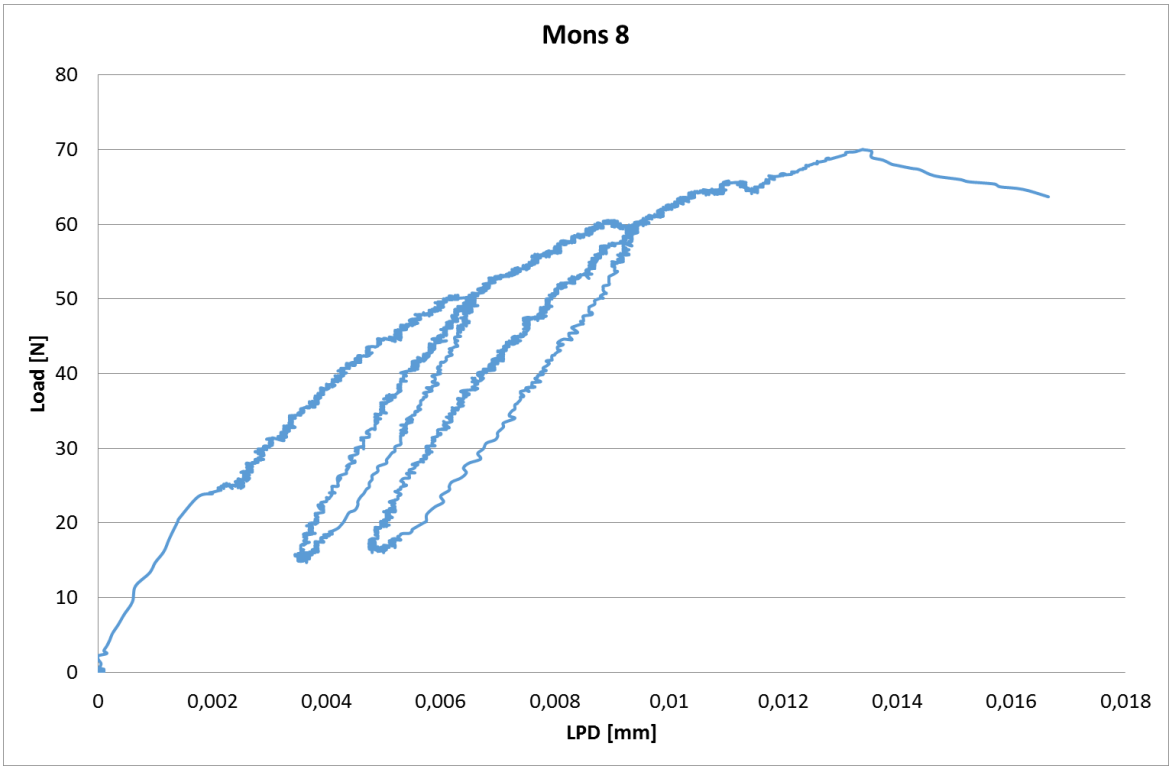

Figure 11-39: Load vs LPD for Mons 8. Diameter is 37.27 mm

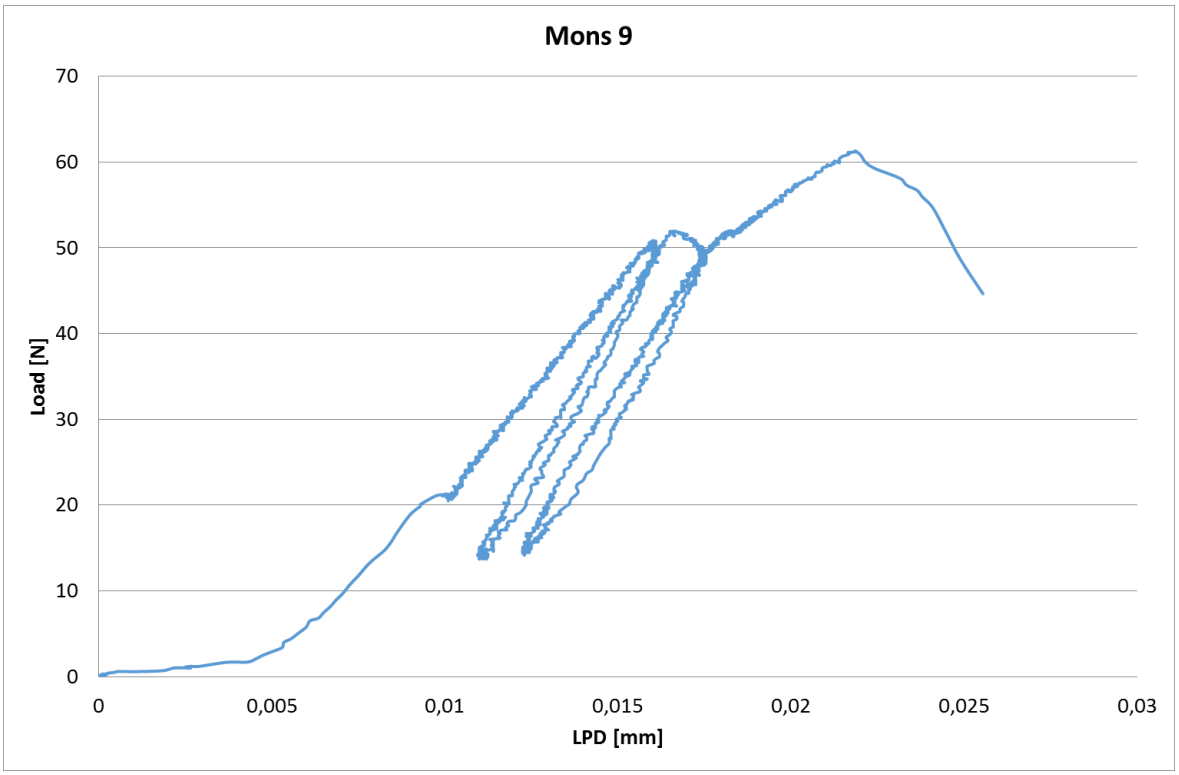

Figure 11-40: Load vs LPD for Mons 9. Diameter is 37.25 mm

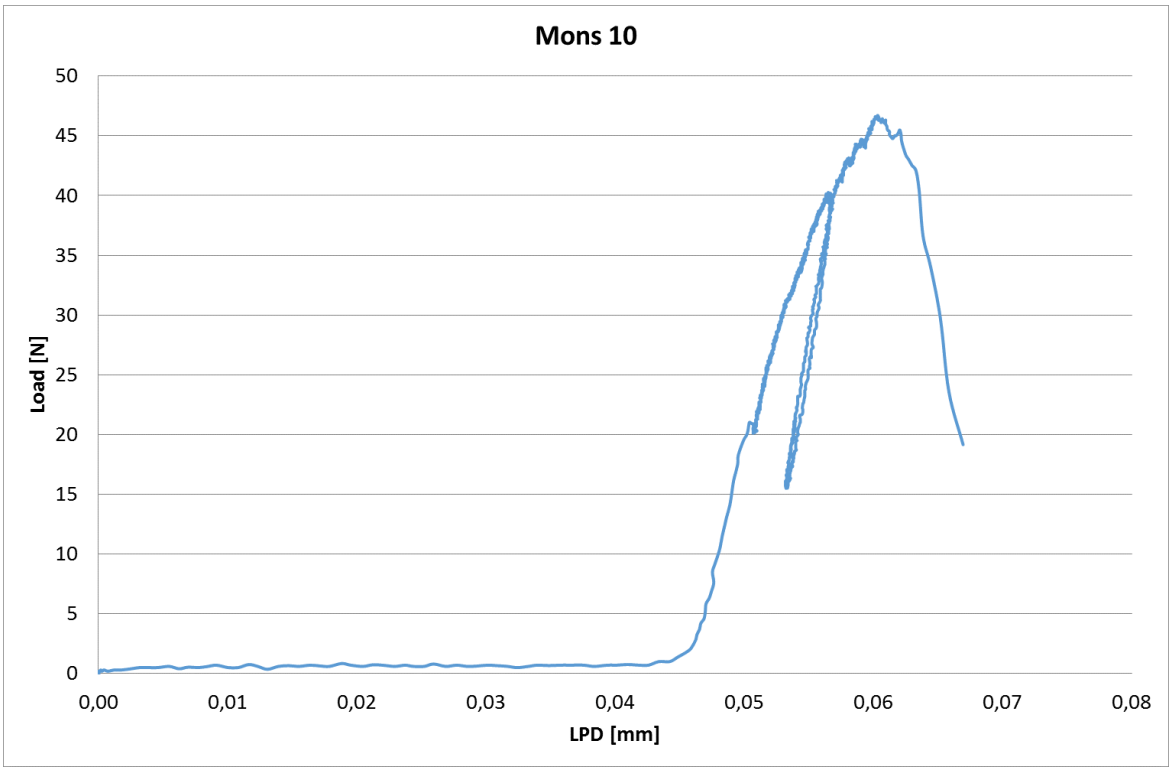

Figure 11-41: Load vs LPD for Mons 10. Diameter is 37.31 mm

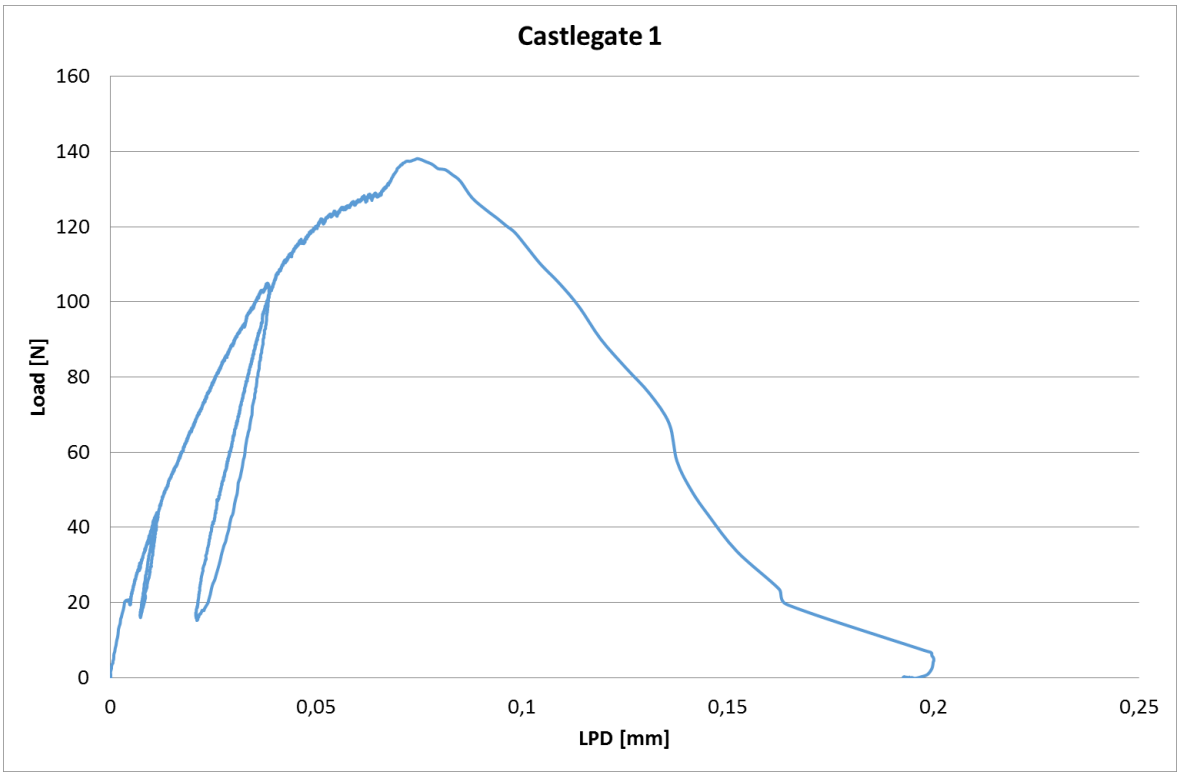

Figure 11-42: Load vs LPD for Castlegate 1. Diameter is 51.24 mm

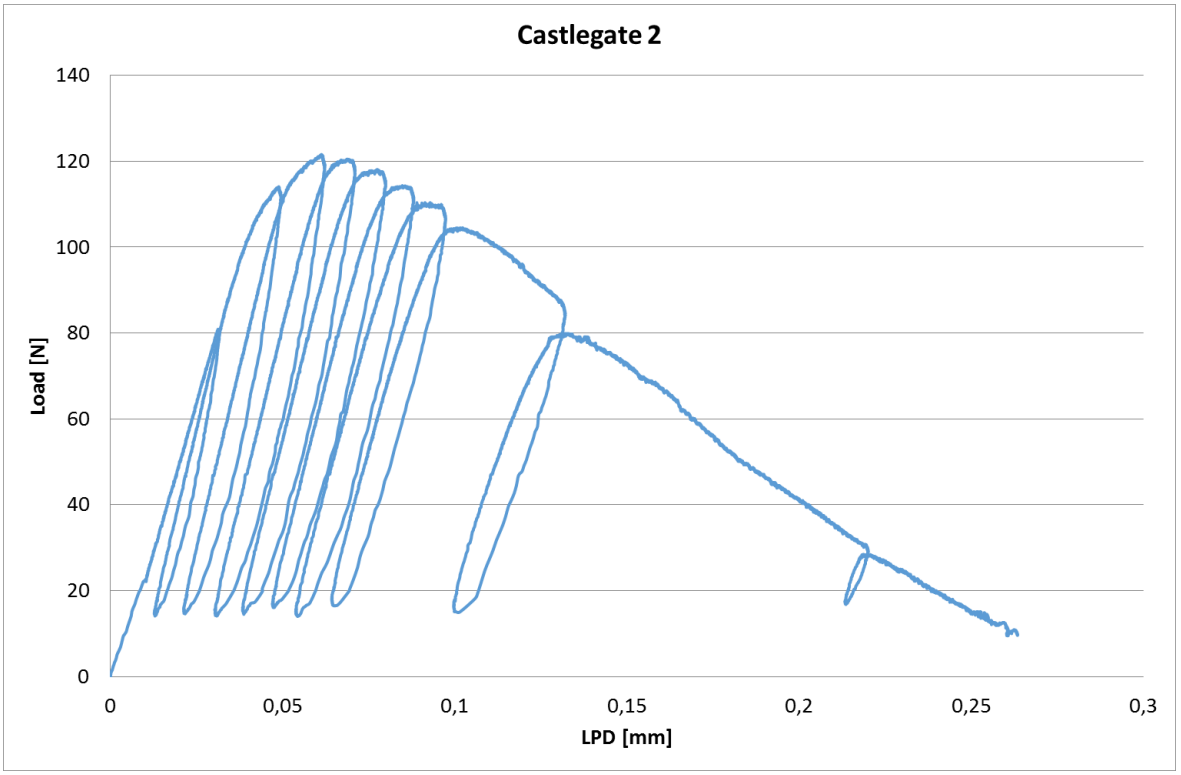

Figure 11-43: Load vs LPD for Castlegate 2. Diameter is 51.40 mm

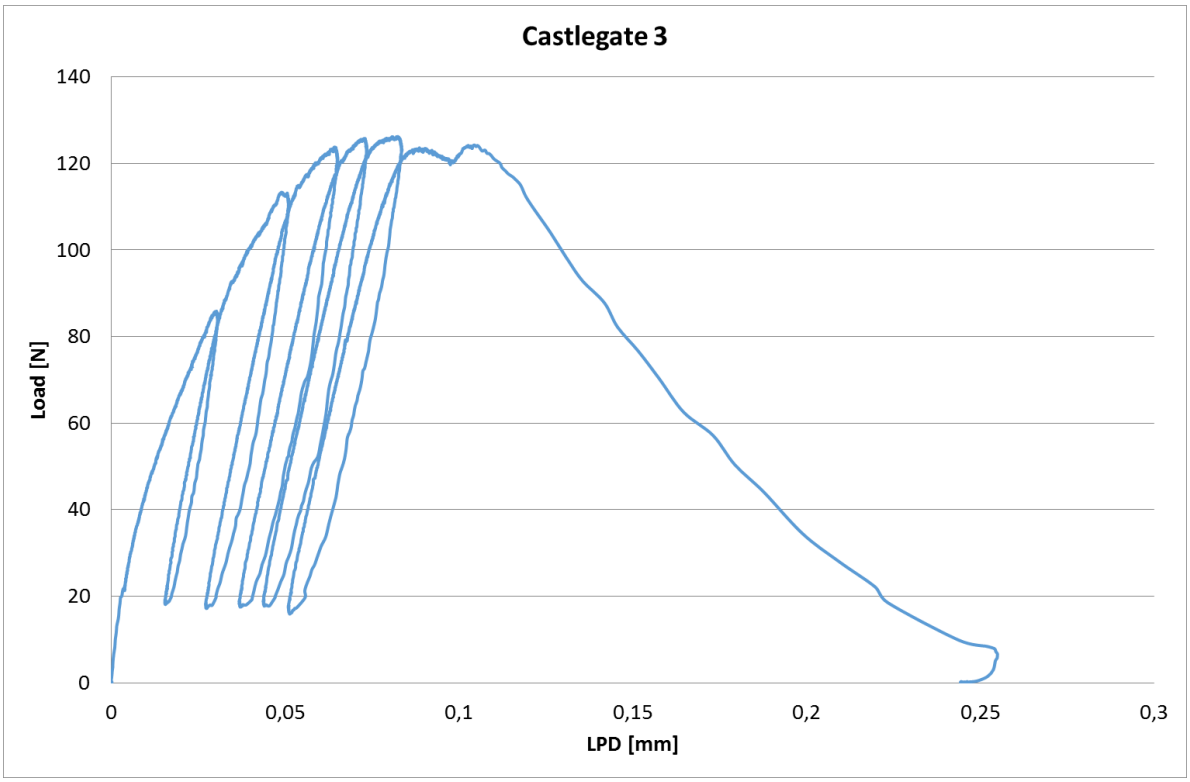

Figure 11-44: Load vs LPD for Castlegate 3. Diameter is 51.26 mm

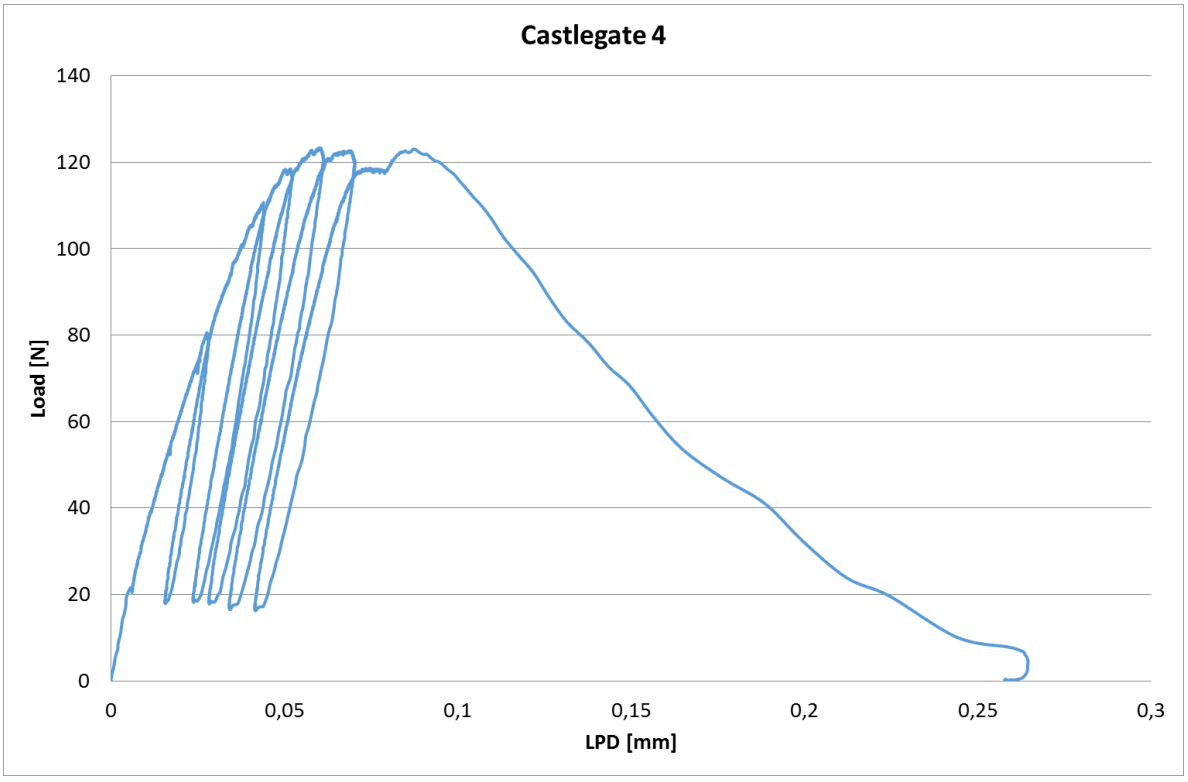

Figure 11-45: Load vs LPD for Castlegate 4. Diameter is 51.36 mm

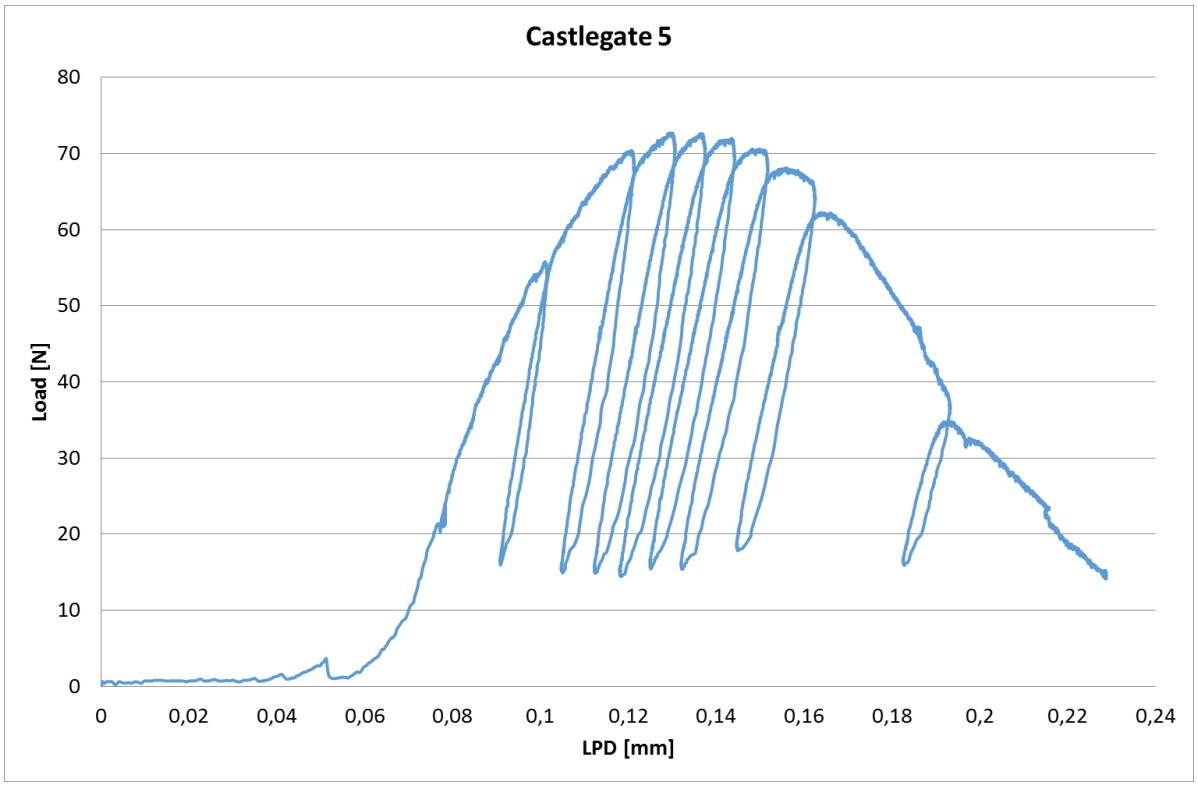

Figure 11-46: Load vs LPD for Castlegate 5. Diameter is 37.39 mm

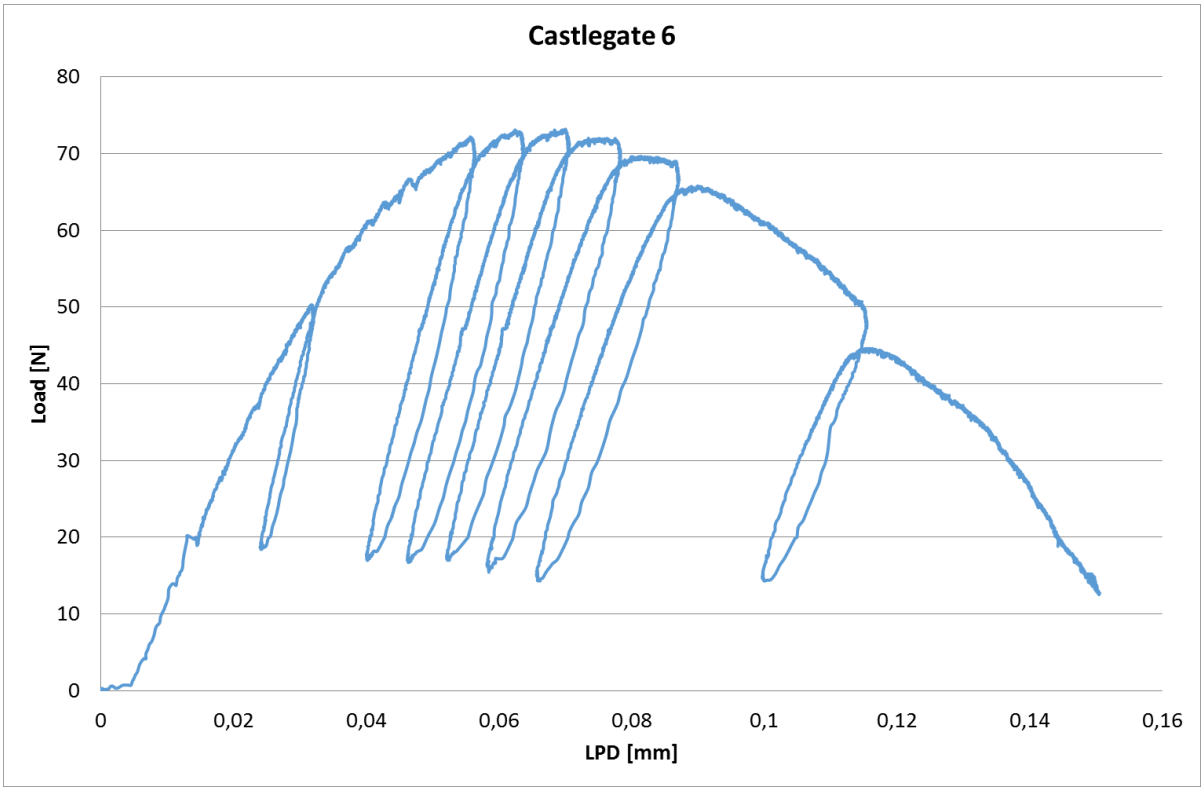

Figure 11-47: Load vs LPD for Castlegate 6. Diameter is 37.39 mm

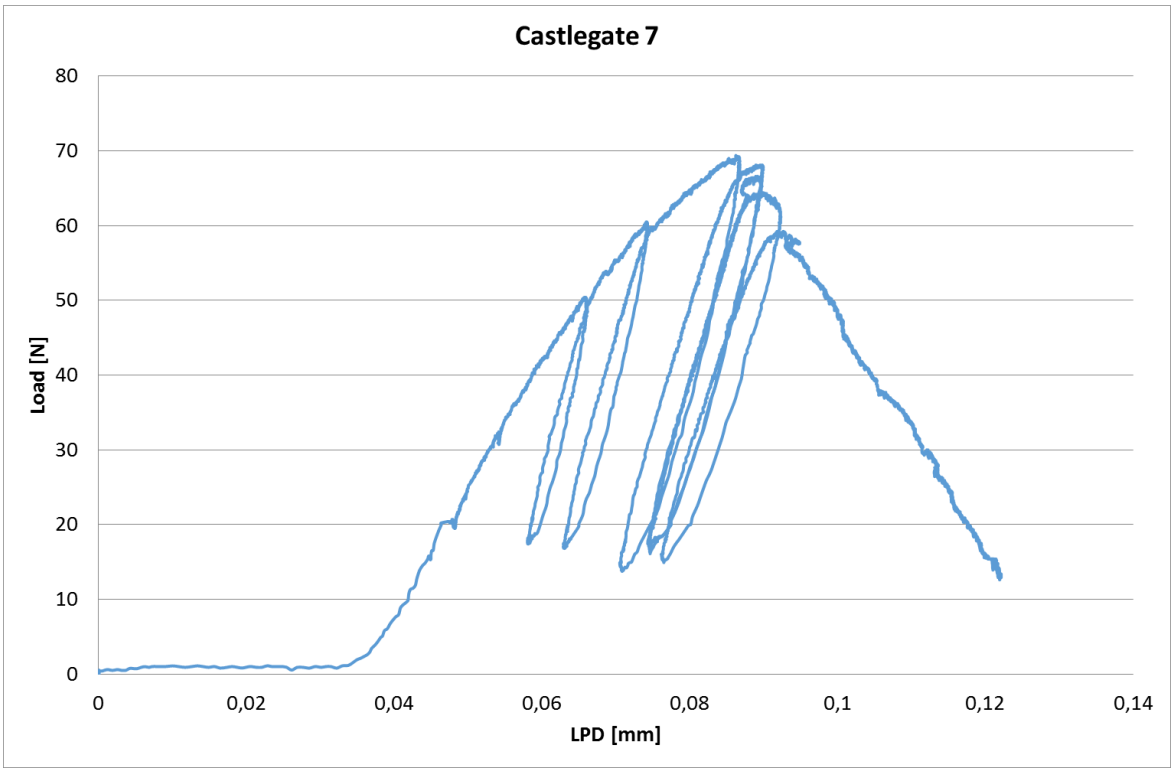

Figure 11-48: Load vs LPD for Castlegate 7. Diameter is 37.35 mm

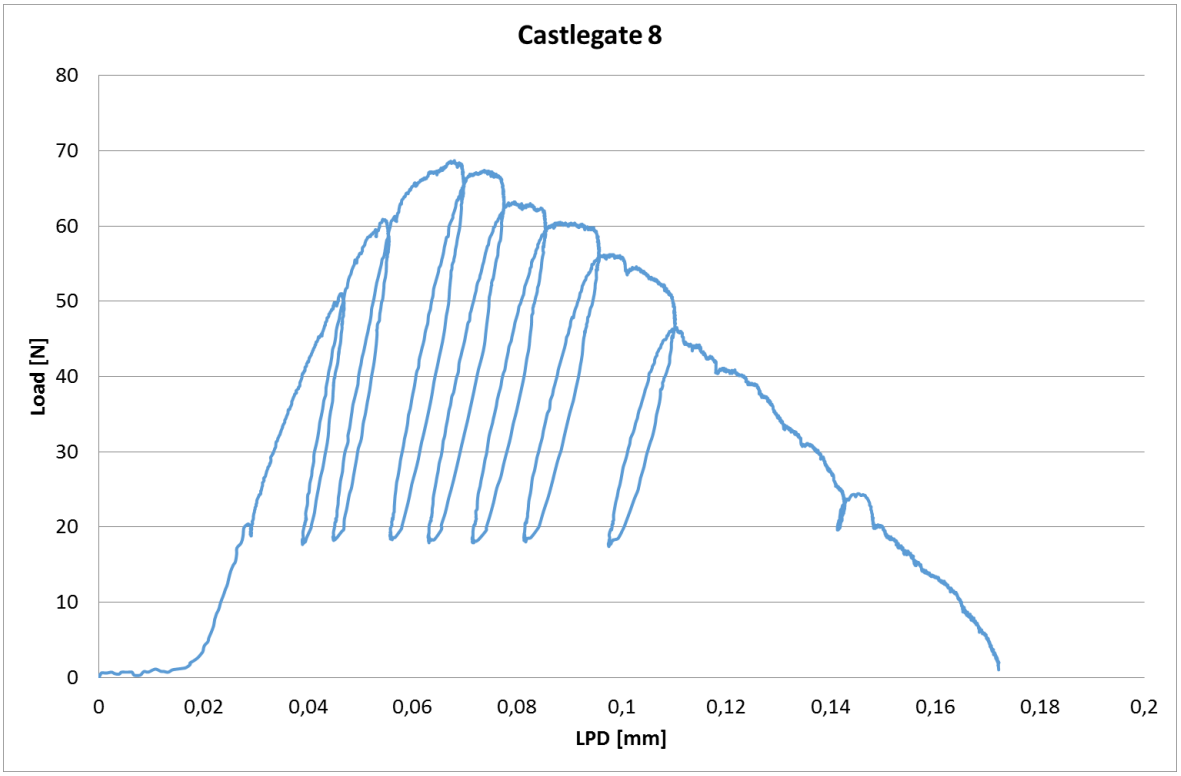

Figure 11-49: Load vs LPD for Castlegate 8. Diameter is 37.42 mm